

# **POLITECNICO DI TORINO**

**Department of Mechanical and Aerospace Engineering**

**Master's degree in Biomedical Engineering**

## **BIOMECHANICAL STUDY OF THE HINGED KNEE ARTHROPLASTY IN PATIENTS WITH VALGUS AND VARUS DEFORMITY**



**Relators:**

Prof.ssa Cristina Bignardi  
Prof. Alberto Audenino

**Supervisor:**

Prof. Bernardo Innocenti

**Candidate:**

Lilia Maestriperi

**A.Y. 2018/2019**

*A mia nonna,  
Pilastro importante della mia vita.  
Per aver creduto sempre in me più di quanto abbia fatto io.*

# INDEX

Abstract	1
1. Introduction	4
1.1 <i>Anatomy of the knee joint</i>	4
1.2 <i>Bones</i>	6
1.3 <i>Soft tissues: Ligaments, tendons and muscles</i>	7
1.3.1 Ligaments	7
1.3.2 Tendons	9
1.3.3 Muscles	9
1.4 <i>Biomechanics of the knee joint</i>	10
1.4.1 Movements	11
1.4.2 Knee joint load	11
1.4.3 Mechanical Alignment	13
1.5 Knee diseases	16
1.6 <i>Primary Total Knee Arthroplasty</i>	18
1.7 <i>Revision Total Knee Replacement</i>	22
1.7.1 Endo-Model Hinged knee Prosthesis	22
2. Aim of the study	27
3. Material and methods	28
3.1 <i>Geometry</i>	28
3.2 <i>Material and Properties</i>	28
3.3 <i>Assembly</i>	29
3.4 <i>Contacts</i>	30
3.5 <i>Load and Boundary Conditions</i>	30
3.6 <i>Cementless models</i>	32
3.6.1 First model	32
3.6.2 Second model	33
3.6.3 Third model	33
3.7 <i>Cemented Models</i>	33
3.7.1 Fourth model	33
3.7.2 Fifth model	34
3.7.3 Sixth model	34
3.8 <i>Osteoporotic configuration</i>	34
3.9 <i>Mesh</i>	35
4. Results	36
4.1 <i>Part I</i>	36
4.2 <i>Part II</i>	67
5. Discussion	84

6. Conclusions	87
7. Figures	88
8. Tables	92
REFERENCES	93

## **Abstract**

### **Introduction**

Restoration of the functional anatomy of the knee is one of the most important challenge today.

The factors that ensure long-term survival and improving function of the replaced knee are alignment, soft tissue balancing and restoration of the joint.

It is essential thus study the anatomy, the biomechanics and the forces transmitted across the articulating surfaces, in order to achieve long-term TKA survival.

Rotating hinge (RH) knee prosthesis is a common solution used for revision procedure. Nevertheless, it is also used in complex primary surgery as an alternative of primary total knee arthroplasty. One of the most used RH implants is the Endo-Model rotating Hinged Knee Prosthesis, which enable knee flexion-extension and intra-extra rotation. The design of this prosthesis consists of a femoral and a tibial component, which are rigidly constrained, and a polyethylene insert placed between these two elements, which prevent luxation without reducing the range of motion. This kind of prosthesis thus is a highly constrained device able to provide the stability needed for arthroplasty in complex situations. It is therefore optimal to deal with such problems of large ligamentous instability, severe bone substance loss, and distal femoral or proximal tibial defects resulting from injury or tumour, severe Varus or valgus deformity. Deviation from neutral alignment could alter mediolateral force distribution, which could cause overloads the bone-implant interface as well as to the bone itself. To date, the use of Endo-Model rotating-hinge is mainly based on surgeon experience and this could represent an important bias for the use of this device and the associated clinical outcomes. This study thus intends to help clinicians and specialists to make a proper decision during surgery about the length and type of stems when a Varus-valgus deformity is present. Due to the impossibility to predict the deficiencies of the bone, it is possible to choose among different lengths of stem and type of fixation, cemented or cementless. Therefore, a biomechanical study is conducted in order to evaluate the performance of Hinged Knee Endo-Model prosthesis in patients with severe Valgus and Varus deformity.

## **Materials and Methods**

3D femur bone model was obtained from Computer Tomography images. While, the design of right side, size medium of Endo-Model prosthesis was reconstructed using industrial CAD designs. A Total of 243 configurations were developed and analyzed in this study. To compute the distribution of mediolateral forces, a simplify mathematical model was used. From the equilibrium of forces and moments in the frontal plane, the medial and lateral forces were derived. A simplify 3D model of femur bone was developed with the use of software Abaqus to obtain the percentage of force distribution in medial and lateral region of tibial component. Starting from physiological configuration, static simulations were performed to analyse the stress distribution on implant components for different Varus and Valgus alignments (5°, 10°, 20° and 30°) at 0°, 5° and 90° of flexion. Three stem lengths (50, 120 and 160 mm) of femoral component and two types of fixation (cemented or cementless) were examined both for physiological and osteoporotic bone. Each configuration underwent was loaded with a constant axial force of 1000N applied on the proximal tibia and the proximal part of the femur was constrained. A Finite Element Analysis was used in order to obtain the average von Mises stress and the contact pressure and area both for polyethylene and bushing components.

The materials properties of the implant and bone were chosen based on literature research.

## **Results and Conclusions**

For all the stem lengths, when the knee has a Varus or Valgus configuration, it will cause an increase of stress on polyethylene component compared to the aligned configuration. The tibiofemoral force at the medial side increased in Varus configurations; accordingly, the stress on lateral side was higher for Valgus configurations. The trend of mediolateral force for 50 and 160 mm cementless stem was similar. In particular, the percentage of force increased sharply after 10° of Varus and Valgus alignment, with values of 100% of total force in medial and lateral region. While, the model with 120 mm cementless stem showed a roughly linear trend between -10°

and 10° of Valgus and Varus alignment. Moreover, the values obtained from this model demonstrated a better distribution of force on each side for severe Varus and Valgus alignment at 5° and 90° of flexion, which could mean more stability of the implant. Therefore, 120 cementless stem is a good compromise between 50 and 160 cementless stems. Similar results were found for cemented and osteoporotic models.

## **1. Introduction**

Restoration of the functional anatomy of the knee is one of the most important challenge today. The factors that ensure long-term survival and improving function of the replaced knee are alignment, soft tissue balancing and restoration of the joint.

This articulation allows a complex set of movements, as a result, the knee joint is difficult to analyze and study. Nevertheless, the main goal of total knee replacement (TKR) is to restore painless movements of the knee joint.

The alignment in total knee arthroplasty (TKA) is an important factor to prevent early implant failure. Incorrect alignment may lead to early aseptic loosening, polyethylene wear, patellofemoral maltracking, instability and infection. [1]

Deviation from optimal alignment could increase bone and implant stress, overload the tibial component in medial or lateral compartment and increase the contact forces. [2]

It is essential thus study the anatomy, the biomechanics and the forces transmitted across the articulating surfaces, in order to achieve long-term TKA survival. For instance, in specific cases the use of a rotating hinge knee prosthesis is an alternative in TKA.

### **1.1 Anatomy of the knee joint**

The main parts of the knee joint are bones, ligaments, tendons, cartilages and a joint capsule.

The knee joint is the largest and one of the most complex joints in the human body. The knee consists of two joints: the femorotibial joint and the patellofemoral joint (Fig1). [3]

The femorotibial joint articulates the femur and tibial bone. It is composed of two condyloid articulations. The medial and lateral femoral condyles articulate with the corresponding tibial plateaus. This joint is the biggest of the human body and allows the relative movement between the femur and tibial bone. It is the weight-bearing joint of the knee.

The patellofemoral joint articulates the femur and the patella. This joint is important to knee stability mostly through its role in the extensor mechanism. [3]

The distal end of the femur has a medial and a lateral condyle, each of which has a distinct shape that corresponds to the shape of the tibial plateau (Fig. 2). Instead, the proximal end of the tibia has a plateau with medial and lateral sections divided by the tibial spine (Fig. 3).

The proximal tibia is separated by the intercondylar eminence into an oval, concave medial plateau, and a circular, convex lateral plateau. The medial and lateral compartments are asymmetrical. [3]

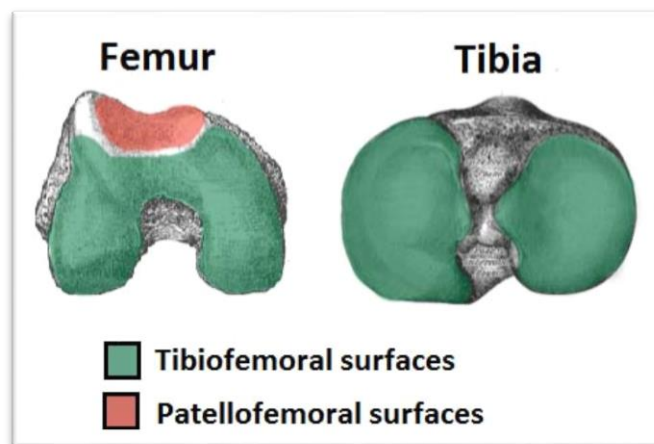


Figure 1, articulations of the knee joint. Distal view of the femur and proximal view of the tibia

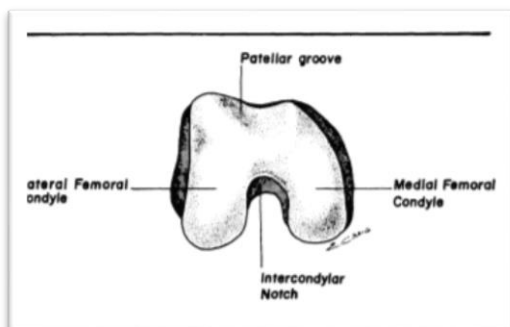


Figure 3, Distal view of femur bone

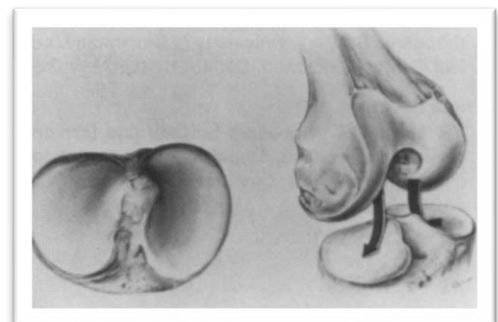


Figure 2, Proximal view of tibia bone

## 1.2 Bones

Four bones make up the knee: femur, tibia, patella and fibula (Fig. 4).



*Figure 4, bones of the knee*

### **Femur**

The femur is the longest and strongest bone in the human body. The proximal end forms the head of the femur, which articulates with the acetabulum in the pelvic bone forming the hip joint. Whereas, the distal end forms a double condyle that articulates with the tibia and patella forming the knee joint. The tibia articulates with the distal lateral and medial femoral condyles. The patella articulates anteriorly to the femoral condyles in the region of the intercondylar fossa.

### **Tibia**

The proximal end of the tibia bone consists of medial and lateral condyles, an intercondylar area, and the tibial tuberosity that articulates with the medial and lateral condyles of the femur. Distally, the tibia articulates with the ankle. The distal and proximal ends of the tibia articulate with the fibula.

## **Fibula**

The fibula is thin bone in the lower leg and runs along the lateral side of the tibia. It articulates with the tibial head and the ankle joint. The fibula is connected to the tibia via the interosseous membrane. The fibula does not articulate with the femur or patella.

Furthermore, the fibula is not directly involved in weight transmission. Its main function is to combine with the tibia and provide stability to the ankle joint. [10]

## **Patella**

The patella is a flat sesamoid bone that articulates with the femur posteriorly. Its function is to protect the anterior surface of the knee joint. [11]

# **1.3 Soft tissues: Ligaments, tendons and muscles**

## **1.3.1 Ligaments**

The ligaments connect the bones providing knee stability and preventing undesired motions. The ligaments of the knee joint can be divided into extracapsular and intraarticular ligaments. The main ligaments in the knee are medial collateral ligament (MCL), lateral collateral ligament (LCL), anterior cruciate ligament (ACL), posterior cruciate ligament (PCL) (fig 5).

The MCL is composed of a superficial and a deep part.

The superficial MCL originates on the medial epicondyle of the femur and runs downward approximately 11 cm to its tibial insertion. [3] The deep part of MCL has the same origin of superficial portion but it inserts on the medial meniscus and the proximal medial tibia plateau.

The main function of the MCL is to restrain Valgus force and contain lateral and medial translation of the tibia.

The lateral collateral ligament (LCL) extends from the lateral epicondyle of the femur to the lateral fibular head. The different from MCL is that the LCL is separated from the lateral meniscus. The LCL is a primary restraint to Varus at all positions of flexion [3].

The collateral ligaments help to stabilise the knee joint in medial-lateral direction.

The ACL arises from the medial side of the lateral femoral condyle and runs an oblique course through the intercondylar fossa distoanteromedial to the insertion at the medial tibial eminence. It prevents anterior dislocation of the tibia onto the femur [5].

The PCL originates from the lateral surface of the medial condyle and inserts onto the posterior aspect of the tibia. It prevents posterior dislocation of the tibia onto the femur [3].

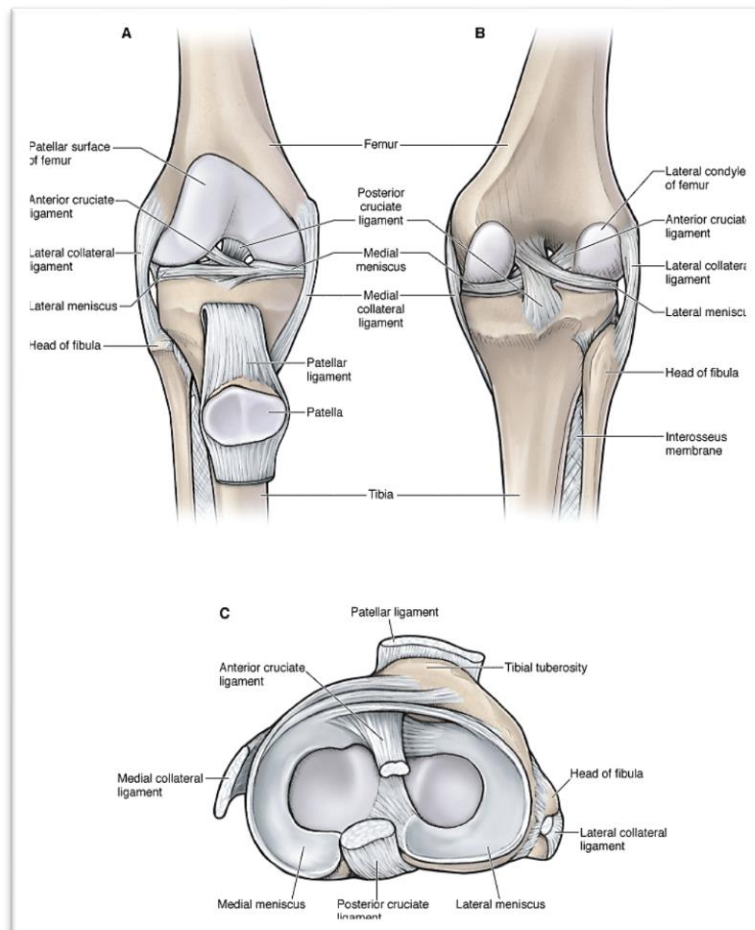


Figure 5, (A) Anterior view of the distal femur and the proximal tibia. (B) Posterior view of the distal femur and the proximal tibia. (C) Top view of the proximal tibia

### 1.3.2 Tendons

The tendons connect muscles to bone. Their biomechanical function is to transmit forces from muscles to bone and modulate forces during knee activities. The two major tendons in the knee are quadriceps tendon and patellar tendon.

### 1.3.3 Muscles

The main motion of the knee is flexion and extension. There are two main muscle groups involved in this kind of motions: the quadriceps and hamstrings.

Femoral quadriceps control the extension of the knee. It is made up of four extensor muscles: vastus medialis and lateralis, rectus femoris and vastus intermedius (Fig.6). They are responsible of stabilizing the patella and the knee joint during gait. They also play a crucial role in walking, running, jumping and squatting.

Flexion is caused by the hamstrings muscles, which include semitendinosus, semimembranosus and biceps femoris (fig.7). These muscles on the back of the thigh flex the knee and extend the hip. The hamstrings have the same role of the femoral quadriceps in daily activities such as walking, running, jumping and squatting. Especially during walking they play an important role as antagonist muscles to the quadriceps in the deceleration of knee extension [12].

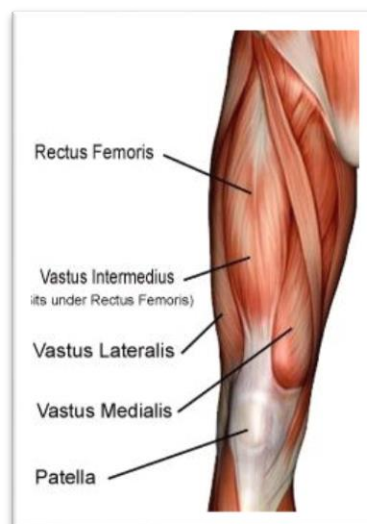


*Figure 6, Anterior view of quadriceps*

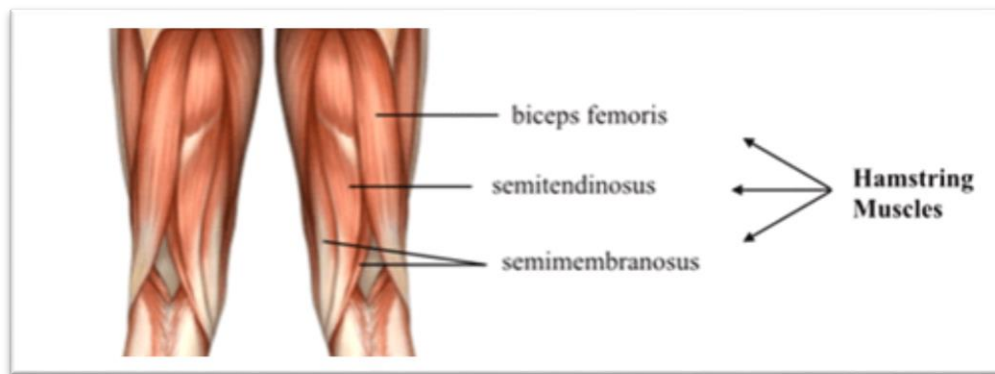


Figure 7, Posterior view of hamstrings muscles

## 1.4 Biomechanics of the knee joint

The study of the kinematics, related to the human body, is important to evaluate the behaviour of the joints as motions of biologic system.

The purpose of kinematics study is to understand the behaviour of normal joint for comparing the injured knee joint with a no injured ones and for evaluating the success of treatment protocols. With this knowledge can be decided the correct treatment and management of all knee lesions.

For example, excessive knee motion in a certain direction during examination may be an indication that a specific structure within the knee has been damaged [6].

Movement of knee joint can be described with six degrees of freedom: three translations and three rotations along three principle axes: the tibial shaft axis, the epicondylar axis, and the anteroposterior axis, which is perpendicular to the other axes.

Translations along these axes are referred to as proximal-distal, medial-lateral, and anterior-posterior translation, respectively. Rotations about these axes are referred to as internal-external rotation, flexion-extension, and Varus-Valgus rotation, respectively [6].

### **1.4.1 Movements**

The knee joint is the largest joint in the human body and allows a complex set of movements.

Knee flexion-extension involves a combination of rolling and sliding called “femoral roll back” between femur and tibia. Starting from the full extension position, the condyle begins to roll without slither, and then the sliding becomes progressively predominant so at the end of the flexion there is only slipping of the condyle without rolling.

Because of asymmetry between the lateral and medial femoral condyles, the rolling phase is then different between the condyles. In early flexion, 10°-15° of knee flexion are characterised by rolling of medial condyle, and then the rolling continues up to 20° of flexion with lateral condyle. The rolling movement translates the point of tibiofemoral contact posteriorly. The gliding movement takes place with flexion angle greater than 20°, and in this configuration, there is a greater posterior translation of the lateral tibiofemoral contact point in relation to the medial contact point.

During the flexion-extension movement, the intra-extra rotation is possible with 25-30 degrees of rotation.

Translations are in the order of the millimetre, 5-10 mm of anteroposterior translation and 1-2 mm of mediolateral translation. [8]

### **1.4.2 Knee joint load**

The knee joint can be divided into three compartments, two tibiofemoral and one patellofemoral and the presence of menisci, which contribute significantly in the transfer of contact stresses from one articular surface to another [7].

The tibiofemoral joint is subject to forces due to combination of transmission of the body weight across the joint and the contraction of muscles around the knee. Forces transmitted across the articulating surfaces are determined by a combination of the alignment, movement and integrity of anatomical structure [8].

The forces acting on the knee joint are (Fig. 8):

- Axial force along the axis of the tibia.
- The forces in the anterior-posterior and / or mediolateral direction resist (or induce) translations.
- The torque around the mediolateral axis resists (or induces) flexion and extension.
- The torque around the anteroposterior axis resists (or induces) adduction and abduction.
- The torque around the tibial axis resists (or induces) medial or lateral rotation

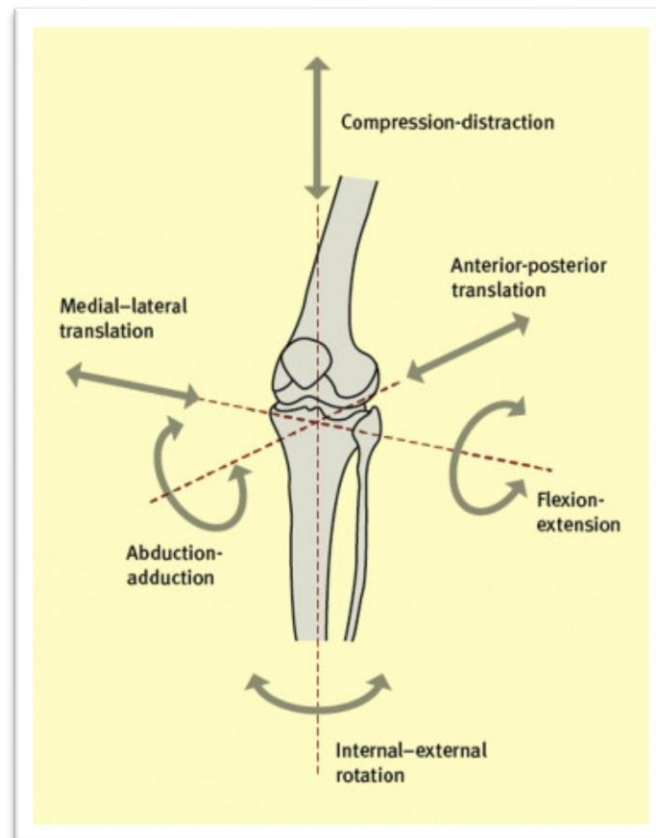


Figure 8, forces and moments of the knee with six degrees of freedom

The knee joint has a primary role in all human activities as walking, squats, climbing stairs and sport activities.

Biomechanical studies estimate that during a level walking the tibiofemoral contact forces are two to five times the body weight, while the patellofemoral ones are around half of the body weight.

In a physiological knee the compressive force is resisted by the joint reaction force. Therefore, the stresses depend on the contact area. [9]

### **1.4.3 Mechanical Alignment**

The knowledge of lower limb alignment is important to understand the parameters and limits of normal alignment.

The axes considered are mechanical axis and anatomic axis (Fig 9).

The mechanical axis of the lower limb originates from the centre of the femoral head to the centre of the ankle joint. Moreover, it is that along which the weight load is applied.

The anatomical axis of the femur and the tibia is a straight line drawn along their intramedullary canals.

The mechanical axis of the femur is not parallel to the vertical axis, which is a vertical line that extends distally from the centre of the pubic symphysis. This axis forms an angle of three degrees with the vertical line.

The anatomical axis of the femur makes an angle of 5°-7° degrees with the mechanical axis in the frontal plane. Consequently, the anatomic axis of the femur has an approximate 5°-7° of inclination difference than the vertical axis. While the anatomical and mechanical axis of the tibia corresponds to each other. [13]

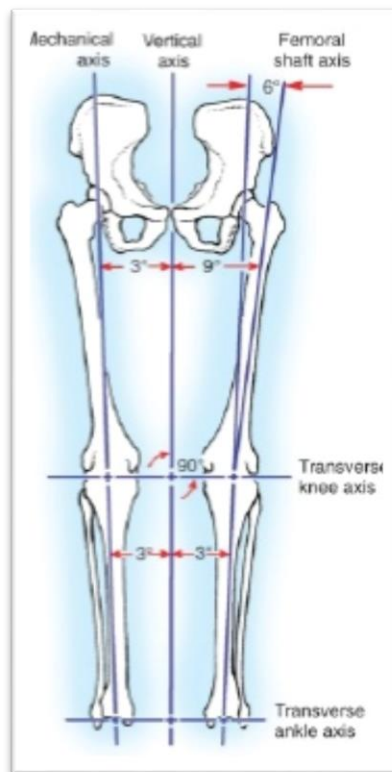


Figure 9, mechanical and anatomical axis of the lower limb.

Frontal plane tibiofemoral alignment can influence the distribution of tibiofemoral contact forces. Malalignment can lead to unphysiological mediolateral force distribution. Varus and valgus deformities can be representative of knee misalignment (Fig 10).

In details, genu Valgum is a knee misalignment that turns the knee inwards. In a valgus (knock-knee) knee, the axis passes lateral to knee center, increasing force across the lateral compartment.

Genu Varum is a knee misalignment that turns the knee outwards. In a Varus (bow-leg) knee, this line passes medial to the centre of the knee, increasing force across the medial tibiofemoral compartment.

Hence, the alignment of the femur and bone is a key determinant of load distribution, especially in terms of stability and function of the knee joint.

One of the most important prerequisites for a long-term TKA survival is the restoration of neutral mechanical alignment [2]. Malalignment could increase mediolateral force distribution, which causes overloads the bone-implant interface as well as the bone itself. Moreover, it may induce polyethylene wear, leading to osteolysis and loosening of the implant.

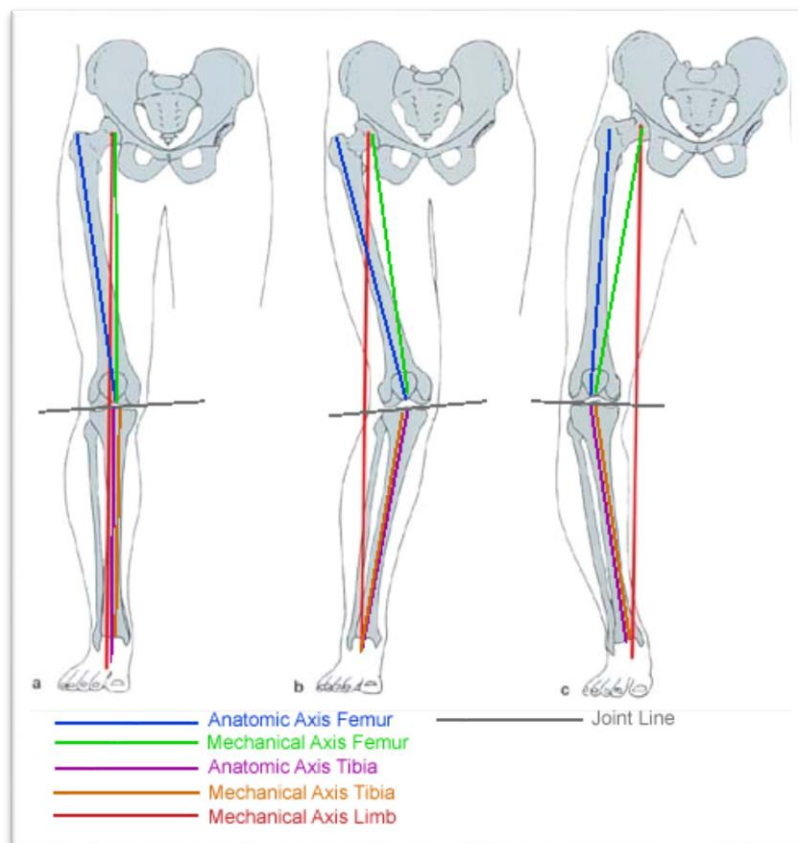


Figure 10, physiological knee (a), Valgus knee (b), Varus knee (c)

## 1.5 Knee diseases

The knee is the largest joint in the body, for this reason, the risk of injuries and diseases is quite high.

In physiological knee, all components are balance to each other. Nevertheless, disease or injury can lead to loss of this stability, resulting in pain, muscle weakness and reduced function.

Knee problems are very common, and they occur in a large portion of people. They can interfere with daily activities and have a big impact with the quality of life. Treatment of knee problems depends on the causes and severity of the injury. In cases where preventive measures cannot be taken, surgical operation can restore the functionality of the knee joint.

The most common reason of knee replacement surgery is osteoarthritis. It is a chronic degenerative disorder characterised by gradual loss of articular cartilage. Therefore, the thickness of the cartilage decreases until it disappears, causing damages in the joint. Osteoarthritis is characterized by deterioration of articular cartilage, osteophyte formation and bone remodelling.

Osteophytes are bone spurs that form along joints; they can cause pain and limiting joint motions (Fig 11).

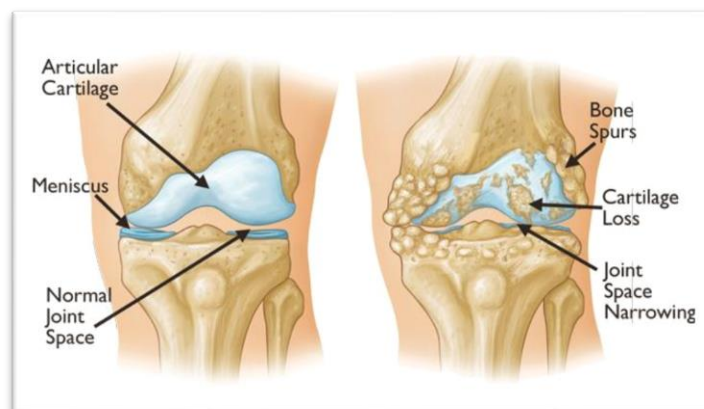


Figure 11, healthy knee joint (left), osteoarthritic knee (right)

The most common risk factors for osteoarthritis are:

- Age: osteoarthritis affects elderly population but can involve also young adult people.
- Trauma: cruciate, collateral ligaments and joint fractures can lead increase risk of osteoarthritis.
- Gender and ethnicity: men under the age of 50 have a higher prevalence and incidence than women. However, the women up to 50 are affected more than men. Instead, the difference tends to become less evidence with the increase of age, in particular after 80.
- Genetics: there is a genetic susceptibility to the disease. Indeed, many genes are related to osteoarthritis. The defective genes are often coding for structural proteins of the extracellular matrix of the joint and collagen proteins.
- Obesity: increasing weight can lead the risk of osteoarthritis, since excessive weight can put stress on joints and cause cartilage damage.
- Diet: lack of vitamin C and vitamin D could increase the risk of osteoarthritis progression. In detail, vitamin C has antioxidant and collagen promoting properties that may delay the onset of osteoarthritis. On the other hand, people with low levels of vitamin D had an increased risk of osteoarthritis knee progression.
- Bone density: high bone density is a risk factor for development, but low bone density is a risk factor for progression of knee osteoarthritis [14].
- Biomechanical: joint injury, reduced muscle strength, joint laxity, joint malalignment.

There are many treatments for osteoarthritis both non-surgical and surgical interventions.

The most important surgical procedure is arthroplasty that is an intervention to replace or restore a severely osteoarthritic joint in order to relieve pain and improve mobility, thereby adding to the patient's quality of life [15].

## 1.6 Primary Total Knee Arthroplasty

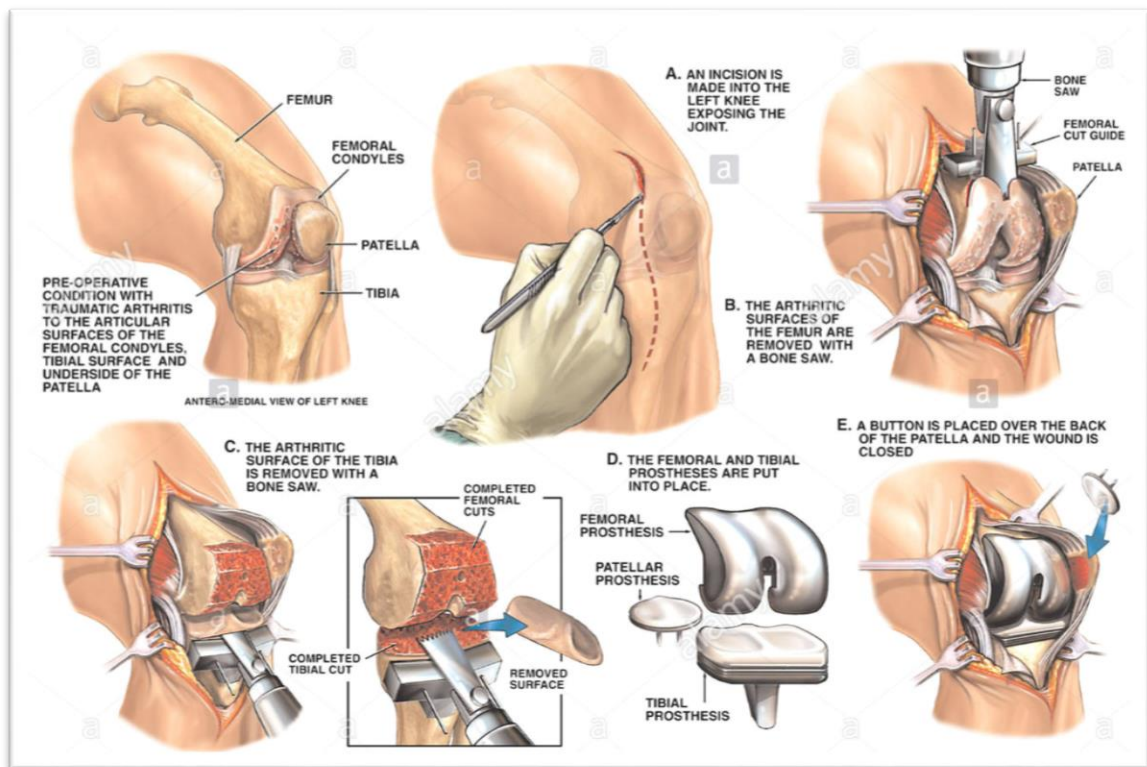


Figure 12, Procedure of TKA

Total Knee Replacement, also known as Total Knee Arthroplasty, is the most common surgical procedure performed in all countries of the world. Nowadays this procedure is not limited to the elderly population but is performed also in younger patients. In the last few decades, in the US, the number of annual primary TKA is increased by 161.5%, from more than 93,000 to more than 226,000 cases [17]. Approximately 700,000 knee replacement procedures are performed annually in the US. Studies estimated that the number of TKR procedure will increase to 3.48 million per year within 2030 [16].

The main goal of TKR is to relieve pain and to restore function of the knee joint, arising from Osteoarthritis and other pathologies that damage the articular surface of the knee. Restoration of biomechanical functions of the knee, such as alignment, soft tissue balancing and joint line, are factors that guarantee long-term TKA survival.

TKR is a surgical procedure that consists to remove the damage surfaces of the bones and replace them with an artificial implant. An incision is made with the knee slightly

flexed to expose the joint. After that, knee flexion is increased and the patella is shifted laterally to open the anterior knee. Then, distal femur and proximal tibia are cut to remove the damaged surfaces to fit the shape of the implant. Finally, the femoral and tibial components are put into place (Fig. 12). The prosthetic implant consists of a femoral and a tibial component, which are rigidly constrained, and a polyethylene insert placed between these two elements.

Femoral component is placed in the distal part of the femur and due to its shape covers the lower end of the femur. Whereas tibial plate is flat and has a stem that inserts into the centre of the tibial bone. The third component is a plastic insert typically made up of polyethylene, placed between femoral and tibial components. It has an important role to create a smooth gliding

surface and role of damper to adsorb shocks and prevent luxation without reducing the range of motion. To avoid friction and creation of debris, metal surfaces never come into contact with one another. In some cases, also the patella can be replaced with a prosthetic component made of polyethylene. It improves extensor function by increasing its lever arm [8] (fig.13).

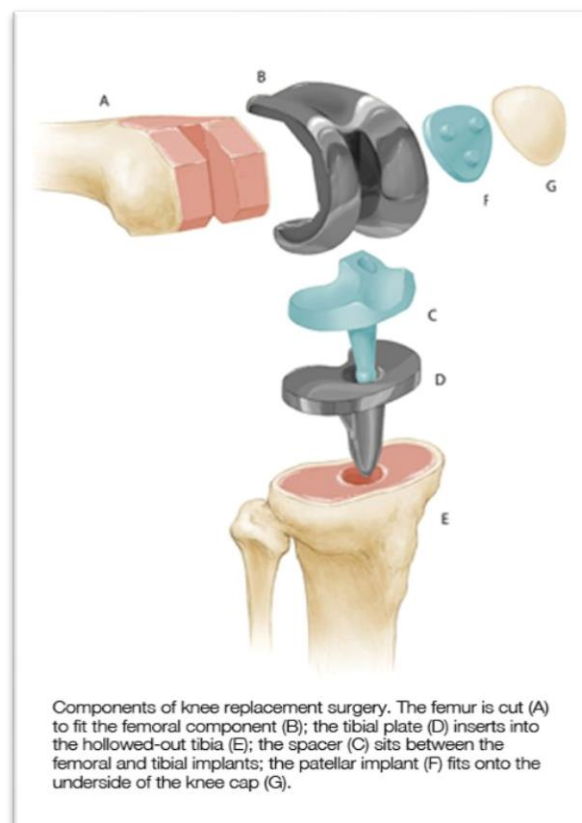
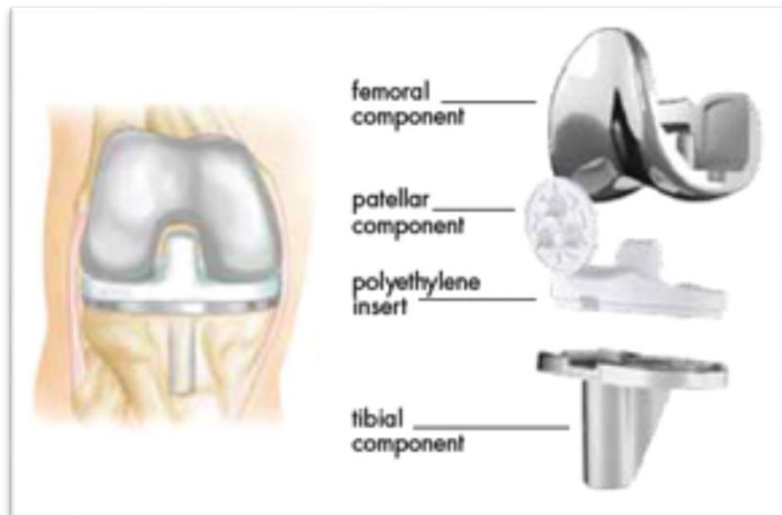


Figure 13, femur, tibia and patella after bone resection. The damaged joint is completely removed. The TKA is performed

The components in contact with the bones are made up of metal, usually alloys of cobalt-chromium and titanium, because they are strong enough to take weight bearing loads. Therefore, Metal-Polyethylene-Metal is the most combination used in knee replacement implant and the best association of materials in this kind of prosthesis. Since polyethylene resists to wear and degradation, is placed between the two metal components, in fact wear of components is an important problem in TKA, that must be avoid. The common features of materials are biocompatibility, because they are insert into the body, also they must to be flexible to bear stress and able to keep their strength and shape for long time (Fig 14).



*Figure 14, components of TKA*

There are different types of total knee replacement, in general they are divided into unconstrained, semi-constrained and constrained devices. Consequently, the choice of type of design, rather than another one, depends on evaluation of bone loss and extent of instability. Additionally, the choice among all types of implants is usually based on surgeon preferences as good clinical mid-term results.

Furthermore, the weight and gender are taken in consideration on implant selection. For example, nowadays there is a gender-specific “woman’s knee”, which is designed to comply the bone structure of the distal part of woman’s femur. [18]

There are several reasons of failure of total knee replacement, among these the most important are polyethylene wear, aseptic loosening, instability, infection, malalignment or malposition of components.

Wear of polyethylene is an important problem in TKA, nonetheless it can be reduced by improving PE manufacturing process or by reducing the contact stress at the joint surfaces.

Unfortunately, wear debris remains the major factor that leads to aseptic loosening of the implant. It can be caused by initial fixation, mechanical loss of fixation over time or biologic loss of fixation caused by particle-induced osteolysis around the implant. [19]

Instability can be associated with different factors as loosening of component, bone loss, fracture of prosthetic component, inadequate size or position, wear or collateral ligament laxity.

Infection is caused by formation of biofilms on the implant surfaces. Biofilm is an aggregate of microorganisms in which cells are adherent to each other and/or to a surface. Bacteria secrete a substance that forms the basic architecture of biofilms. This matrix isolates bacteria from the rest of environment and help bacteria to survive in the biofilm. Consequently, the antibiotics are not efficacy. [20]

Malalignment of the components leads to unphysiological distribution of the contact forces between the medial and lateral compartment, which overloads the bone and bone-implant interface. Misalignment thus may induce wear of polyethylene and/or aseptic loosening. [2]

In all cases, which the Primary Total Knee Replacement does not provide the required performances, a Revision Total Knee Replacement is needed.

## **1.7 Revision Total Knee Replacement**

Revision total knee replacement is used when the primary Total knee Arthroplasty is failed for all sort of reasons. For instance, loosening of the implant, infection of the joint, instability of the knee and malalignment of the parts. This procedure consists to remove some or all parts of the primary surgery and replace them with new ones. Both primary and revision replacement have the same goal, but revision surgery is more complicated than a primary total knee replacement, because it requires removing the previous implant, which placed into the existing bone. Therefore, once surgeons remove the implant there is less bone remaining. However, it is not possible to predict the quantity of damage bone, so it does not exist a standard total knee implants for revision knee replacement. Finally, obtaining a knee that is flexible and stable enough to allow motion and to keep you steady, respectively, are major challenges. Revision TKR is a complex procedure that requires an experienced surgeon, proper pre-operative planning and specialized tools to achieve good outcomes. [21]

The revision prosthesis consists of three components like the primary implant. The tibial component, femoral component and patellar component. The tibial and femoral component usually have a long stem placed into the bone for extra support.

### **1.7.1 Endo-Model Hinged knee Prosthesis**

Rotating hinge knee prosthesis is used in complex primary surgery, it is thus an alternative in total knee arthroplasty. The first implant was designed by Judet and by Walldius and Shiers in 1950. This kind of prosthesis had a considerable number of complications as loosening and infection. Therefore, new modifications were performed in order to improve different aspects and evolve the second generation of prosthesis. The main models were the GUAPAR implant in 1970, the Stanmore prosthesis in 1971 and the Saint Georg in 1979. Nevertheless, some complication was reported such as material fractures or rupture of the extensor apparatus, so the third generation of prosthesis were designed. The main implant was Endo-Modell (Link) rotating hinge knee prosthesis, which functions as flexion-extension and intra-extra rotation.

This prosthesis attempts to reproduce the movements of a physiological knee. The flexion movement is around an axis with no change in the center of rotation. Whereas, during rotational movement the transmitted torque force to the bone-cement interface by components increases the risk of loosening. Therefore, the aim of this prosthesis is to reduce this problem with ramps shaped like tibial component to lead flexion, in order to limit the rotation depending on the flexion. In full extended knee the intra-extra rotation movement is not allowed, but it rises during flexion- extension movement by 15-20° from 50° of flexion. Flexion and rotation of the knee prosthesis occurs in a cross joint [22].

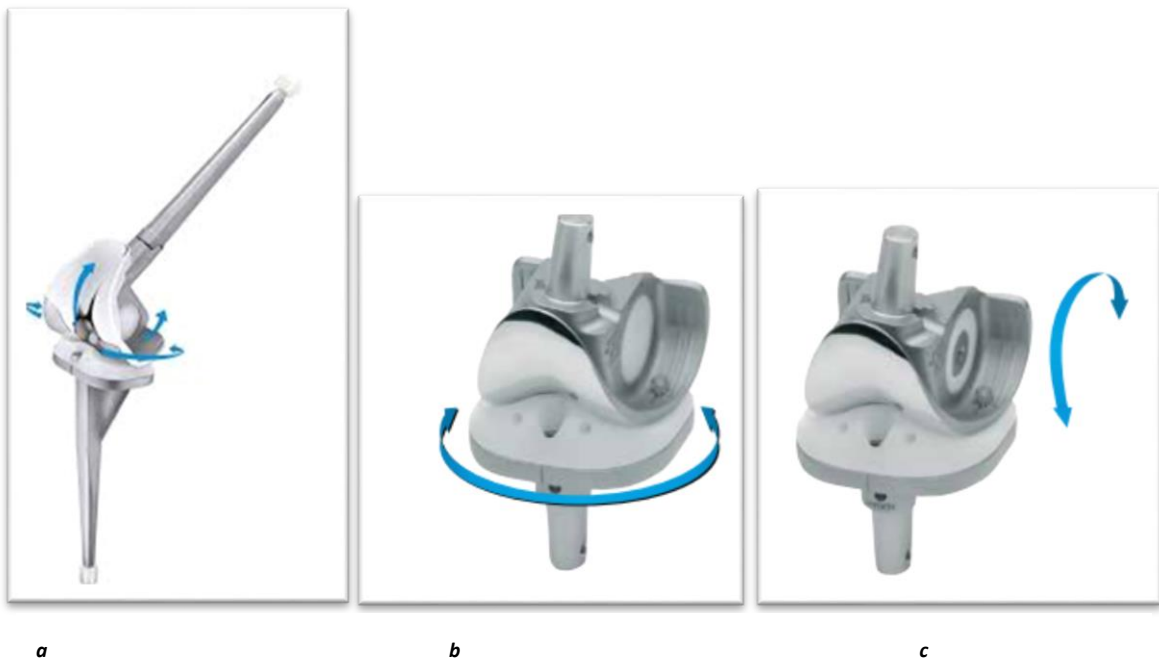


Figure 15, Movements of Hinged Knee Prosthesis (a), Rotational (b) and flexion movement(c).

The design of this prosthesis consists of a femoral and a tibial component, rigidly constrained, and a polyethylene insert placed between these two elements, which prevent luxation without reducing the range of motion. The distal femur and proximal tibia were prepared using the oscillating saw, and then the UHMWPE tibial plateau is positioned using a special instrument. Endo-Model includes also two stems placed into the femur and tibia bones. They can be used with cement or without (fig 16 and 17); stems represent a significant part of modular knee system. Moreover, the stems are available in different lengths of 50 to 280 mm. The possibility to interchange the size

and dimensions of prosthetic component is a worthwhile element. This means to choose independently to each other components according to fit on their respective bones. The modularity is very beneficial for revision surgery when deficiencies of the bone cannot be totally predicted.



*Figure 16, Cemented Stems*



*Figure 17, Cementless Stems*

Figure 16 and 17 show cemented and cementless stems respectively. The first stem is characterized with no structuring and the tips are fitted with star shaped UHMWPE centralizers in order to position the stem in the middle of the medullary canal. Hence, direct contact of the metal stems with the internal wall of the bone is prevented. While cementless stems have a longitudinal structuring and a microporous surface.

Regarding the assembly of plateau with anti-luxation system, first, the femoral component is lifted slightly, then the UHMWPE plateau is placed between the proximal and distal component of the prosthesis. After that, it is necessary to make sure that the chamber of the plastic plateau merges with the flange of the femoral component, and recess on the underside of the plastic plateau snaps into the marginal groove on the metal tibial tray. Finally, the UHMWPE plateau is pressed down and fixed into place by the self-locking fixation screw (fig 18).

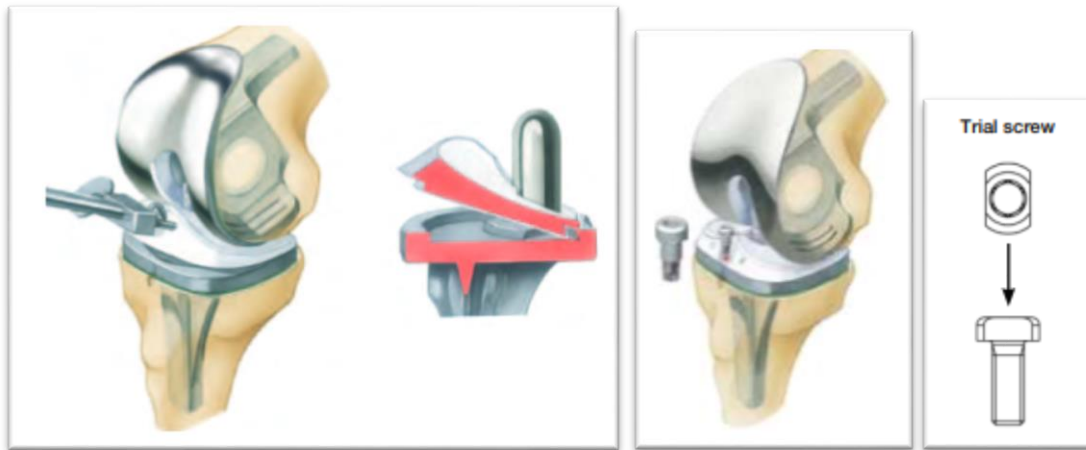


Figure 18, the UHMWPE plateau is pressed down into the metal tray and firmly fixed by the self-locking screw

After that, modular stems are linked by a cone assembly to the femoral and tibial components. There are two opposite flanges, which are inserted in the medial and lateral grooves at both the tibial and femoral components, to provide rotational stability (fig. 19 and 20).

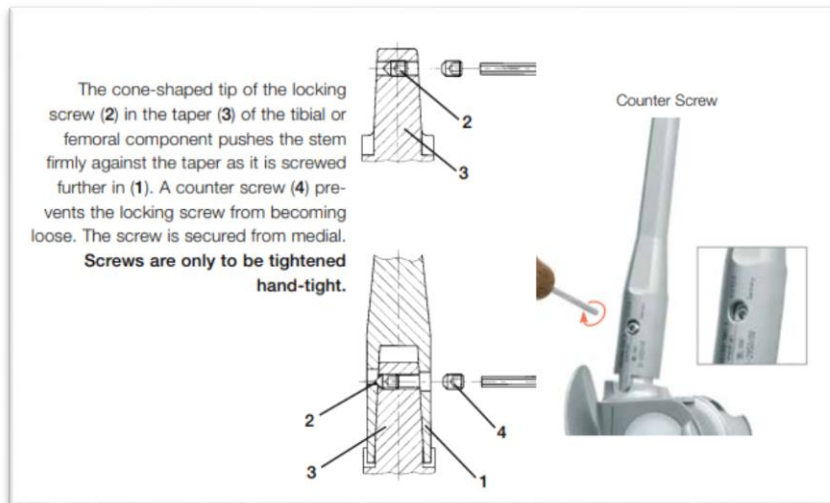


Figure 20, Screw fixation



Figure 19, Insertion of modular stems

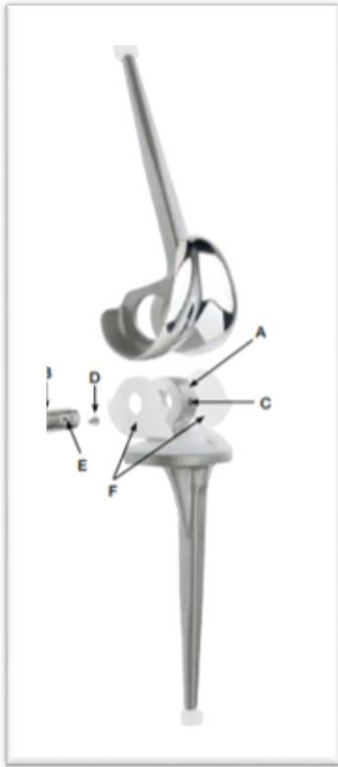


Figure 21, internal components of Endo-Model Hinge Knee Prosthesis

Finally, the inner of Endo-Model Hinge Knee is made up of several components (fig 21). The piece **A** is placed on tibial components and it has an important role to connect it to the femoral component. It is drilled through to accommodate the joint axis **B**. Also, it has a ventral hole **C** for the grub screw **D** whose tip fits into the recess **E** on the axis and locks the latter once the upper and lower components have been joined.

Moreover, there are two polyethylene bearings **F** which are placed between femoral component and connecting piece **A**. They are pushed into medial and lateral boreholes. In conclusion, the upper and lower prosthesis components are joined by the tibial connecting piece into the intracondylar box of the femoral component. Articulation takes place between the prosthesis axis and the two

bearings. The Endo-Model® Hinge Knee Prosthesis is delivered ready assembled in a sterile condition.

Because of its dimensions, Endo-Model® Standard/ – M requires an only minimal resection of 14 mm on the tibia-femur joint plane. As a result, there is a less resection than with a total knee prosthesis. [23]

Rotating-hinge device is therefore optimal to deal with such problems of large ligamentous instability, severe bone substance loss, and distal femoral or proximal tibial defects resulting from injury or tumour, severe Varus or Valgus deformity both in primary and revision surgery. This kind of prosthesis thus is a highly constrained device able to provide the stability needed for arthroplasty in complex situations, both in primary and revision surgery.

In the other hand, complications are frequent after this type of arthroplasty. Infection is the main frequent complication. The other two common causes are aseptic loosening and polyethylene wear. The reasons could be an insufficient long-term fixation and an increased amount of constraint.

## **2. Aim of the study**

The aim of this study is to evaluate the performance of Hinged Knee Endo-Model prosthesis by LINK company in patients with Valgus and Varus deformity. In particular, evaluate the distribution of stress and contact area on polyethylene and plastic bushing components. To reach this goal, Abaqus, which is a software suite for Finite Element Analysis (FEA), was used to perform all the simulations.

The purpose of this study is to assess the performance of this kind of prosthesis when two versions of stems (cemented and cementless) of different lengths are used. The main goal is to obtain significant result that could be useful for surgeon to make decision during surgery about the length and type of stems.

A static analysis is conduct in full extension ( $0^\circ$ ) and in flex-extension (both  $5^\circ$  and  $90^\circ$ ) both for cemented and cementless stems of three different lengths of femoral component (50 mm, 120 mm and 160 mm). Each model is thus performed for different Varus and Valgus configurations in order to evaluate the effect on the fixation and load transmission when using different stem lengths of femoral component.

Finally, each model is also performed for osteoporotic bone in order to predict the behaviour of the implant and extract data providing information on contact force and pressure.

To date, the use of Endo-Model rotating- hinge is mainly based on surgeon experience and this could represent an important bias for the use of this device and the associated clinical outcomes. This study thus intends to help clinicians and specialists to choose a device rather than another. Therefore, it may aid in the surgeon's treatment decision and in the development of patient-specific treatments.

### **3. Material and methods**

#### **3.1 Geometry**

In this study, a modular Endo-Model prosthesis (LINK), right side, size medium, was considered for the numerical analysis. The design of the prosthesis was reconstructed using industrial CAD designs. For the bone geometry, a physiological three-dimension femur bone was obtained from Computer Tomography images. The femoral bone consists of two parts: cortical bone and cancellous bone. Three stem lengths (50, 120 and 160 mm) of femoral component and two types of fixation (cemented or cementless) were examined both for physiological and osteoporotic bone for Valgus and Varus deformity. While the tibial component had a stem of 50 mm length. The size of polyethylene insert and tibial component remained the same in all configurations.

#### **3.2 Material and Properties**

The materials properties of the implant and bone were chosen based on literature research. The materials used in this study were assumed to be linear elastic, this means a better approximation of all materials in order to achieve a qualitative comparison among different configurations [2]. In particular, implant materials as femoral component and tibial tray were cobalt-chromium (CoCr), whereas the material of tibial insert was ultra-high-molecular-weight-polyethylene (UHMWPE), which has a yield point of approximately 20MPa. These materials were assumed to be homogeneous and isotropic. In detail, the material properties, i.e., the Young's modulus ( $E$ ) and Poisson's ratio ( $\nu$ ), were as follow: CoCr:  $E=240$  GPa,  $\nu=0.3$  and UHMWPE:  $E=0.685$  GPa,  $\nu=0.4$ . While, materials properties of cortical bone, of femur in physiological case, was considered transversely isotropic, with properties varying along the mechanical axis of the bone. With  $E_1=E_2=11.5$  GPa,  $E_3=17$  GPa,  $\nu_{12}=0.58$ ,  $\nu_{23}=\nu_{13}=0.31$ . On the other hand, the cancellous bone was considered linear isotropic and the materials properties used were  $E=21.3$  GPa and  $\nu=0.3$ . While material properties of osteoporotic bone of compact

bone were  $E_1=E_2=7.82$  GPa,  $E_3=11.56$  GPa,  $\nu_{12}=0.58$ ,  $\nu_{23}=\nu_{13}=0.31$ . For trabecular bone, material properties are different  $E_1=0.724$  GPa and  $\nu=0.3$ .

For cemented configurations, PMMA was placed in the femoral canal. The material properties adopted for PMMA was homogeneous and isotropic with  $E=3$  GPa,  $\nu=0.3$ .

The full overview of the material properties is shown in table 1.

Material models		Elastic modulus (GPa)			Poisson's ratio		
		$E_1$	$E_2$	$E_3$	$\nu_{12}$	$\nu_{23}$	$\nu_{13}$
Cortical bone	Transversely isotropic	11.5	11.5	17	0.58	0.31	0.31
Cancellous Bone	Isotropic	21.3	X	X	0.3	X	X
CoCr	Isotropic	240	X	X	0.3	X	X
UHMWPE	Isotropic	0.685	X	X	0.4	X	X
PMMA	Isotropic	3	X	X	0.3	X	X

Table 1, materials properties used for all models

### 3.3 Assembly

Abaqus/Standard version 6.14-5 was used to assemble all parts of prosthesis with femur bone in order to perform all the finite element simulations. First of all, it was needed to make adjustments where necessary. For instance, fillets of prosthetic components were removed to avoid problems during simulations as considerable stress peaks. After that, to ensure the right position of each component to another one, it was possible to define position constraint by coaxial method. Software rotated and translated the movable part instance until the two selected faces were coaxial and the arrows were pointing in the same direction. It was possible because the faces selected were cylindrical. Finally, it was added femur bone and assembled with other prosthetic components.

### 3.4 Contacts

As regards the definition of contacts between each components of prosthesis a surface to surface contact was defined. While, tie contacts were made between screws and CoCr components, PE and screws, femur bone and CoCr components, because relative micromovements were not take in consideration in this study. Another reason was to avoid any consequential displacement during simulations.

### 3.5 Load and Boundary Conditions

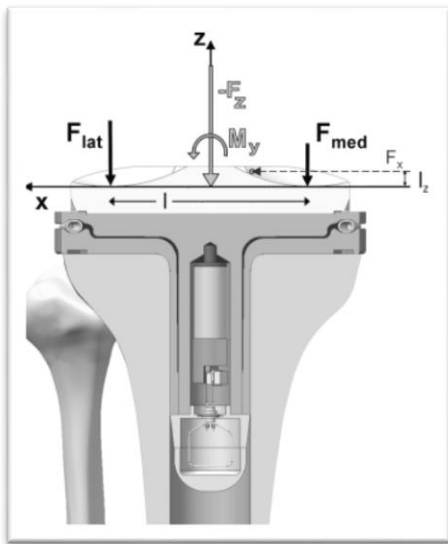


Figure 22, the instrumented baseplate to compute forces and moments.  $M_y$  =moment.  $F_x$  =mediolateral force,  $F_z$  =axial force,  $l$ =distance between condyles,  $l_z$  =lever arm z,  $F_{lat}$  =force on the lateral compartment and  $F_{med}$  =force on the medial compartment.

To compute the distribution of mediolateral forces, a simplify mathematical model was used (fig 22) [24].

From the equilibrium of forces and moments in the frontal plane, the forces  $F_{med}$  on the medial compartment was therefore derived:  $F_{med} = -F_z/2 - M_y/l$ , whit  $l$  the distance between condyles and  $F_{lat} = -F_z - F_{med}$ .  $F_z$  is axial force,  $F_{lat}$  and  $F_{med}$  are respectively the forces on the lateral and medial compartment.

To obtain a qualitative and quantitative data a simplify 3D model of femur bone was developed with the use of software Abaqus. In this way, starting with physiological configuration, medial and lateral forces were calculated for 5°,10°,20° and 30° both for Varus and Valgus deformity. A total of 243 configurations were developed and analyzed in this study. Each configuration was achieved by changing the limb alignment and underwent the same load conditions.

In table 2 are reported percentages of force distribution in medial and lateral compartment with an axial force of 1000 N.

	Medial Force	Lateral Force
<b>30° Varus</b>	<b>91%</b>	<b>9%</b>
<b>20° Varus</b>	<b>82%</b>	<b>18%</b>
<b>10° Varus</b>	<b>64%</b>	<b>36%</b>
<b>5° Varus</b>	<b>60%</b>	<b>40%</b>
<b>Physiological configuration</b>	<b>55%</b>	<b>45%</b>
<b>5° Valgus</b>	<b>43%</b>	<b>57%</b>
<b>10° Valgus</b>	<b>38%</b>	<b>62%</b>
<b>20° Valgus</b>	<b>8%</b>	<b>92%</b>
<b>30° Valgus</b>	<b>0%</b>	<b>100%</b>

*Table 2, Percentage of force applied in all models*

Once the distribution of forces has been estimated, the static simulation was made for nine models. During all simulations the superior part of the femur was constrained, and the forces were applied on the proximal tibia (fig. 23).



*Figure 23, coupling of lateral (a) and medial (b) forces.*

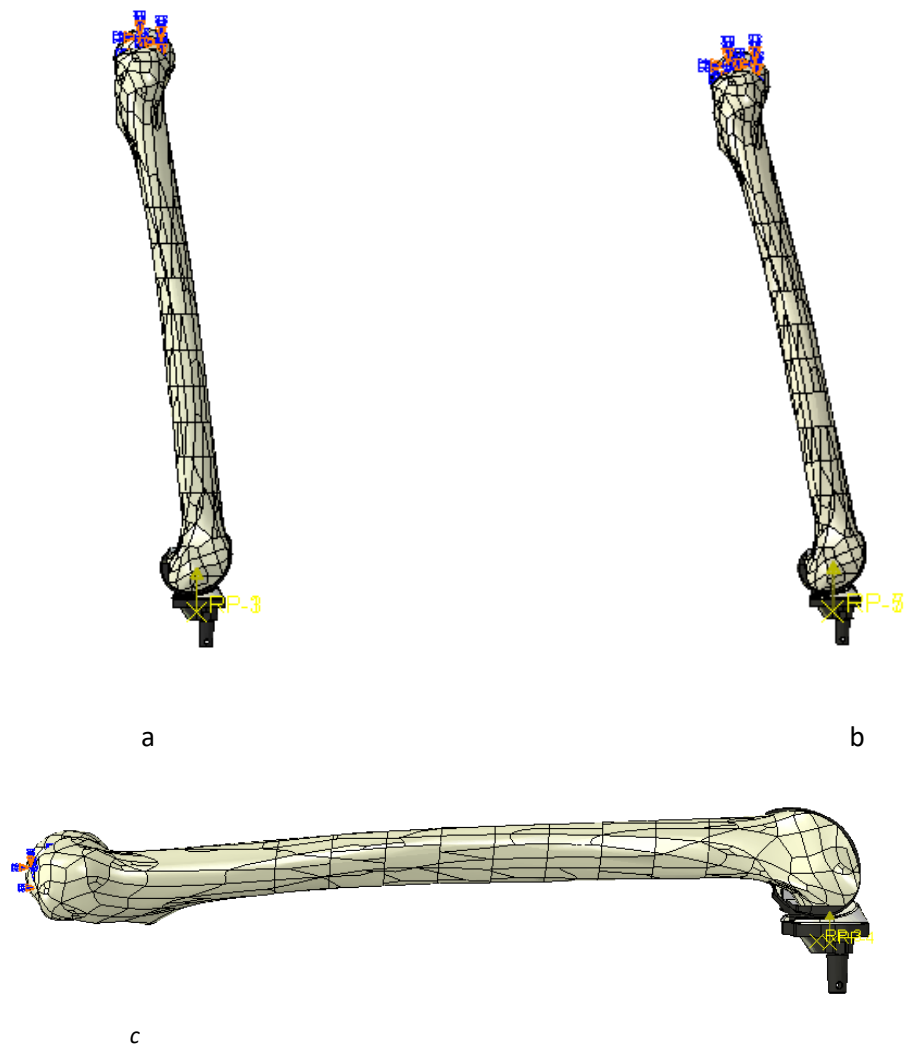


Figure 24, lateral view of femur bone at 0° (a), 5° (b) and 90°(c) of flexion.

## 3.6 Cementless models

### 3.6.1 First model

The first model was performed with cementless femoral stem with a length of 50 mm (fig. 23), the forces were applied in three configurations: in full extension 0°, 5° and 90° flexion.



Figure 25, cementless stem of 50 mm of length

### 3.6.2 Second model

The second model was performed with cementless femoral stem with a length of 120 mm (fig.25), the forces were applied in three configurations: in full extension 0°, 5° and 90° flexion.



*Figure 26, cementless stem of 120 mm of length*

### 3.6.3 Third model

The third model was performed with cementless femoral stem with a length of 160 mm (fig.26), the forces were applied in three configurations: in full extension 0°, 5° and 90° flexion.



*Figure 27, cementless stem of 160 mm of length*

## 3.7 Cemented Models

### 3.7.1 Fourth model

The fourth model was performed with cemented femoral stem with a length of 50 mm (fig.27); the forces were applied in three configurations: in full extension 0°, 5° and 90° flexion.



*Figure 28, cemented stem of 50 mm of length*

### 3.7.2 Fifth model

The fifth model was performed with cemented femoral stem with a length of 120 mm, the forces were applied in three configurations: in full extension 0°, 5° and 90° flexion.



*Figure 29, cemented stem of 120 mm of length*

### 3.7.3 Sixth model

The sixth model was performed with cemented femoral stem with a length of 160 mm, the forces were applied in three configurations: in full extension 0°, 5° and 90° flexion.



*Figure 30, cemented stem of 160 mm of length*

## 3.8 Osteoporotic configuration

Other three models were implemented for osteoporotic bone both with cementless stem with the same configurations seen above.

Finite Element Analysis was used in order to obtain the average von Mises stress and the maximum and average contact pressure and area both for polyethylene and bushing components.

### 3.9 Mesh

The mesh was defined using tetrahedral elements characterized by different elements size according to the region of interest. In detail, an approximate element size of 3 mm was used for each component and a refinement of mesh, with an approximate element size of 1 mm, was performed in the contact area of internal components of the implant, to make sure that the selected mesh did not influence the results. Finally, to check the quality of the mesh a convergence test was performed.

The geometry of the femur bone was more complex than other components, for this reason a virtual topology was done to improve some geometries, as a result more uniform mesh. The mesh size of the bone was chosen based on two factors results and time. Therefore, a compromise between small size and big size was necessary in order to achieve more reliable results in the shortest possible time. Consequently, a mesh with an approximate element size of 3 mm was chosen in the distal part of the femur in contact with metal components, while the proximal part of the bone was performed with an approximate element size of 12 mm.

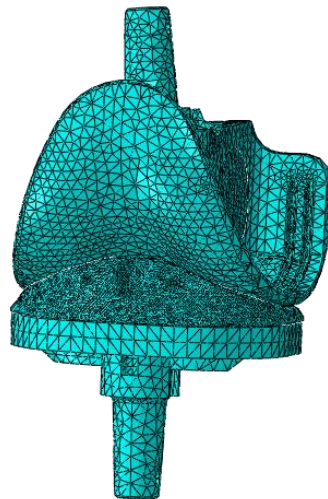


*Figure 31, overview of meshed prosthesis*

## 4. Results

### 4.1 Part I

Fig. 32 reports a graphical overview of the average von Mises stress on polyethylene insert with cementless stem of 50 mm of length. Each row represents Valgus and Varus alignment, while the columns indicate positioning of the knee in three different configurations. In particular, the knee full extended at 0° and flexed at 5° and 90°. While, fig. 33 reports the contact pressure and area. Finally, fig. 34 reports the trend of contact force in tibiofemoral compartment. It is shown the percentage of force in medial and lateral compartment as a function of Varus and Valgus alignment.

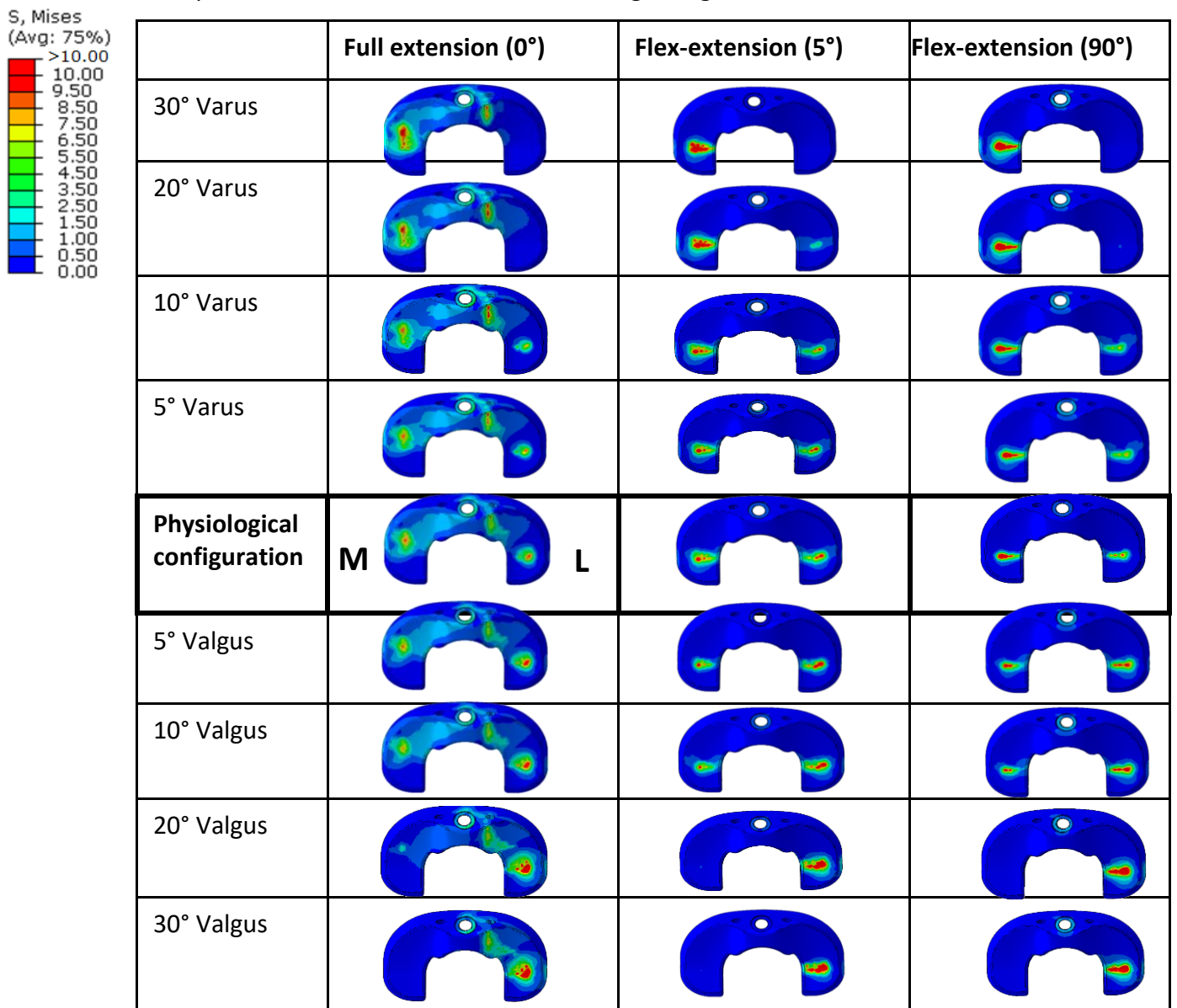


Figure 32, average von Mises stress on polyethylene component. Each row represents a Varus/valgus configuration, while the columns indicate each flexo-extension configuration.

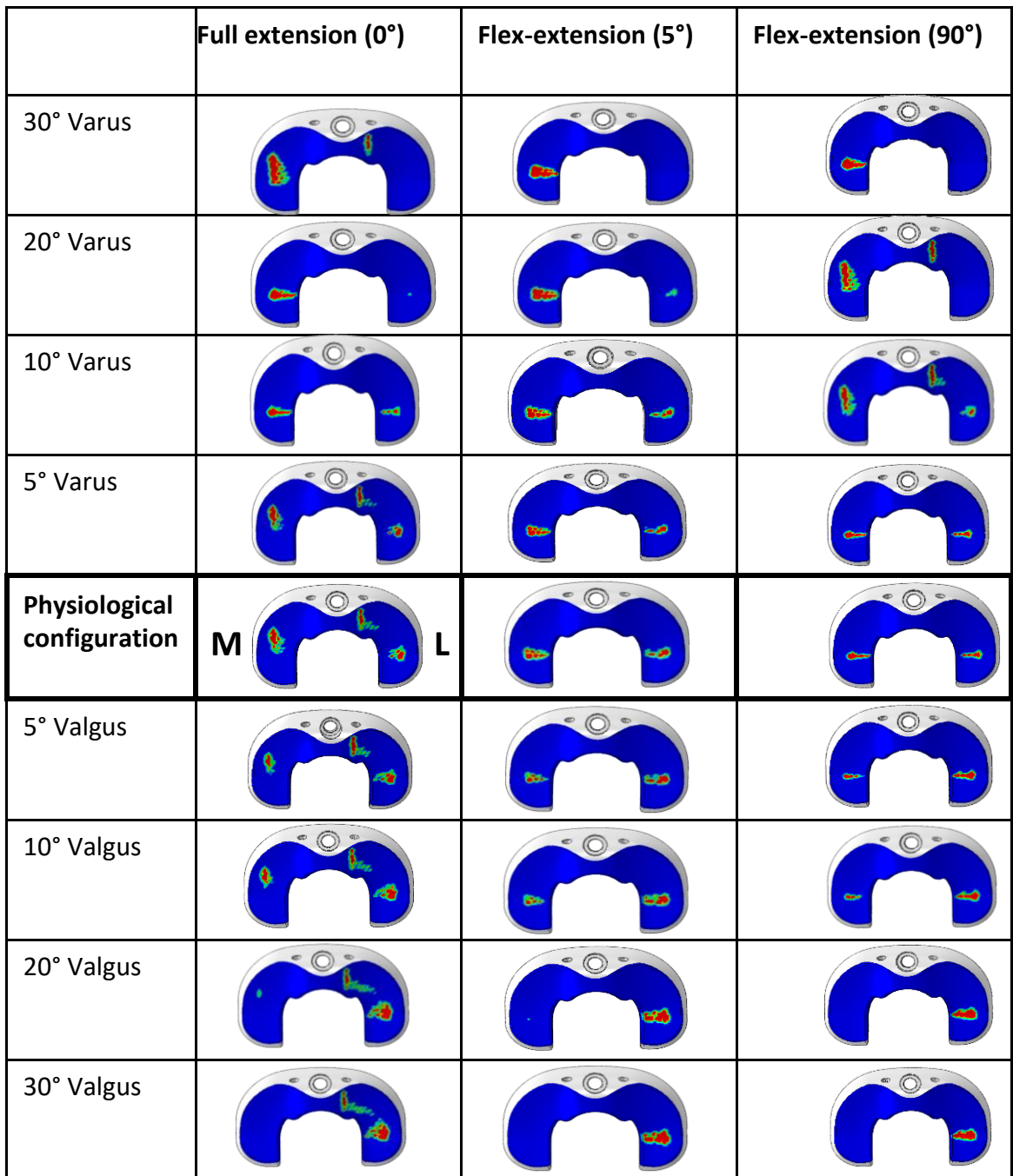
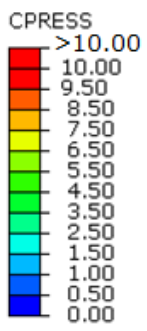


Figure 33, graphical overview of the contact pressure for each configuration.

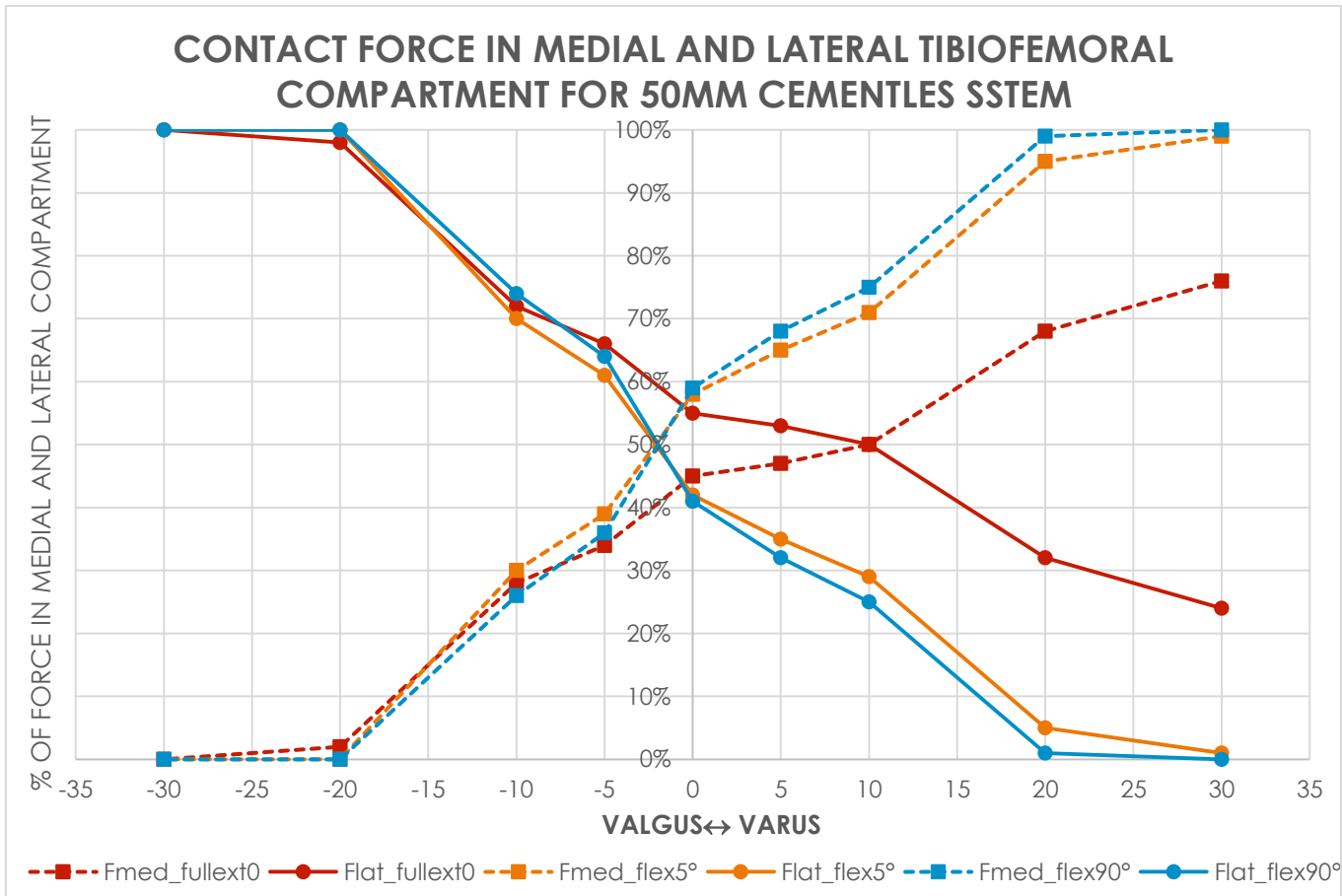


Figure 34, Trend of force in medial and lateral tibiofemoral compartment for Valgus and Varus deformity

Fig. 32 shows a change in stress for Varus and Valgus configurations in the tibial insert compared to the physiological configuration. It is possible to state that the stress at the medial region on polyethylene increases with Varus alignment. While, shifting the alignment from Varus to Valgus configurations leads to an increase of stress in the lateral side. Moreover, considering the first configuration with the knee fully extended at 0°, the distribution of the stress focus is in the anterior and central region of the polyethylene insert. While, the stress moves to the posterior region of the tibial insert with flexion of the knee at 5° and 90°.

Fig. 33 reports the graphical overview of contact pressure and area. Again, shifting from Varus to Valgus configurations induces an increase of contact area respectively in the medial and lateral region. It is important to note that for 30° of Varus and Valgus there is no stress on the polyethylene component.

To better understand the behaviour of the contact force on tibial insert, fig. 34 reports the percentage of force in medial and lateral tibiofemoral compartment as function of Valgus and Varus configurations. Red, orange and blue lines indicate the forces on polyethylene insert at 0°, 5° and 90° of flexion, respectively. The dashed lines represent forces on medial insert; accordingly, the solid lines indicate forces on lateral region. As expected, an increase of Varus alignment cause an increase of stress in medial region and a reduction of stress in lateral region. While, a rise of Valgus malalignment lead to an increment of stress in lateral side and a drop of stress in medial part. This trend of the force is similar for all configurations (0°, 5° and 90°).

Similarly, fig. 35 and fig. 36, report results in terms of von Mises stress and contact pressure for plastic bushing component.

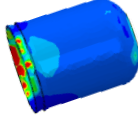
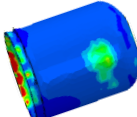
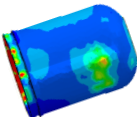
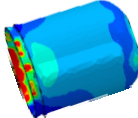
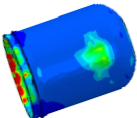
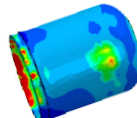
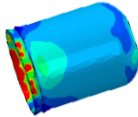
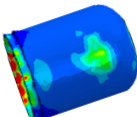
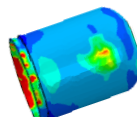
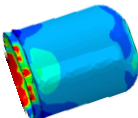
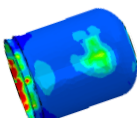
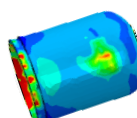
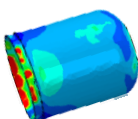
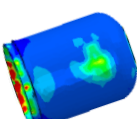
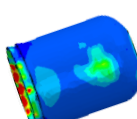
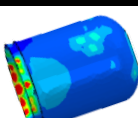
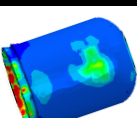
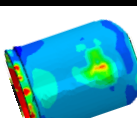
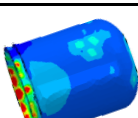
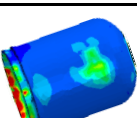
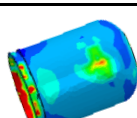
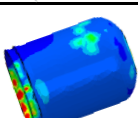
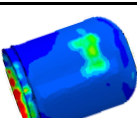
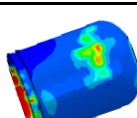
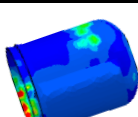
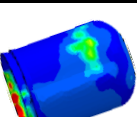
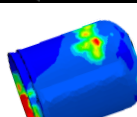
	Full extension (0°)	Flex-extension (5°)	Flex-extension (90°)
30° Varus			
20° Varus			
10° Varus			
5° Varus			
<b>Physiological configuration</b>			
5° Valgus			
10° Valgus			
20° Valgus			
30° Valgus			

Figure 35, average von Mises stress on plastic bushing. Each row represents a Varus/valgus configuration, while the columns indicate each flexo-extension configuration.

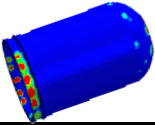
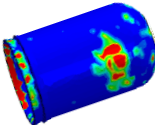
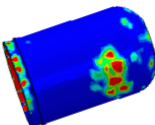
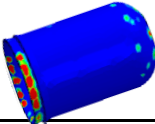
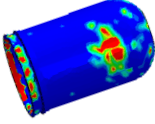
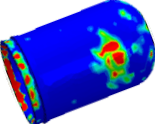
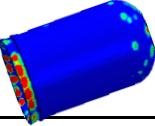
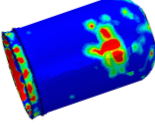
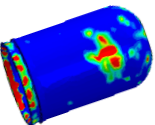
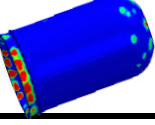
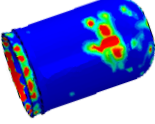
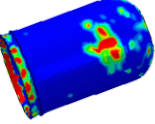
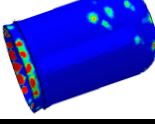
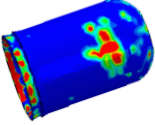
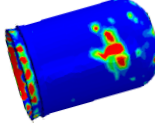
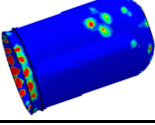
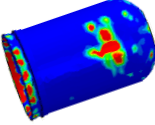
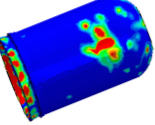
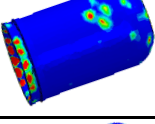
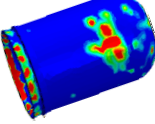
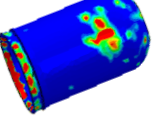
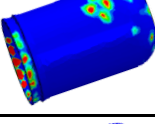
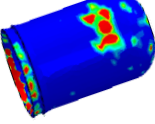
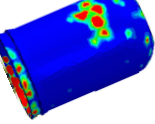
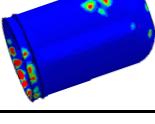
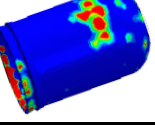
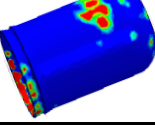
	Full extension (0°)	Flex-extension (5°)	Flex-extension (90°)
30° Varus			
20° Varus			
10° Varus			
5° Varus			
<b>Physiological configuration</b>			
5° Valgus			
10° Valgus			
20° Valgus			
30° Valgus			

Figure 36, graphical overview of the contact pressure for each configuration.

As before, it is noted that there is a shifting of contact pressure and area. In particular, at 5° and 90° of flexion the region of contact area shifts internal compared to physiological configuration.

Fig.37 and fig. 38 report the graphical overview of von Mises stress and contact pressure on polyethylene component, with 120 mm of cementless stem, for each Valgus and Varus configurations, with the knee full extended 0° and flexed at 5° and 90.

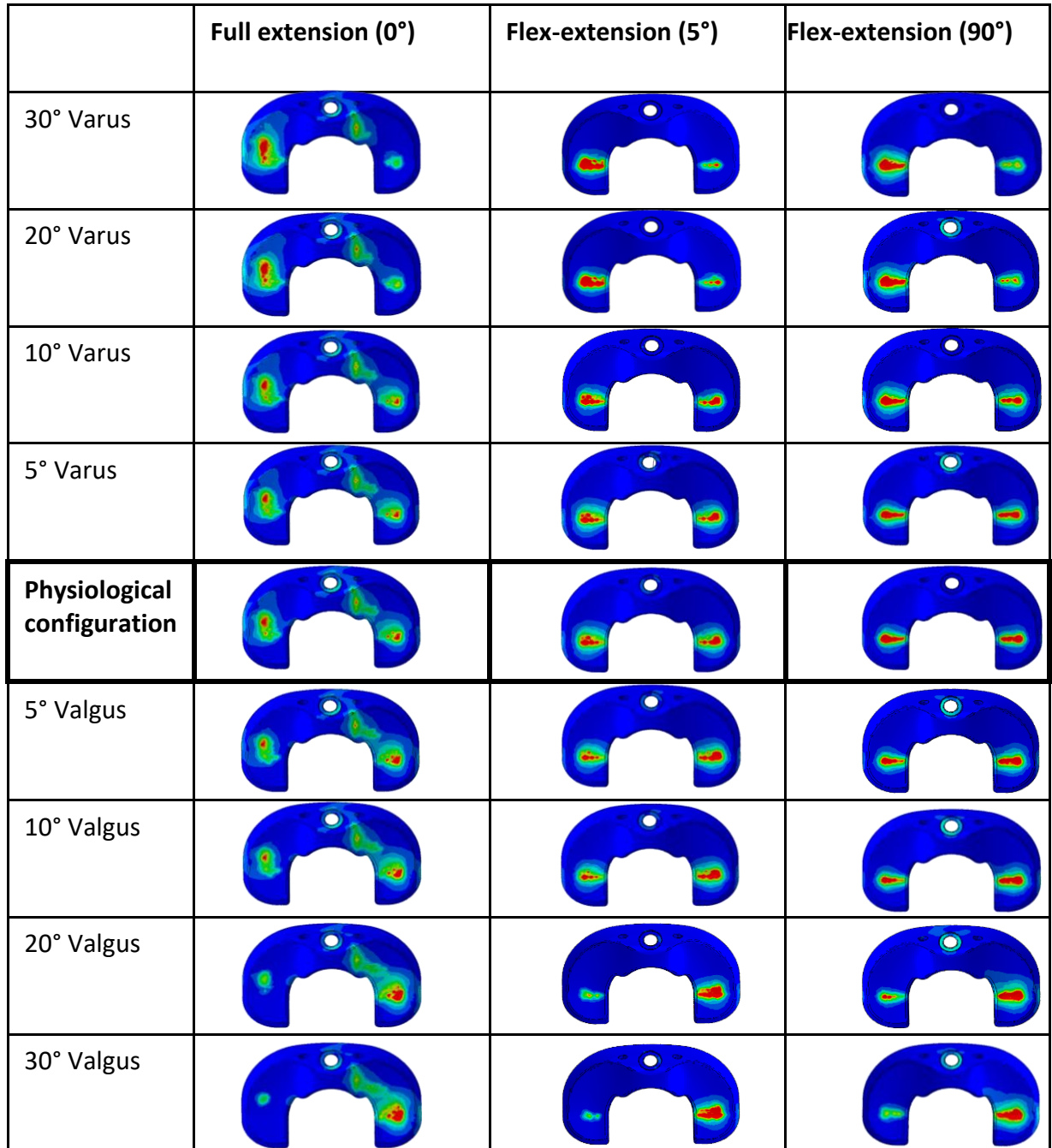


Figure 37, average von Mises stress on polyethylene component. Each row represents a Varus/valgus configuration, while the columns indicate each flexo-extension configuration

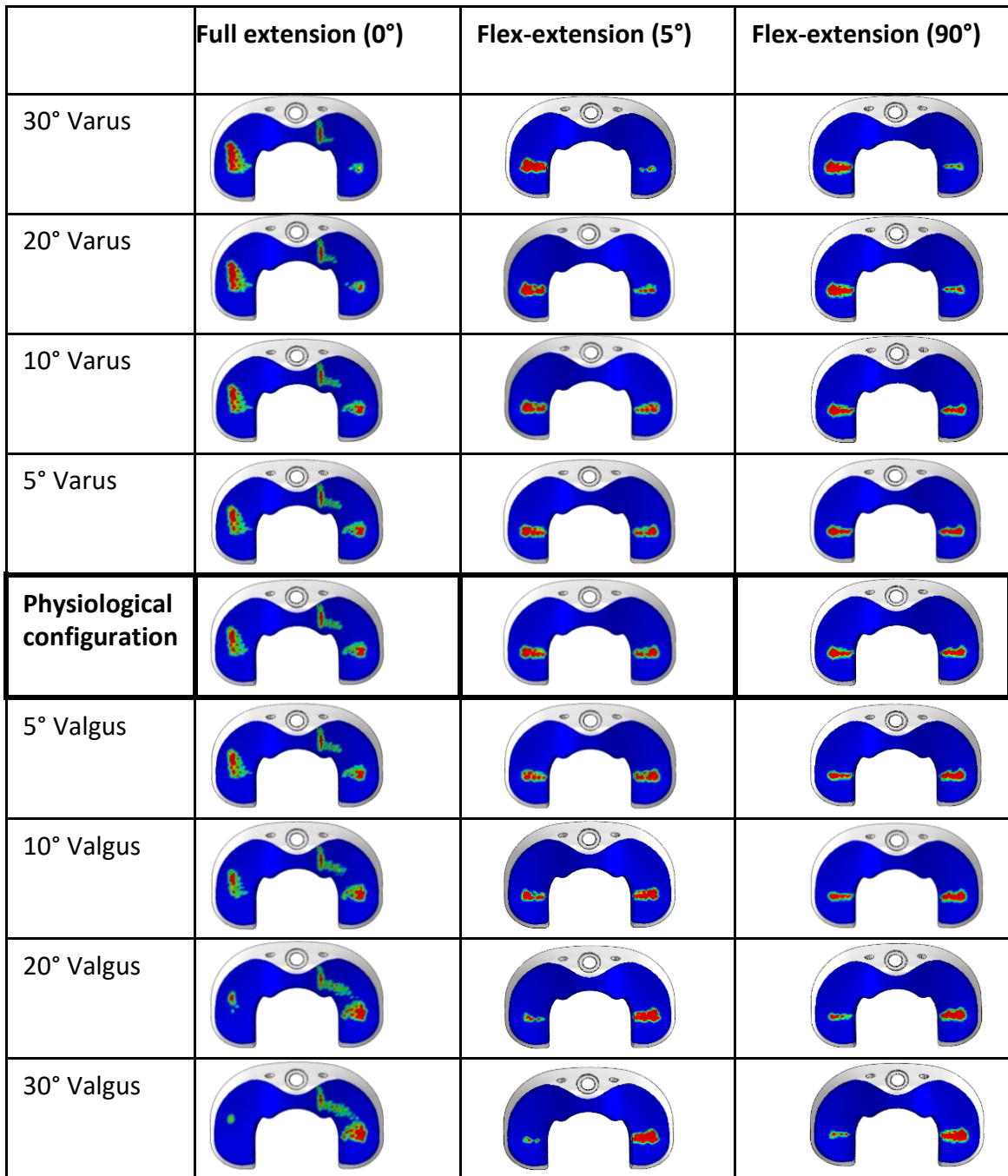


Figure 38, graphical overview of the contact pressure for each configuration

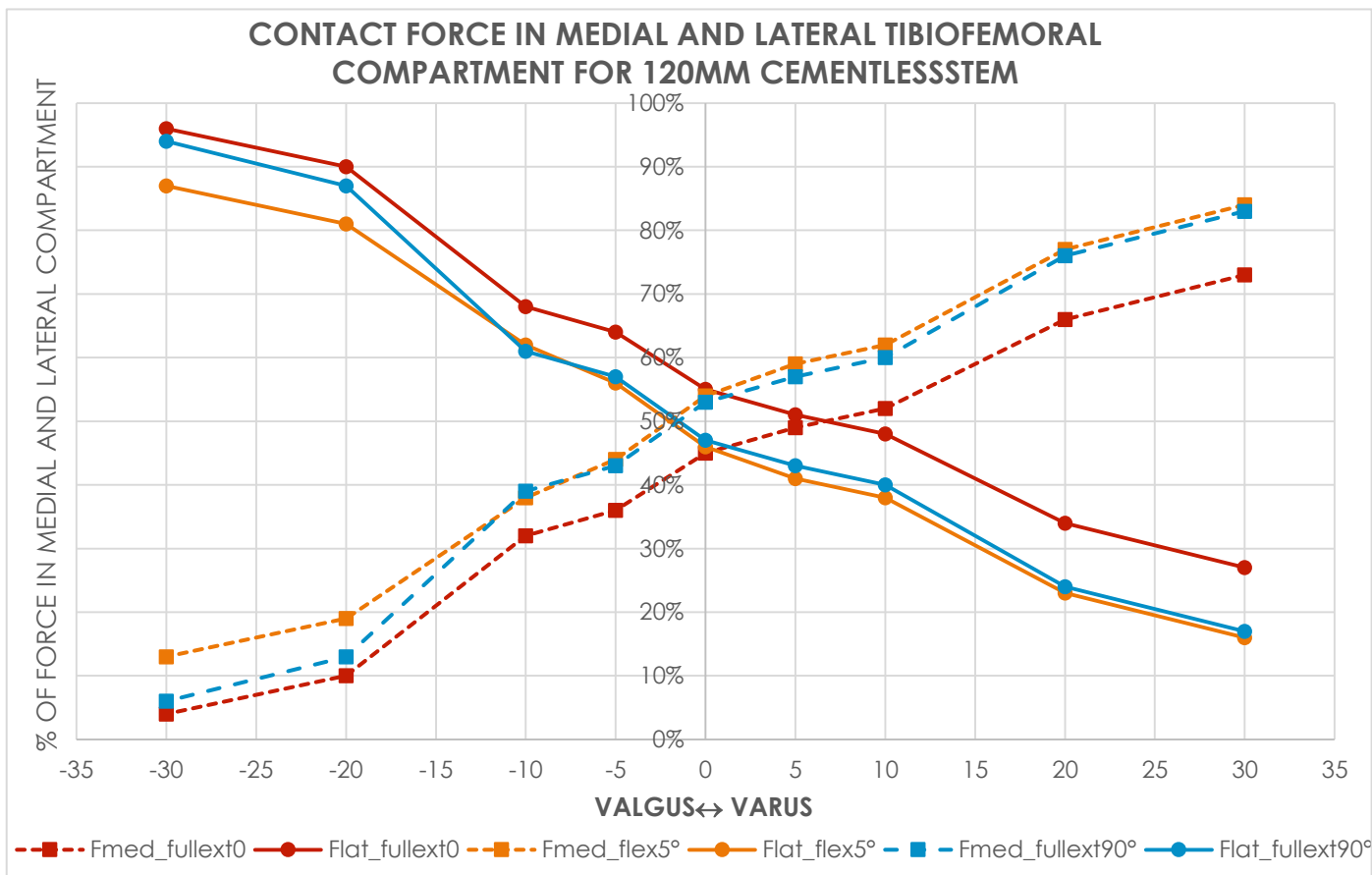


Figure 39, Trend of force in medial and lateral tibiofemoral compartment for Valgus and Varus deformity

Again, Fig. 37 shows a change in stress for Varus and Valgus configurations in the tibial insert compared to the physiological configuration. It is possible to state that the stress at the medial region on polyethylene increases with Varus alignment. On the other hand, shifting the alignment from Varus to Valgus configurations lead to increase of stress in lateral side. Moreover, considering the first configuration with the knee full extended at 0°, the distribution of the stress focus is in the anterior and central region of the polyethylene insert. While, it is possible to note a shifting of stress in the posterior region of tibial insert with configurations at 5° and 90° of flexion.

Fig. 38 reports the graphical overview of contact pressure and area. Again, shifting from Varus to Valgus configurations induce an increase of contact area respectively in medial and lateral region. It is important to note that, respect to the previously model, there is a better distribution of stress on medial and lateral side of polyethylene component at 30° of Varus and Valgus alignment.

To better understand the behaviour of the contact force on tibial insert, fig. 39 reports the percentage of force in medial and lateral tibiofemoral compartment as function of Valgus and Varus configurations. As expected, an increase of Varus alignment causes an increase of stress in medial region and a reduction of stress in lateral region. While, a rise of Valgus malalignment lead to an increment of stress in lateral side and a drop of stress in medial part. Moreover, von Mises stress and contact pressure on plastic bushing are shown in fig. 40 and fig. 41, considering the same configuration.

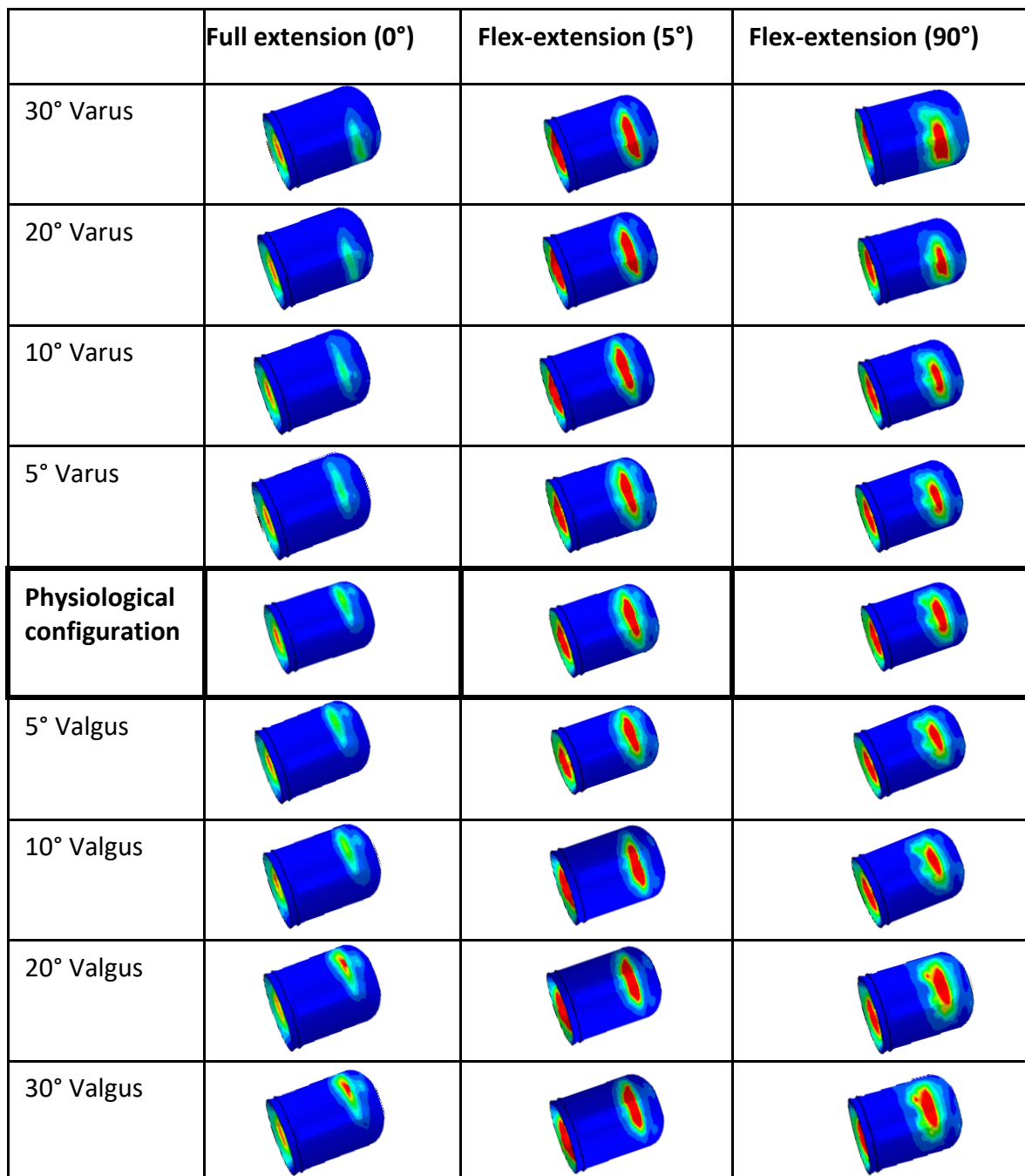


Figure 40, average von Mises stress on plastic bushing. Each row represents a Varus/valgus configuration, while the columns indicate each flexo-extension configuration.

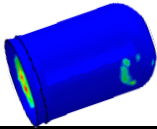
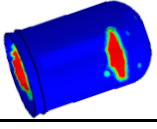
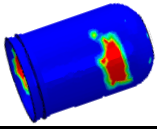
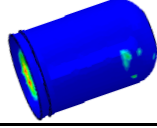
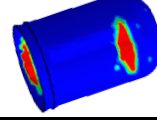
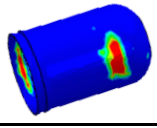
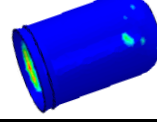
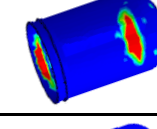
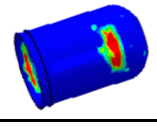
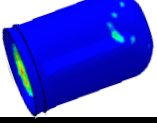
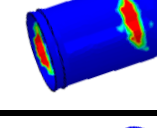
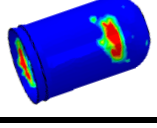
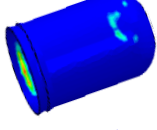
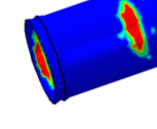
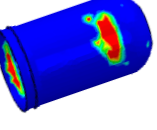
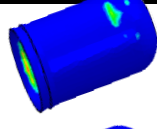
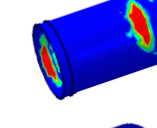
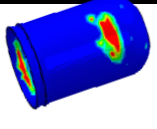
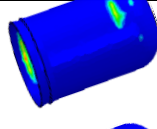
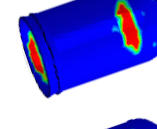
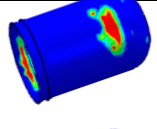
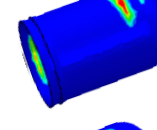
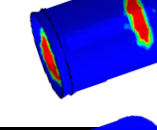
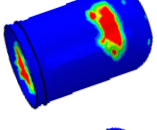
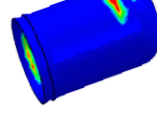
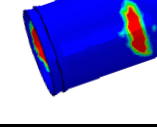
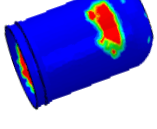
	Full extension (0°)	Flex-extension (5°)	Flex-extension (90°)
30° Varus			
20° Varus			
10° Varus			
5° Varus			
<b>Physiological configuration</b>			
5° Valgus			
10° Valgus			
20° Valgus			
30° Valgus			

Figure 41, graphical overview of the contact pressure for each configuration.

The distribution of von Mises stress and contact pressure on bushing component is more uniform than the previously model. In fact, the stress is focused on the central region of the plastic element. In particular, at 0° of flexion, the contact area shifts internal to the component compared to the physiological configuration. Instead, it is possible to note a wider and mainly constant contact area at 5° and 90° of flexion. The results of von Mises stress and contact pressure on tibiofemoral component for cementless femoral stem with a length of 160 mm are illustrate in fig. 42 and fig. 43. While, the trend of contact force is reported in fig. 44.

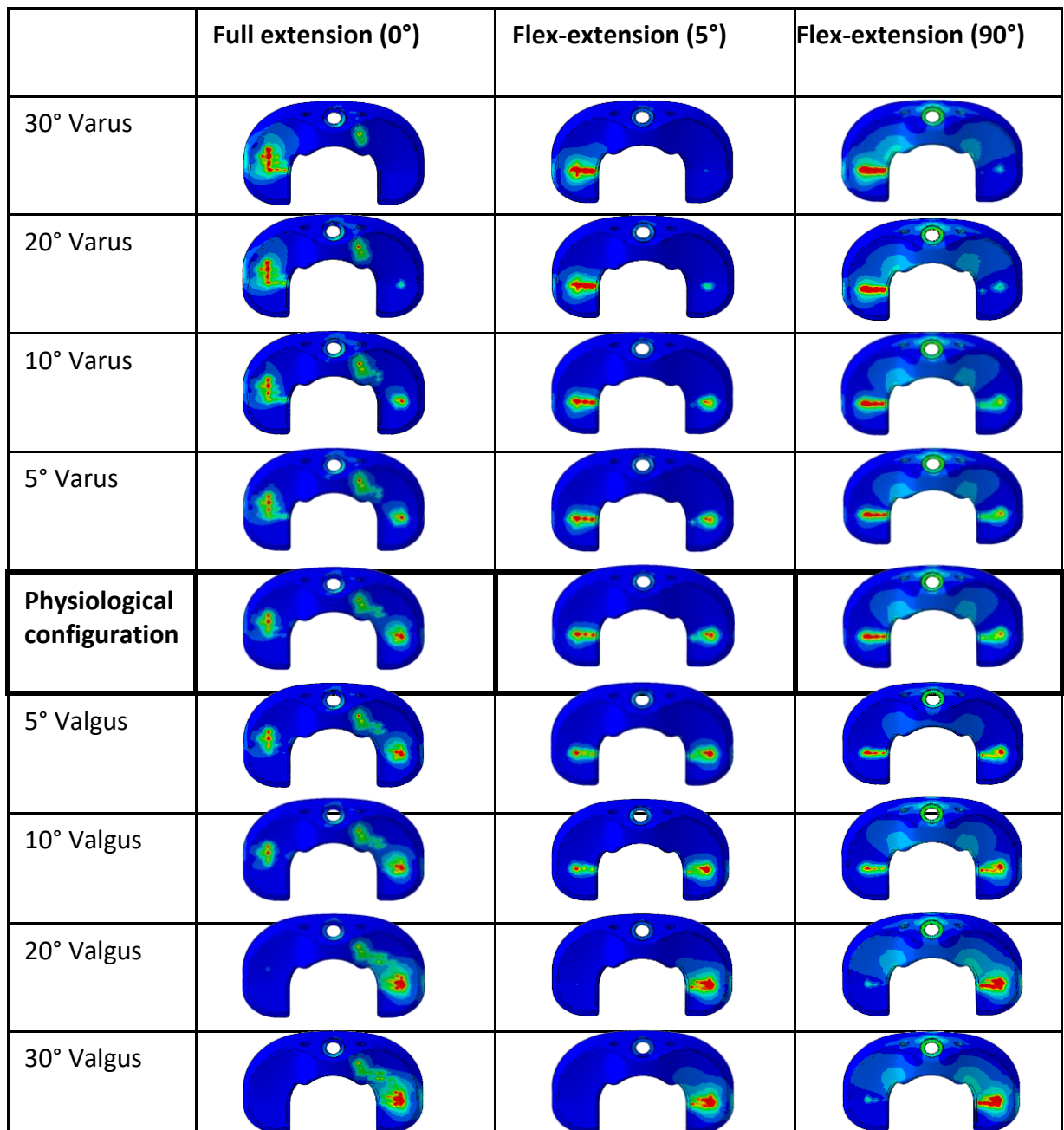


Figure 42, average von Mises stress on polyethylene component. Each row represents a Varus/valgus configuration, while the columns indicate each flexo-extension configuration

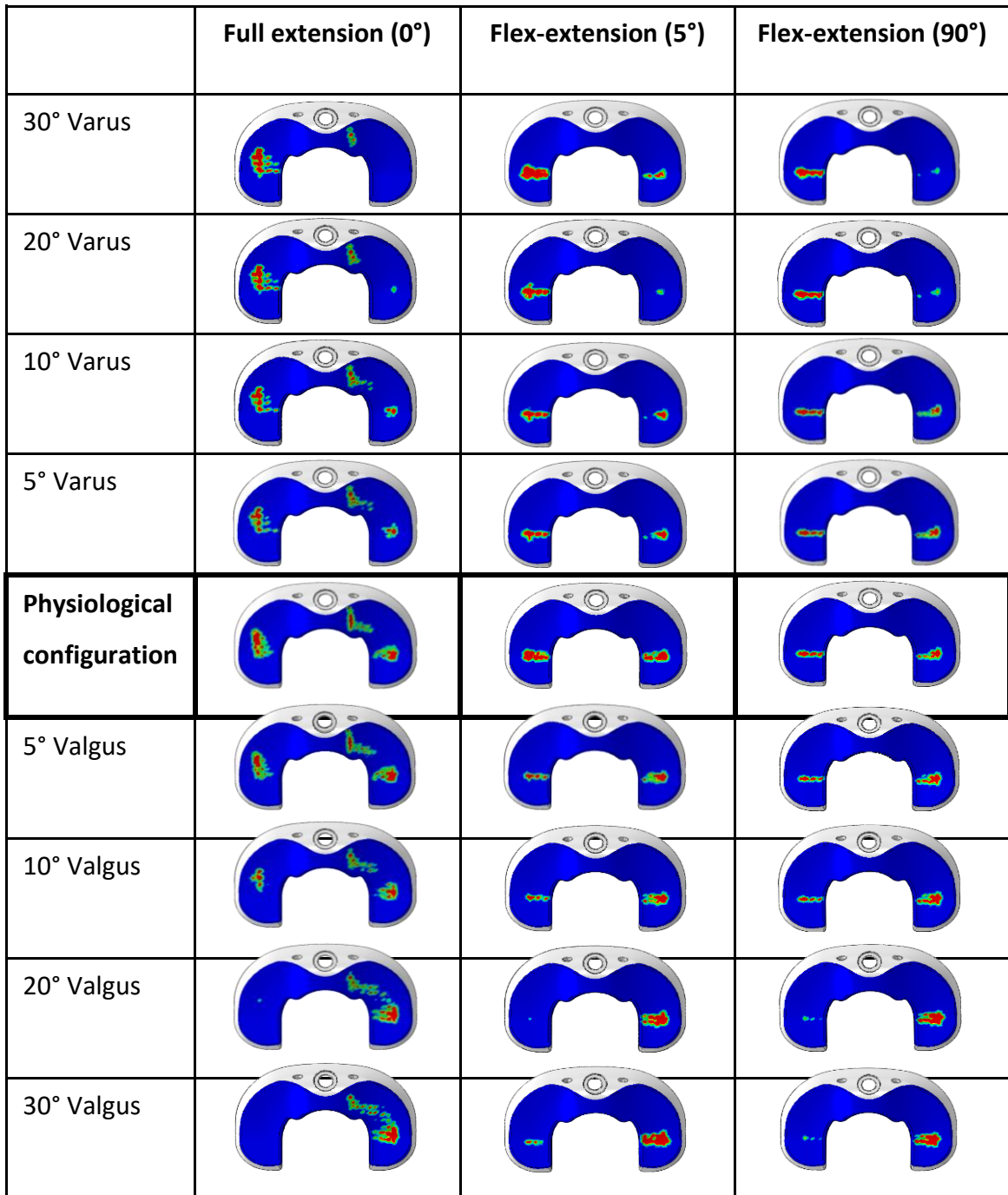


Figure 43, graphical overview of the contact pressure for each configuration

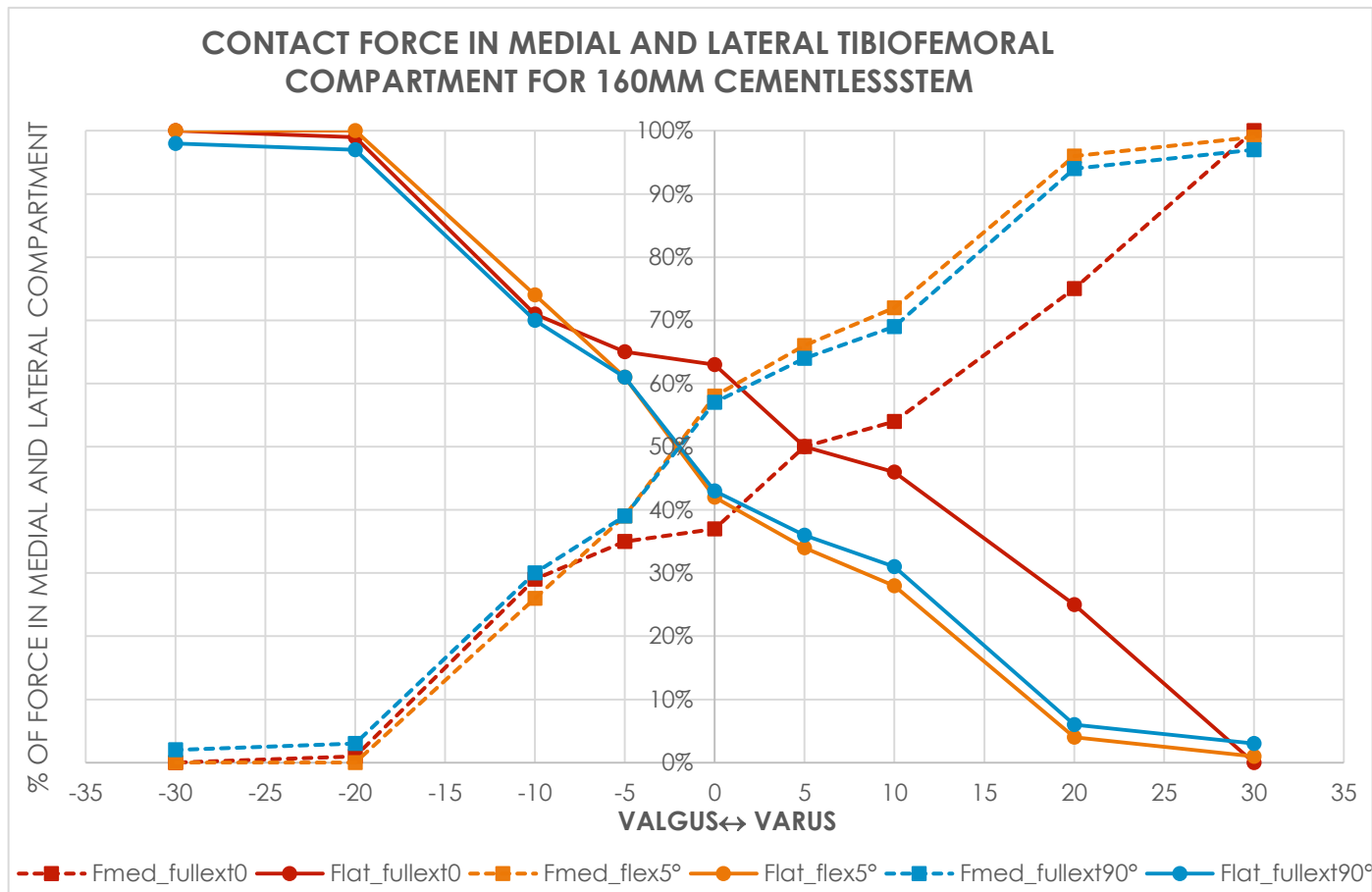


Figure 44, Trend of force in medial and lateral tibiofemoral compartment for Valgus and Varus deformity

As report for previously models, Fig. 42 shows a change in stress for Varus and Valgus configurations in in the tibial insert compared to the physiological configuration. The stress at the medial region on polyethylene increases with Varus alignment. While, shifting the alignment from Varus to Valgus configurations lead to increase of stress in lateral side. Again, considering the first configuration with the knee full extended at 0°, the distribution of the stress focus is in the anterior and central region of the polyethylene insert. While, regarding the flexion of the knee at 5° and 90°, it is possible to note a shifting of stress in the posterior region of tibial insert.

Fig. 43 reports the graphical overview of contact pressure and area. As before, shifting from Varus to valgus configurations induce an increase of contact area respectively in medial and lateral region. It is important to note that, the behaviour of contact force and pressure on polyethylene component is similar to the first model with short stem.

To better understand the behaviour of the contact force on tibial insert, fig. 44 reports the percentage of force in medial and lateral tibiofemoral compartment as function of Valgus and Varus configurations. As expected, an increase of Varus alignment cause an increase of stress in medial region and a reduction of stress in lateral region. While, a rise of valgus malalignment led to an increment of stress in lateral side and a drop of stress in medial part. Moreover, von Mises stress and contact pressure on plastic bushing are shown in fig. 45 and fig. 46, considering the same configuration.

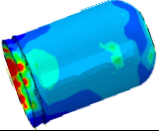
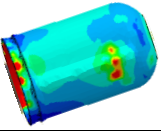
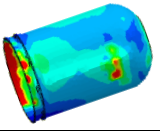
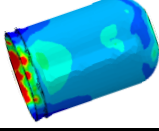
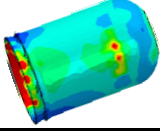
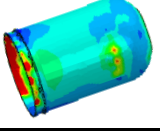
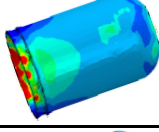
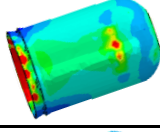
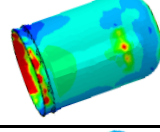
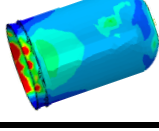
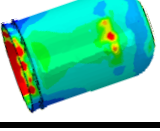
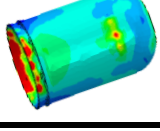
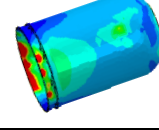
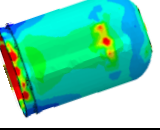
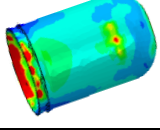
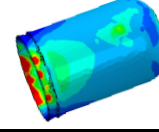
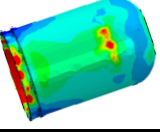
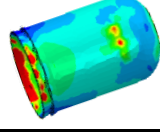
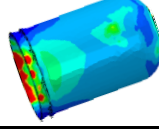
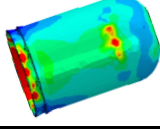
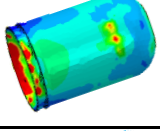
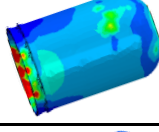
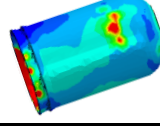
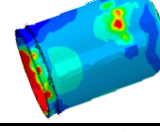
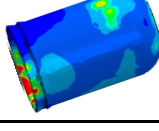
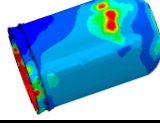
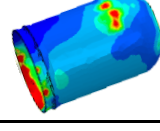
	Full extension (0°)	Flex-extension (5°)	Flex-extension (90°)
30° Varus			
20° Varus			
10° Varus			
5° Varus			
<b>Physiological configuration</b>			
5° Valgus			
10° Valgus			
20° Valgus			
30° Valgus			

Figure 45, average von Mises stress on plastic bushing. Each row represents a Varus/valgus configuration, while the columns indicate each flexo-extension configuration.

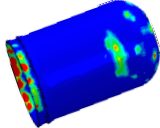
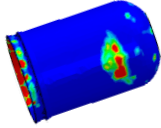
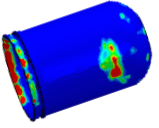
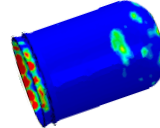
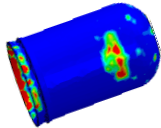
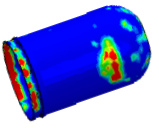
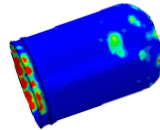
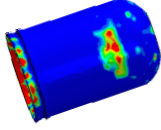
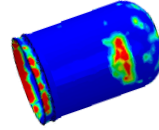
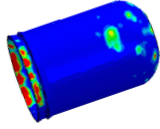
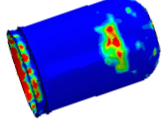
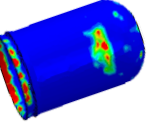
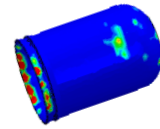
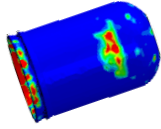
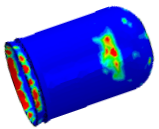
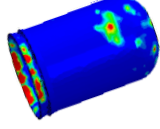
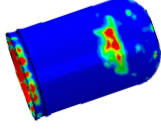
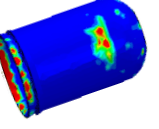
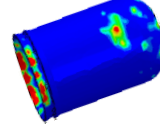
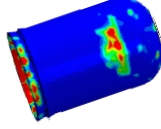
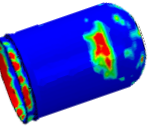
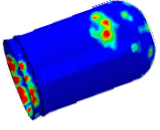
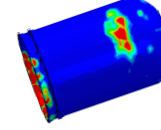
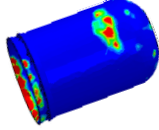
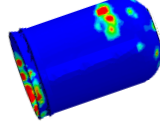
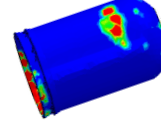
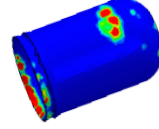
	Full extension (0°)	Flex-extension (5°)	Flex-extension (90°)
30° Varus			
20° Varus			
10° Varus			
5° Varus			
<b>Physiological configuration</b>			
5° Valgus			
10° Valgus			
20° Valgus			
30° Valgus			

Figure 46, graphical overview of the contact pressure for each configuration.

Fig 47, 48 and 49 report a comparison of contact force in medial and lateral tibiofemoral compartment both for 50, 120 and 160 mm cementless stem in terms of percentage as a function of Varus and Valgus alignment for all configurations (0°, 5° and 90°).

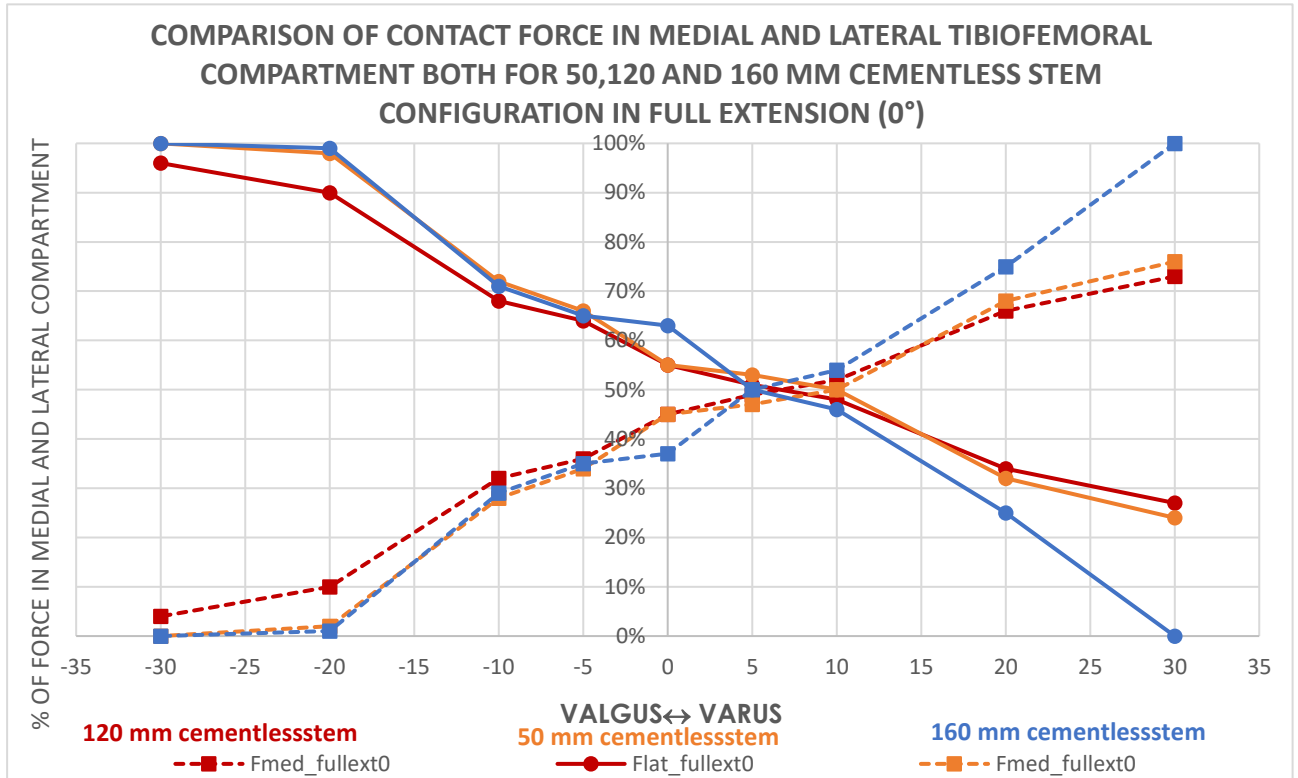


Figure 48, Trend of force in medial and lateral tibiofemoral compartment for Valgus and Varus deformity at 0° of flexion

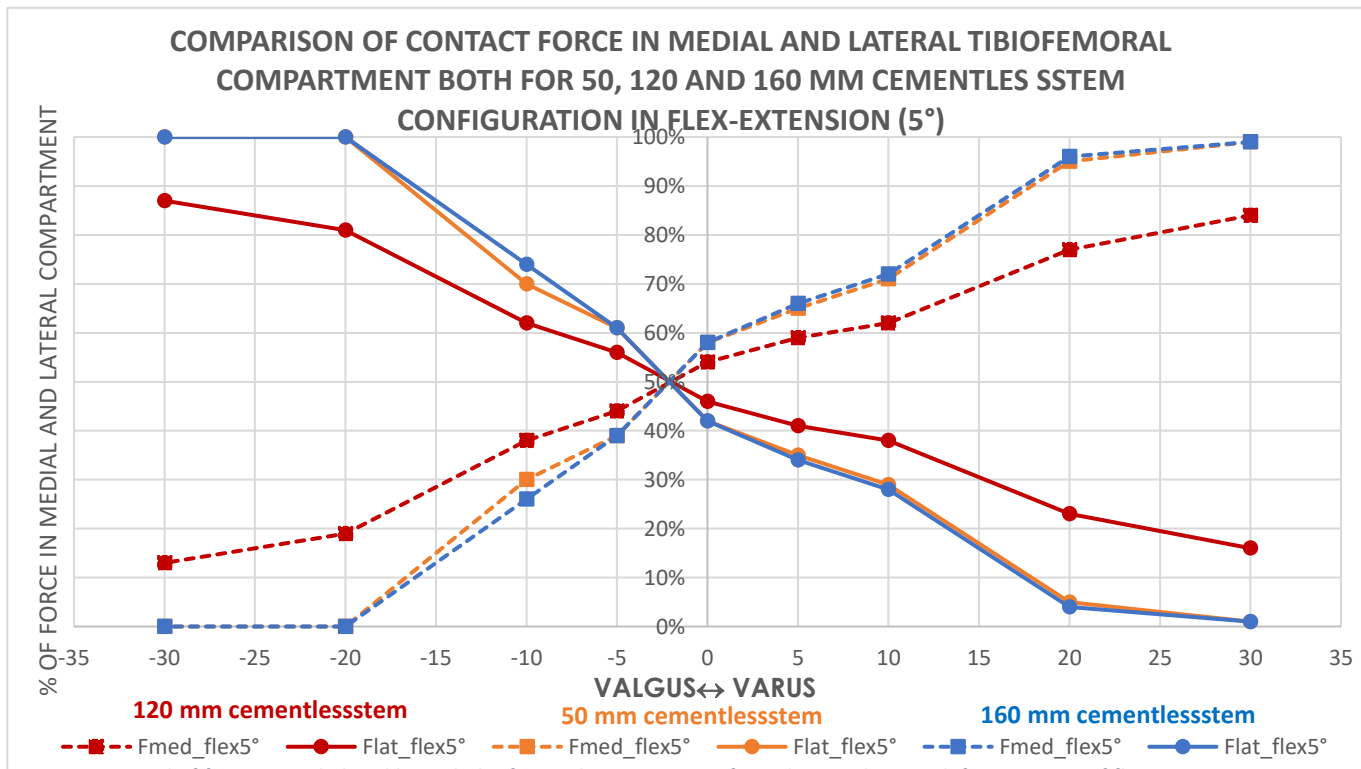


Figure 47, Trend of force in medial and lateral tibiofemoral compartment for Valgus and Varus deformity at 5° of flexion

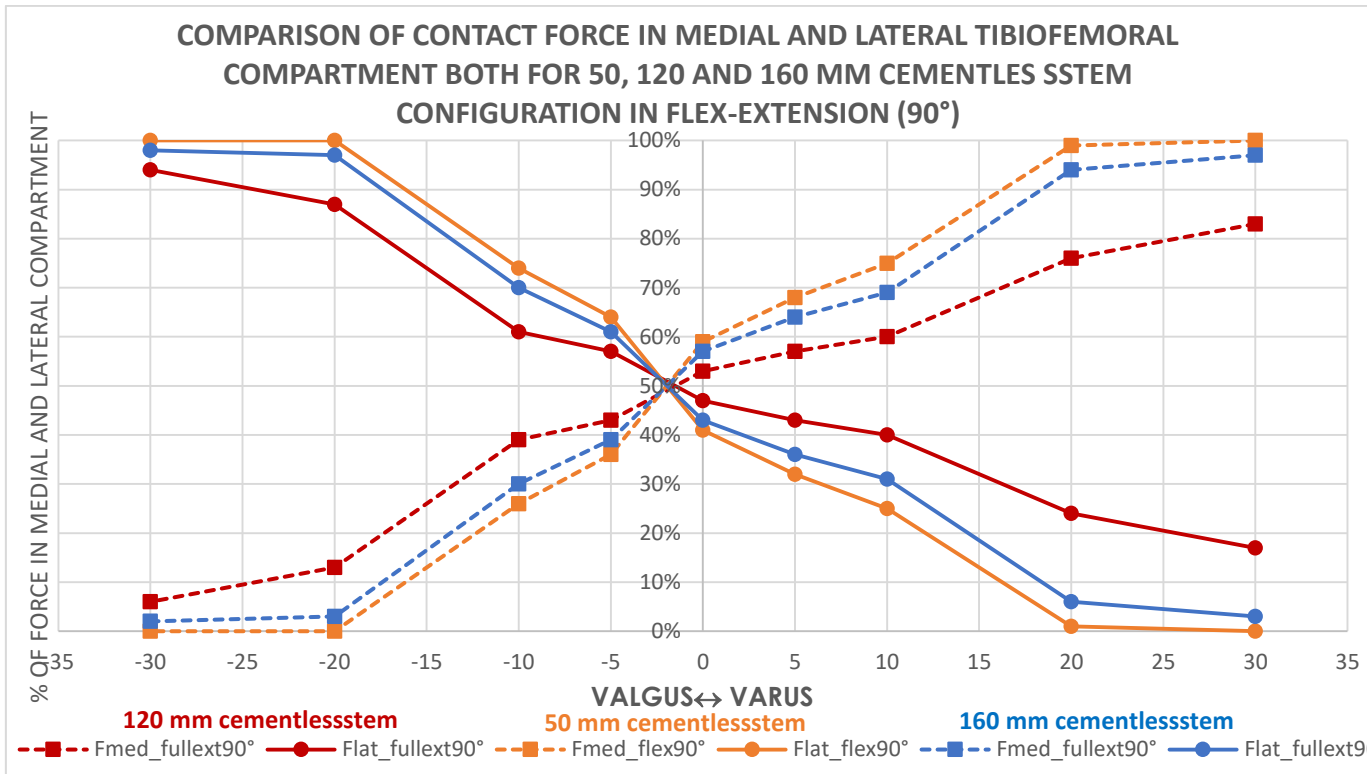


Figure 49, Trend of force in medial and lateral tibiofemoral compartment for Valgus and Varus deformity at 90° of flexion

To better understand the difference between 50, 120 and 160 mm cementless stems, Fig. 47, 48 and 49 report a comparison of contact force in medial and lateral tibiofemoral compartment at 0°, 5° and 90° for 50, 120 and 160 mm cementless stems. Red lines indicate the trend of force for 120 mm cementless stem, orange lines represent the percentage of force for cementless stem of 50 mm of length and blue lines indicates the trend of contact force with the model using 160 mm cementless stem.

It is possible to note that the model with 120 mm cementless stem has a quite linear trend at 5° of flexion. While, the other two models follow a similar trend.

To better understand results of contact force, the quantitative results about contact pressure are shown below. Fig 50, 51 and 52 report histograms of maximum contact pressure (MPa), for medial and lateral contact area on polyethylene component, as function of 5°, 10°, 20° and 30° of Varus and Valgus alignments for each configuration and for all models. While, fig 53 reports histograms of average contact pressure on polyethylene component for all configurations.

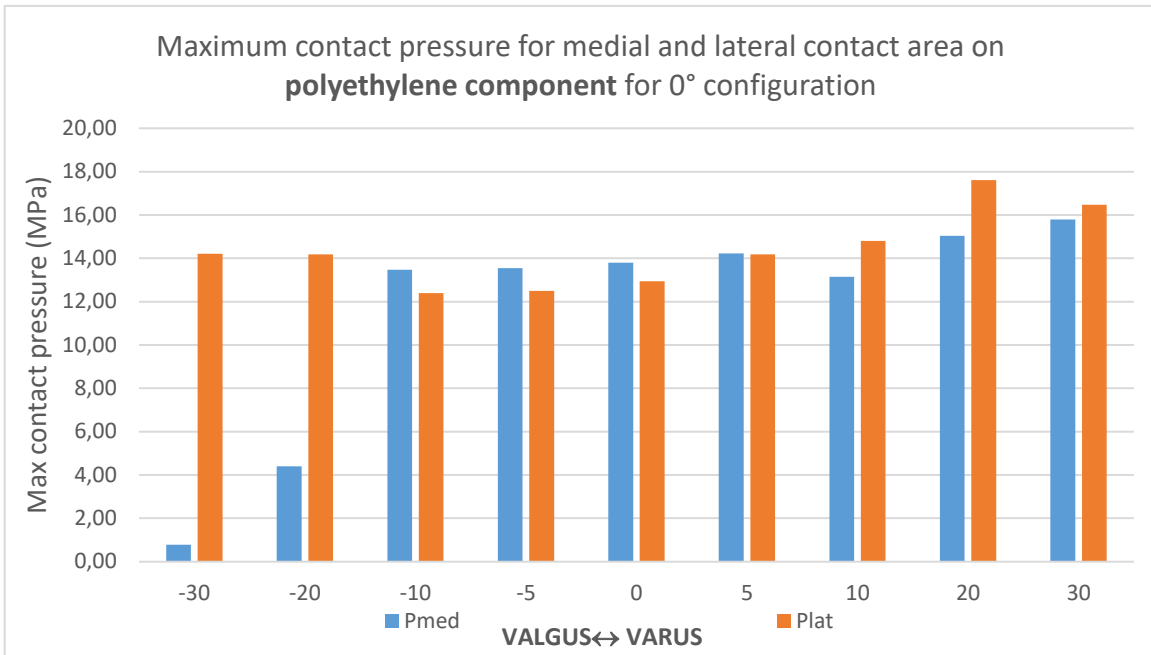


Figure 51, Maximum contact pressure for medial and lateral contact area on polyethylene component for 0° configuration with the cementless stem of 50 mm.

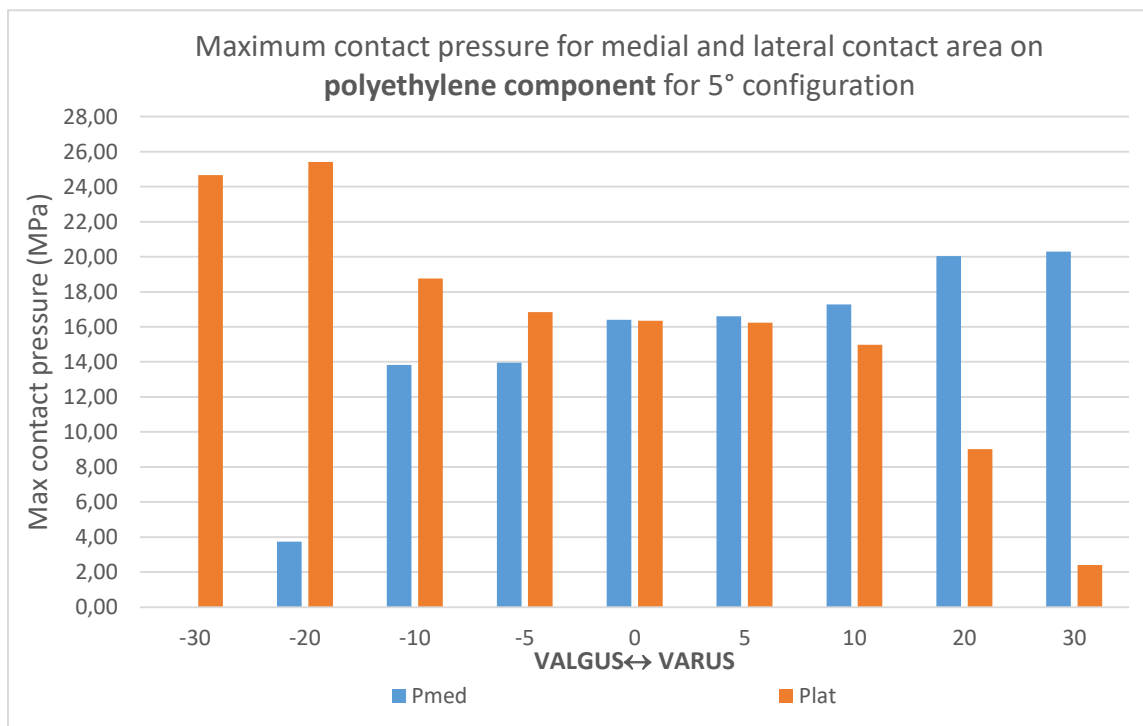


Figure 50, Maximum contact pressure for medial and lateral contact area on polyethylene component for 5° configuration with the cementless stem of 50 mm

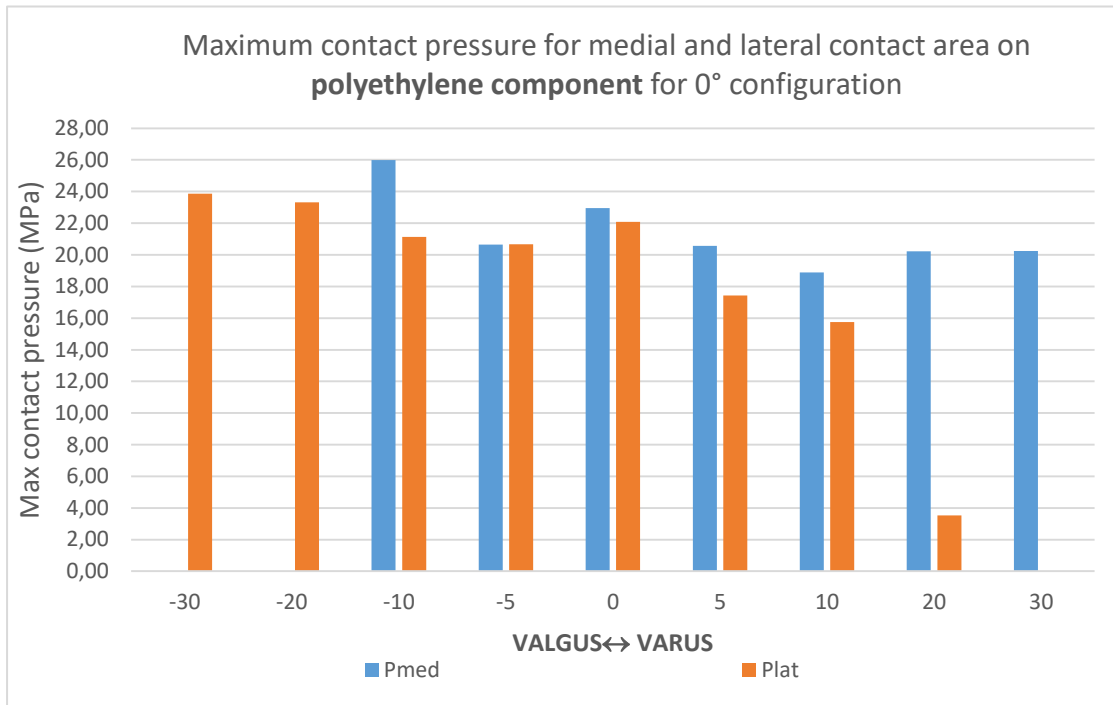


Figure 53, Maximum contact pressure for medial and lateral contact area on polyethylene component for 90° configuration with the cementless stem of 50 mm

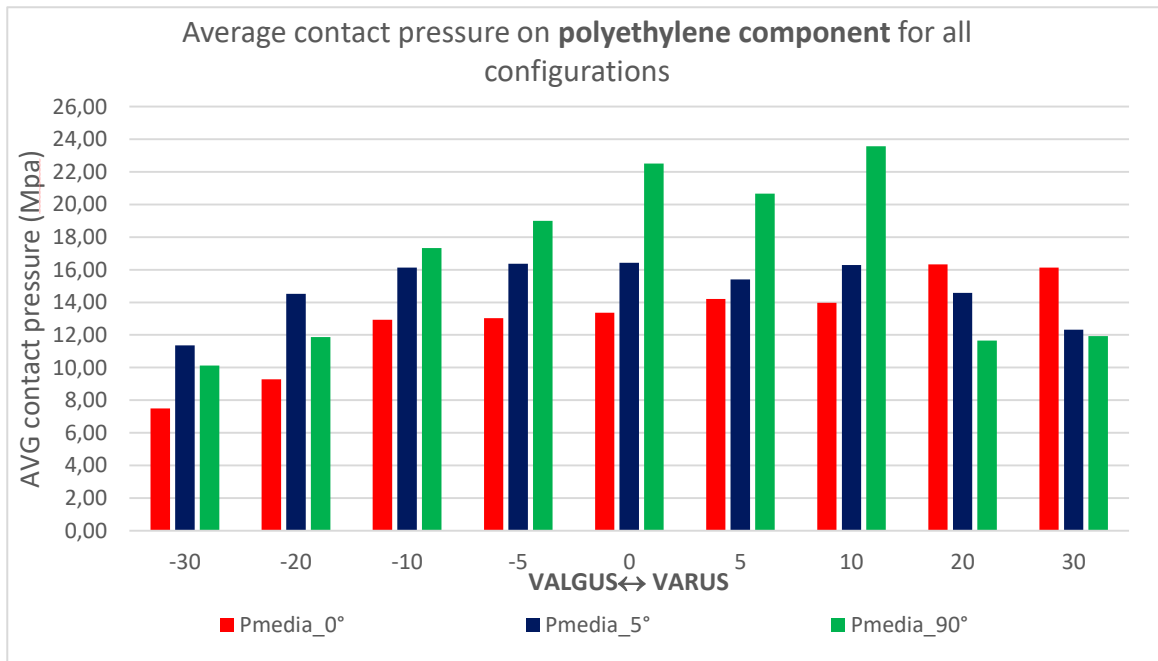


Figure 52, Average contact pressure on polyethylene component for all configurations with the cementless stem of 50 mm for 0°, 5° and 90° of flexion.

The values of contact pressure in medial and lateral area of polyethylene are indicated by colours, with orange the pressure in lateral side and light blue the pressure in medial region. According to qualitative results, Fig 50, 51 and 52 confirm that maximum values of pressure are mainly located on the medial side for Varus configurations. While, contact pressure increases in lateral side with Valgus configurations. This state is evident at 5° and 90° of flexion. Moreover, contact pressure increases with flexion achieving values in a range between 0 and 26 MPa. The results about the average contact pressure are shown in Fig.53. Red, dark blue and green bar diagrams indicate the values of average contact pressure on polyethylene for 0°, 5° and 90° respectively.

Similarly, fig. 54, 55, 56 and 57 report quantitative results in term of maximum and average contact pressure in the internal and external contact area of plastic bushing component with cementless stem of 50 mm. black and grey bar diagrams indicate the values of contact pressure in external and internal area.

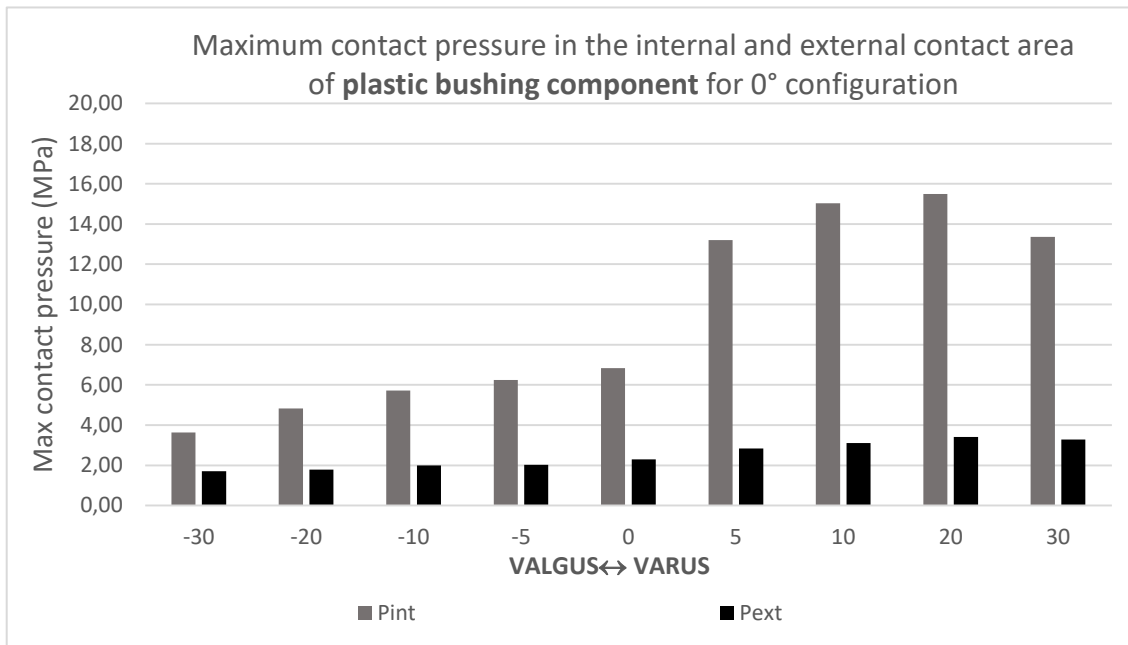


Figure 54, Maximum contact pressure in the internal and external contact area of plastic bushing component for 0° configuration with cementless stem of 50 mm

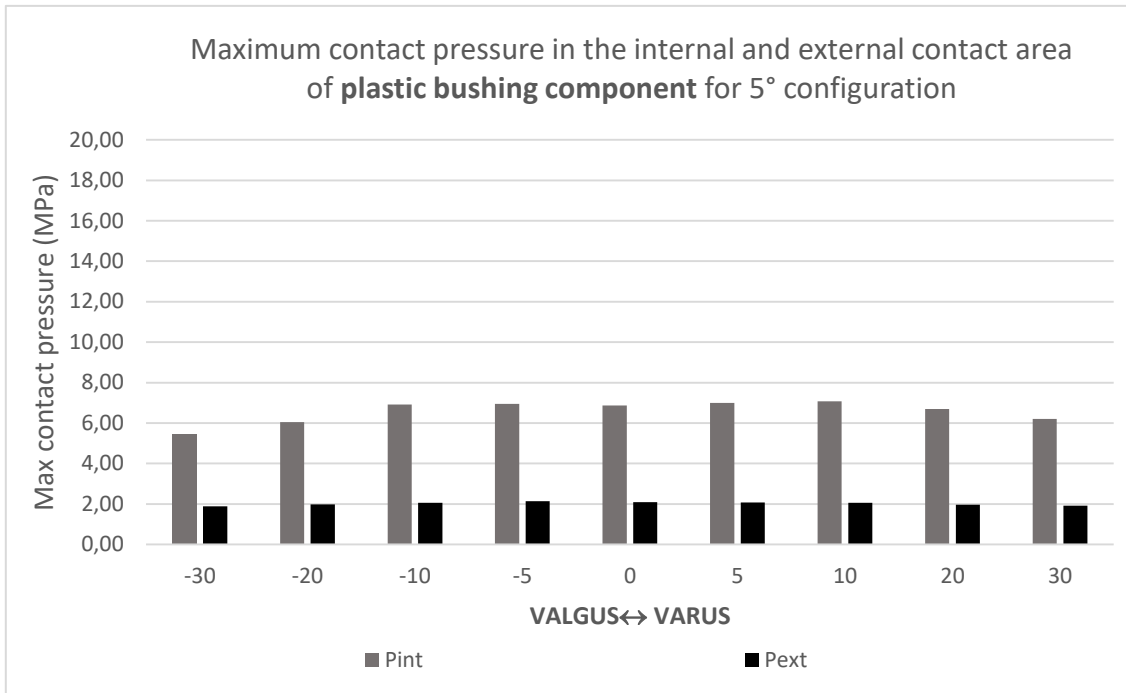


Figure 56, Maximum contact pressure in the internal and external contact area of plastic bushing component for 5° configuration with cementless stem of 50 mm

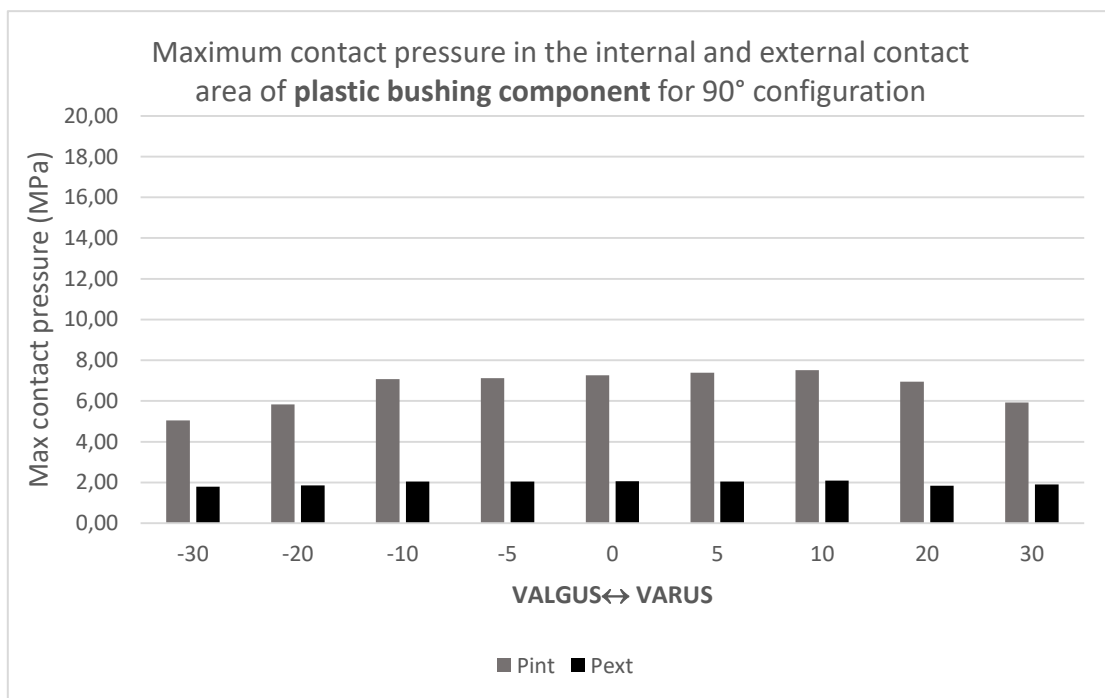


Figure 55, Maximum contact pressure in the internal and external contact area of plastic bushing component for 90° configuration with cementless stem of 50 mm

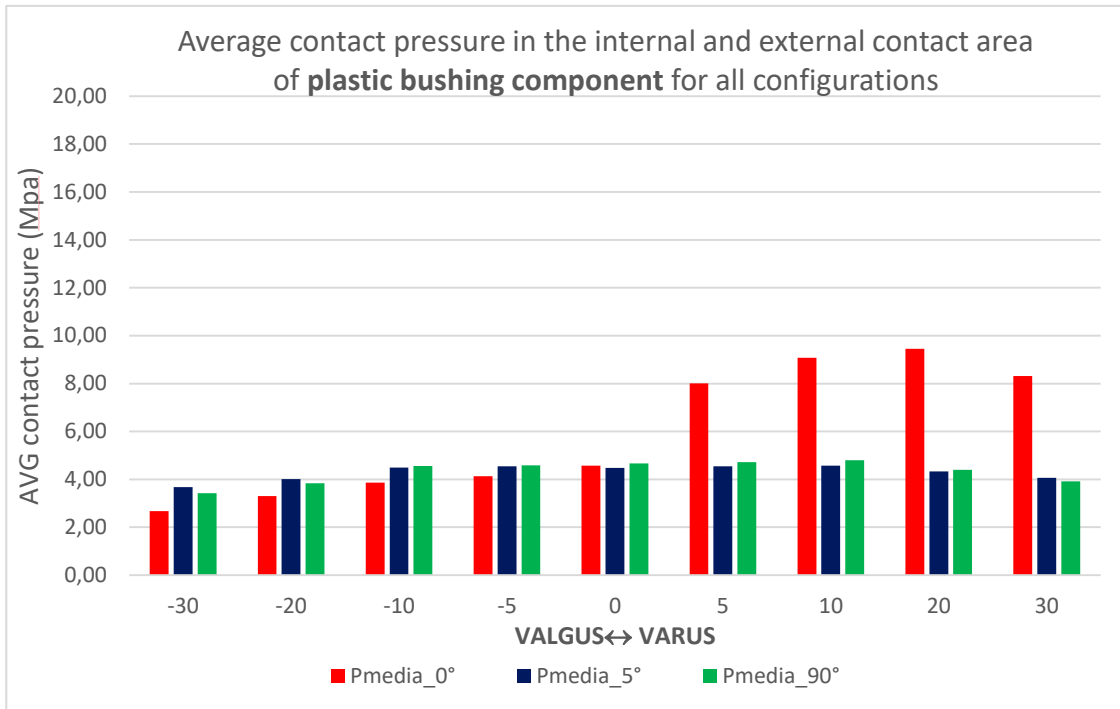


Figure 57, average contact pressure in the internal and external contact area of plastic bushing component for all configurations with cementless stem of 50 mm at 0°, 5° and 90° of flexion.

As before, fig. 58, 59, 60, 61, 62, 63, 64 and 65 illustrate the values of maximum and average contact pressure for both polyethylene and plastic bushing components for all the analysed configurations with cementless stem of 120 mm.

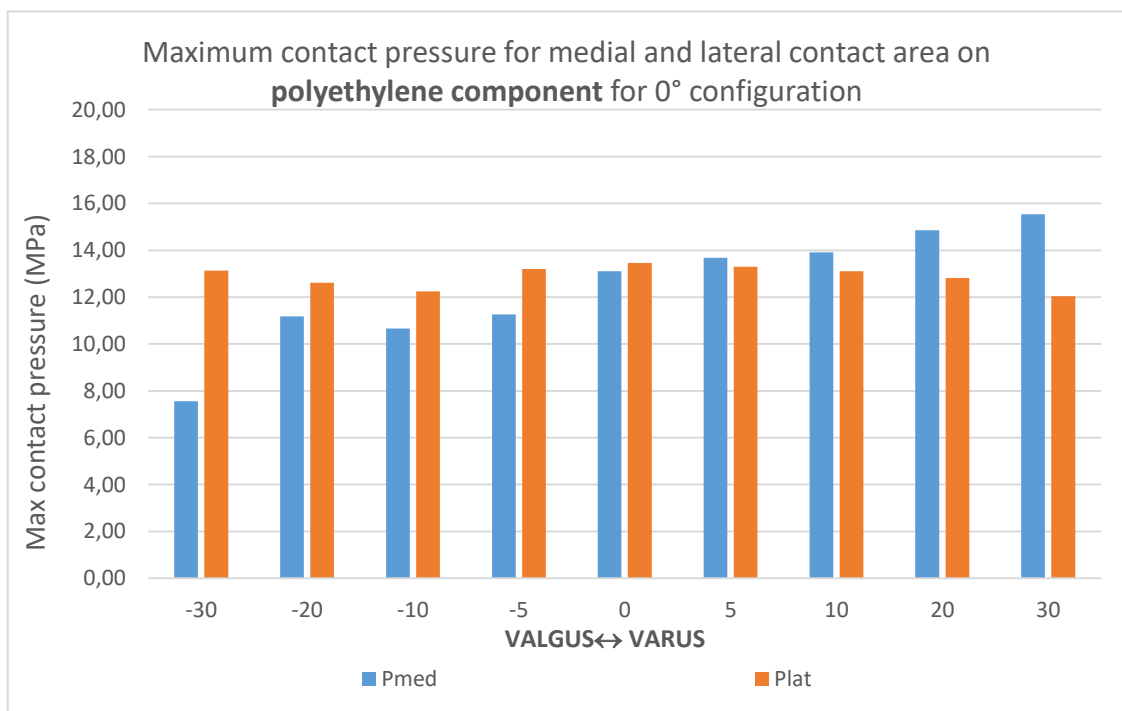


Figure 58, Maximum contact pressure for medial and lateral contact area on polyethylene component for 0° configuration with cementless stem of 120 mm.

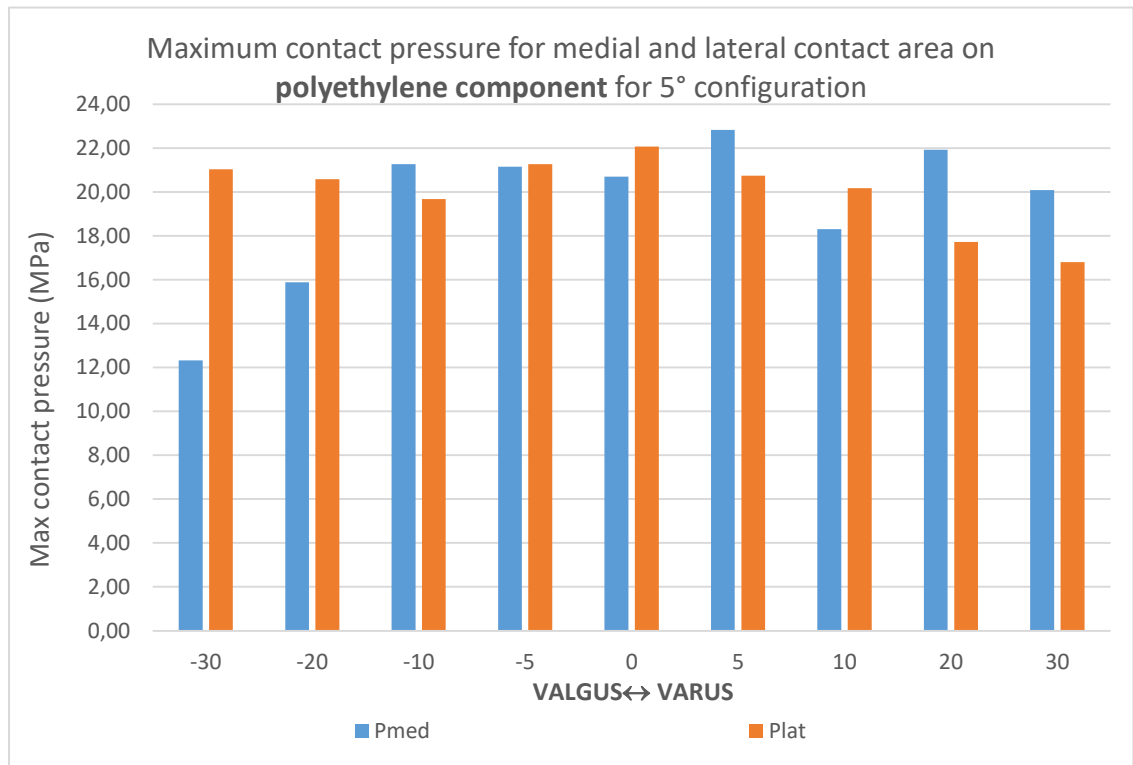


Figure 59, Maximum contact pressure for medial and lateral contact area on polyethylene component for 5° configuration with cementless stem of 120 mm.

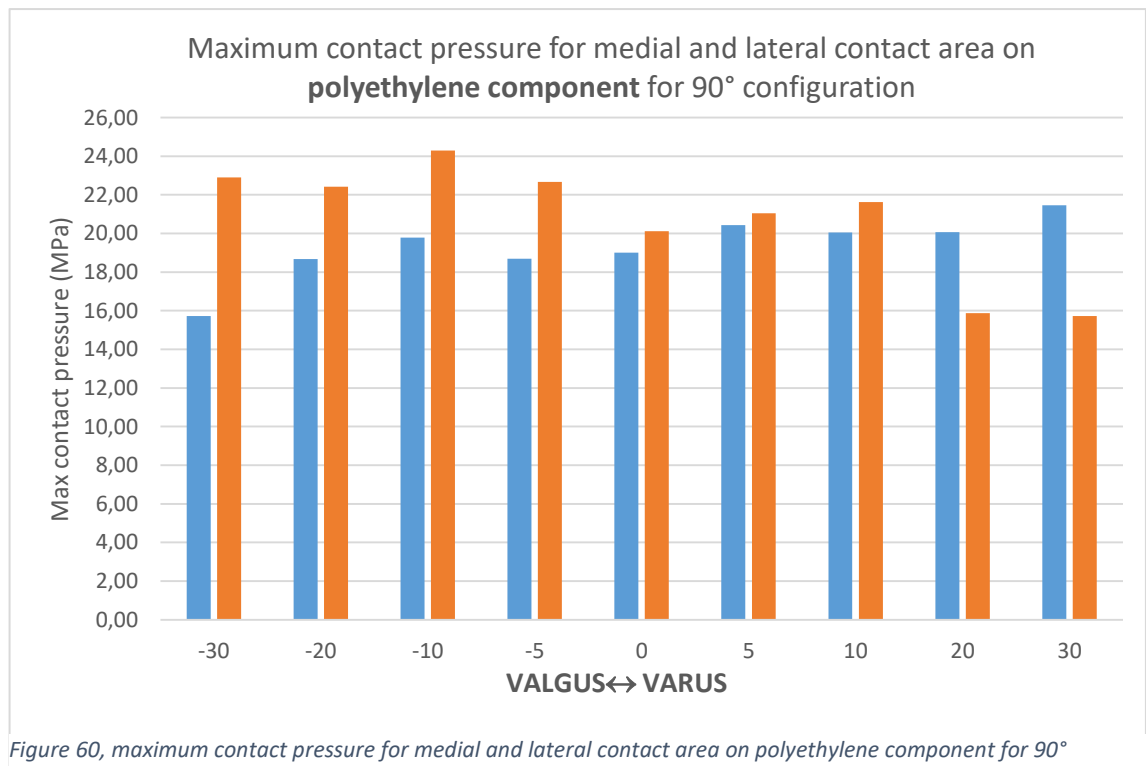


Figure 60, maximum contact pressure for medial and lateral contact area on polyethylene component for 90° configuration with cementless stem of 120 mm

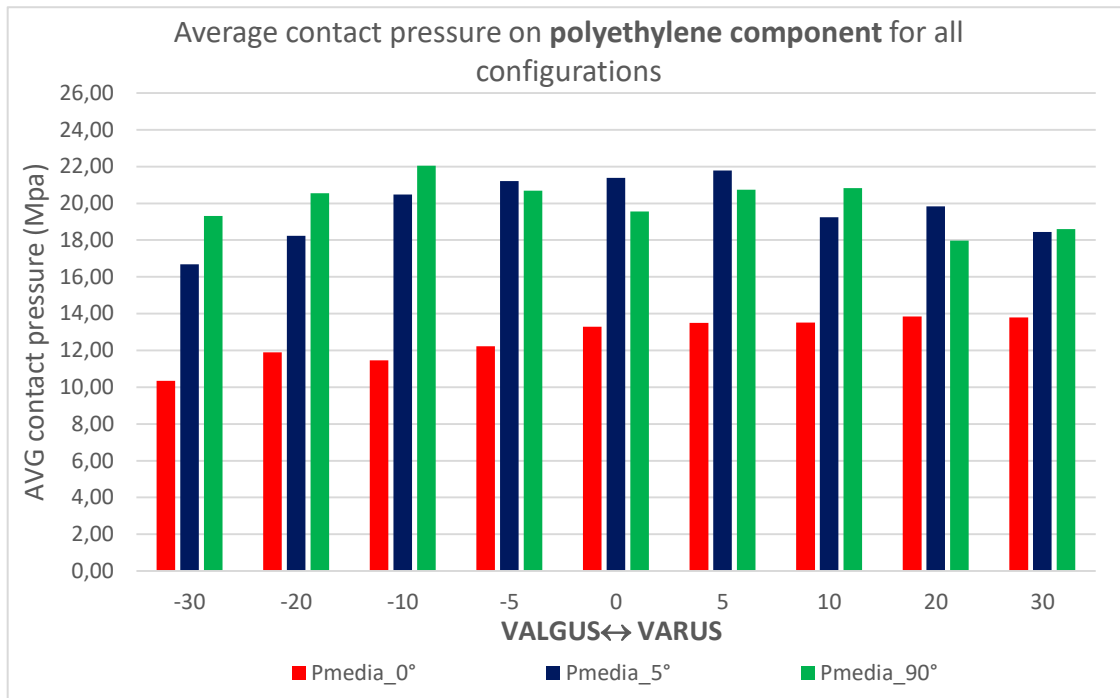


Figure 62, average contact pressure on polyethylene component for all configurations with cementless stem of 120 mm

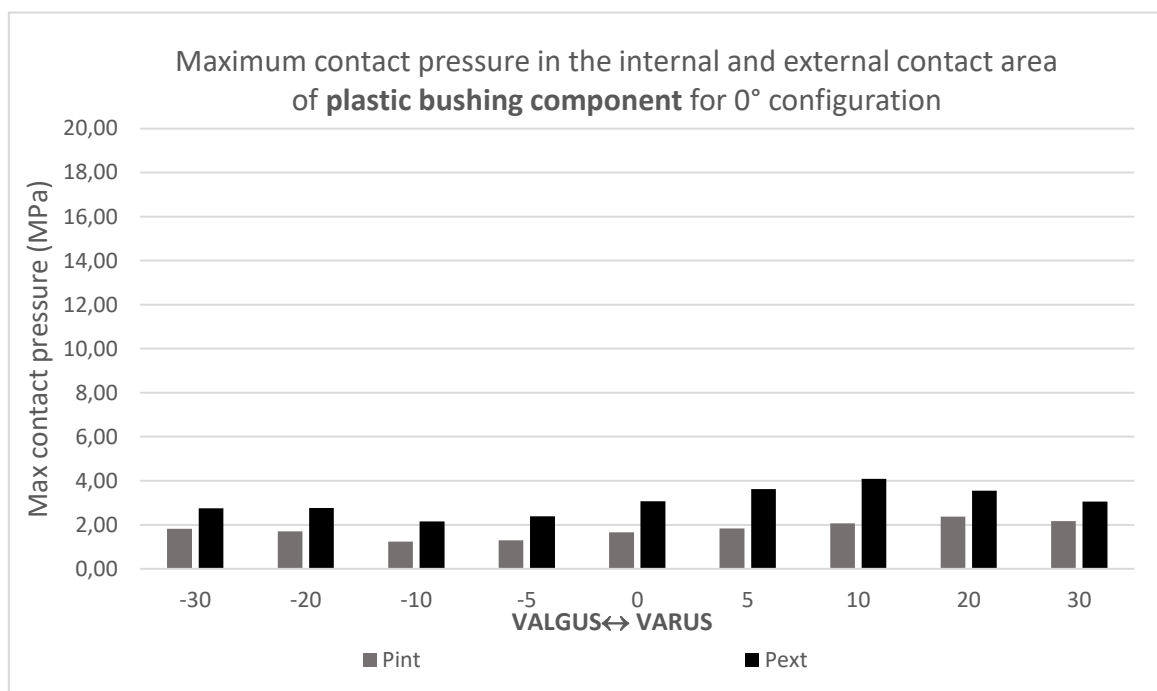


Figure 61, Maximum contact pressure in the internal and external contact area of plastic bushing component for 0° configuration with cementless stem of 120 mm

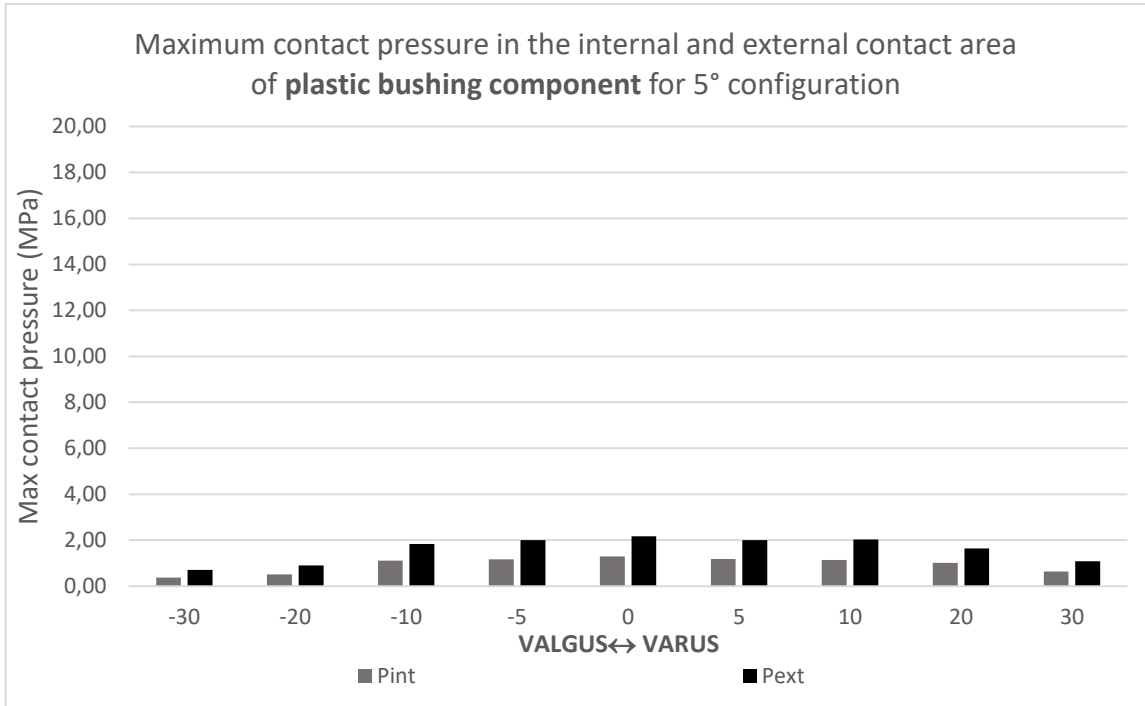


Figure 64, Maximum contact pressure in the internal and external contact area of plastic bushing component for 5° configuration with **cementless stem of 120 mm**

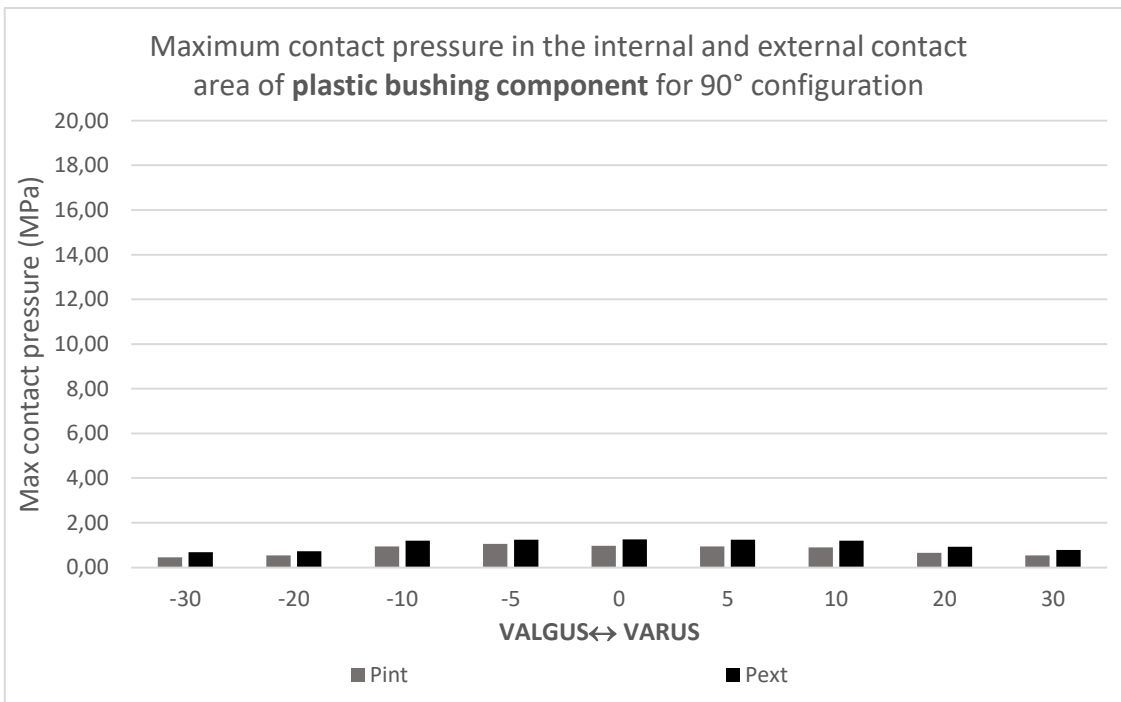


Figure 63, maximum contact pressure in the internal and external contact area of plastic bushing component for 90° configuration with **cementless stem of 120 mm**

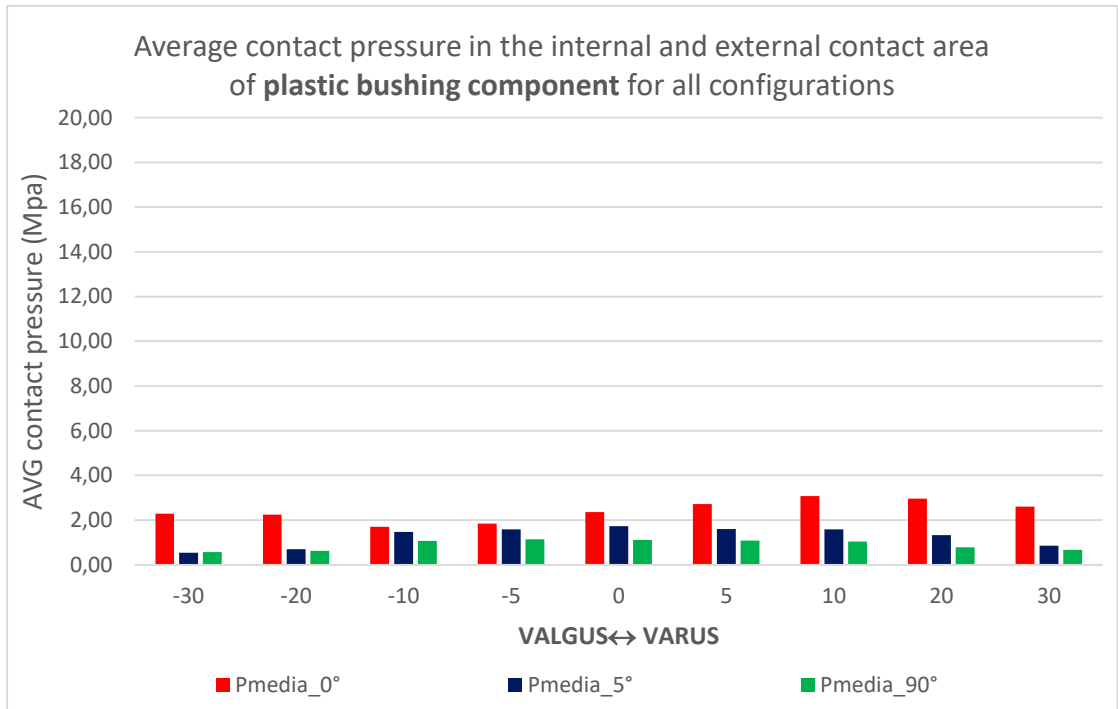


Figure 65, average contact pressure in the internal and external contact area of plastic bushing component for all configurations with cementless stem of 120 mm

As illustrates for the other models, fig. 66, 67, 68, 69, 70, 71, 72 and 73 report the quantitative values of maximum and average contact pressure on polyethylene and plastic bushing components for all the analysed configurations with cementless stem of 160 mm.

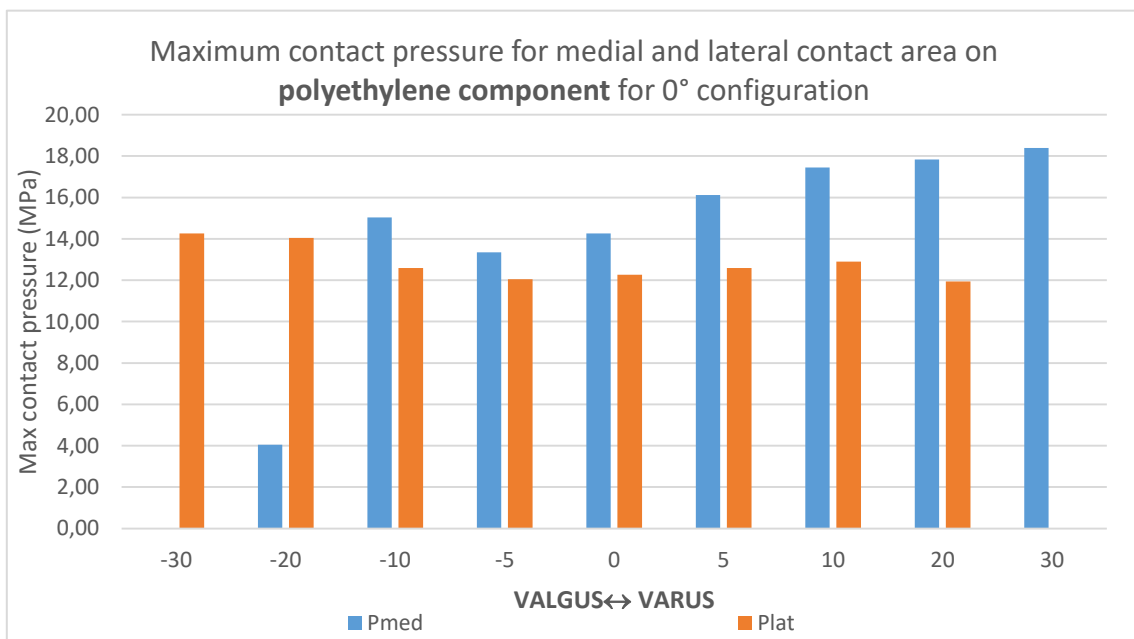


Figure 66, Maximum contact pressure for medial and lateral contact area on polyethylene component for 0° configuration with cementless stem of 160 mm

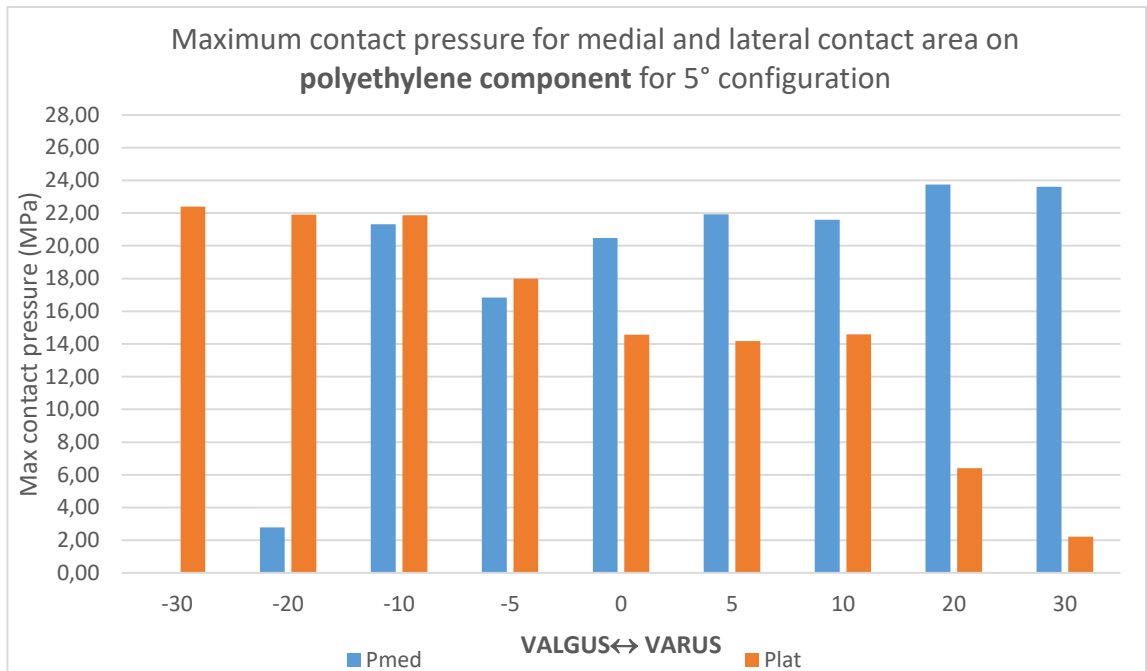


Figure 67, Maximum contact pressure for medial and lateral contact area on polyethylene component for 5° configuration with cementless stem of 160 mm

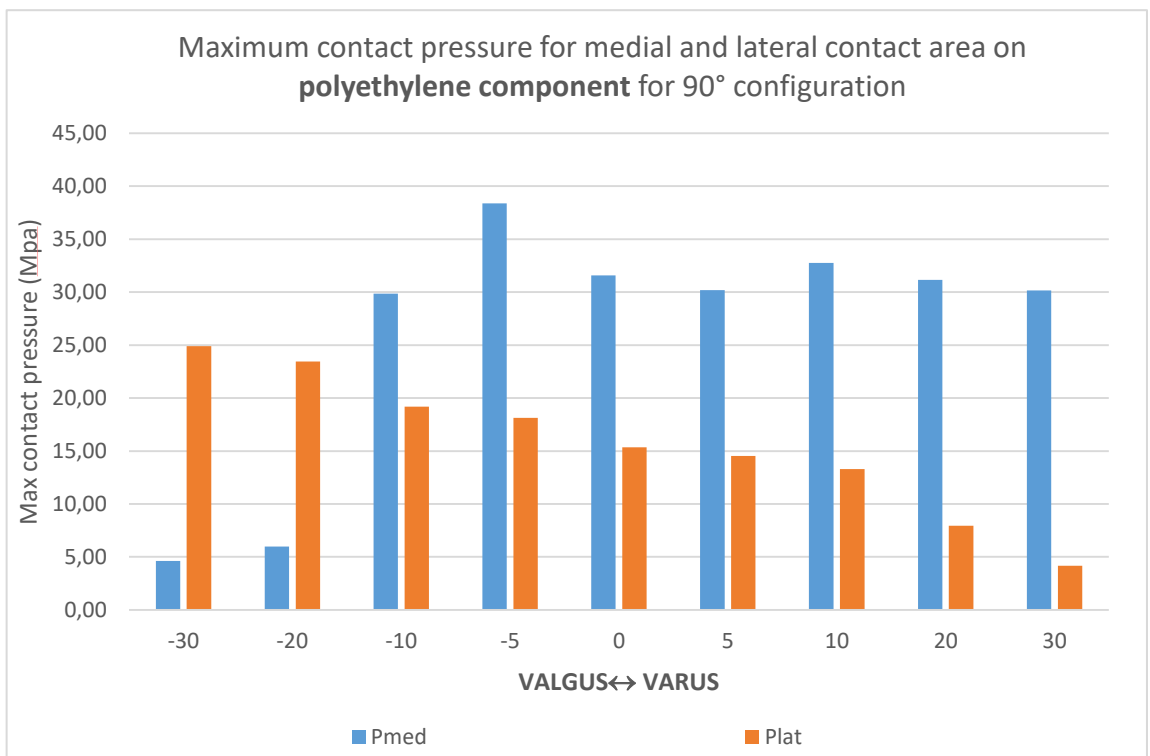


Figure 68, Maximum contact pressure for medial and lateral contact area on polyethylene component for 90° configuration with cementless stem of 160 mm

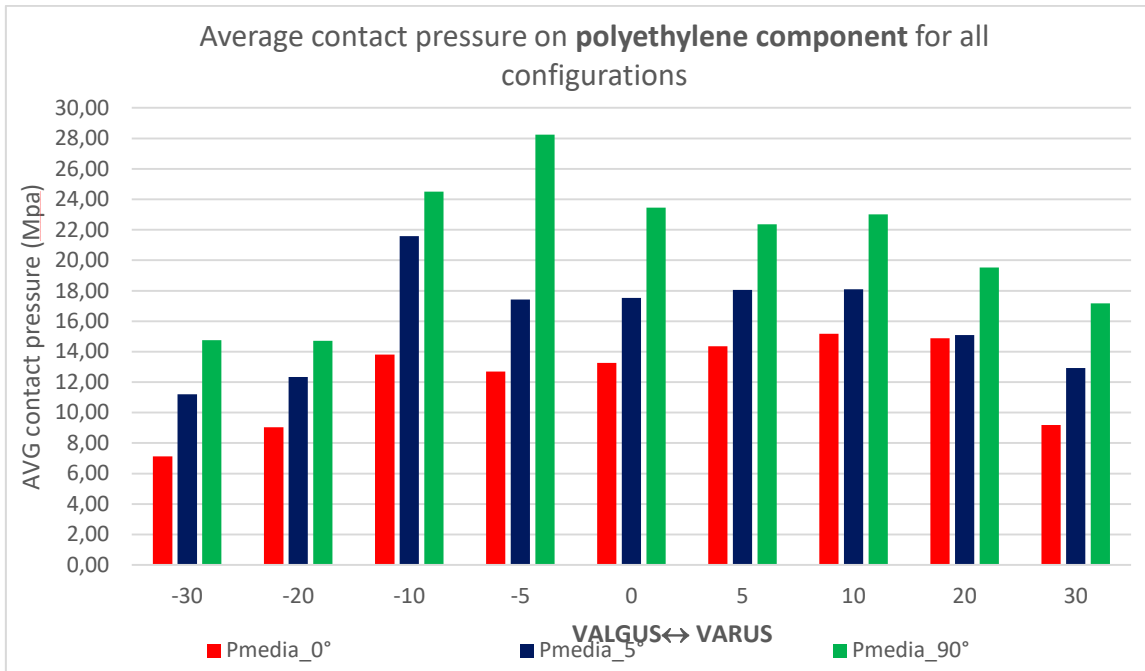


Figure 69, average contact pressure on polyethylene component for all configurations with cementless stem of 120 mm

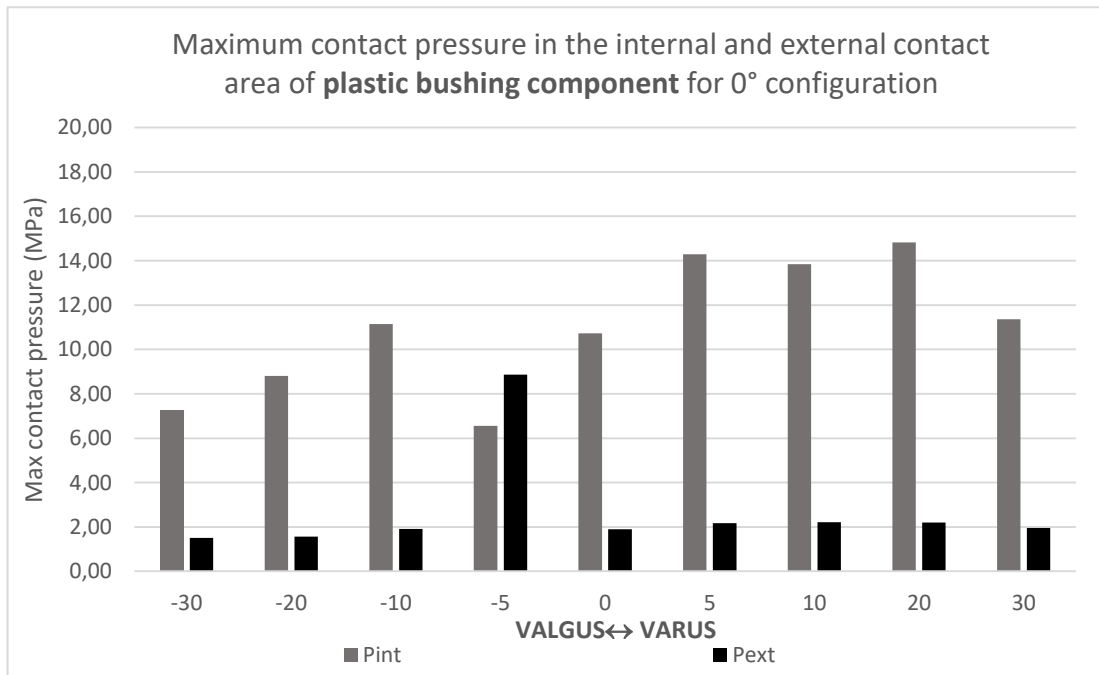


Figure 70, Maximum contact pressure in the internal and external contact area of plastic bushing component for 0° configuration with cementless stem of 160 mm

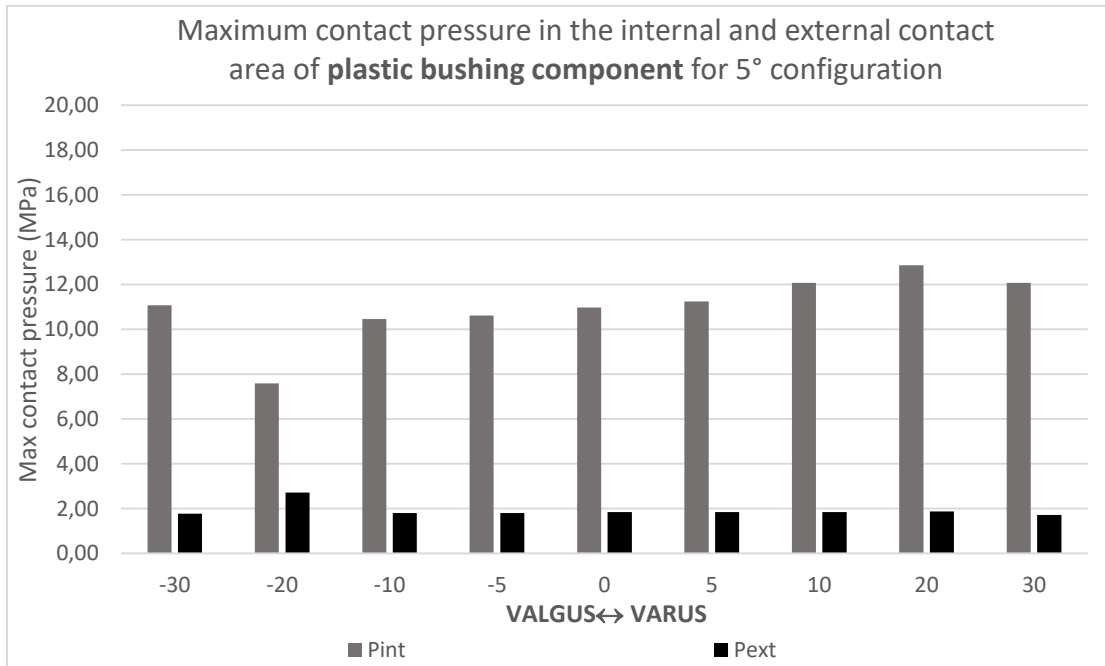


Figure 71, Maximum contact pressure in the internal and external contact area of plastic bushing component for 5° configuration with cementless stem of 160 mm

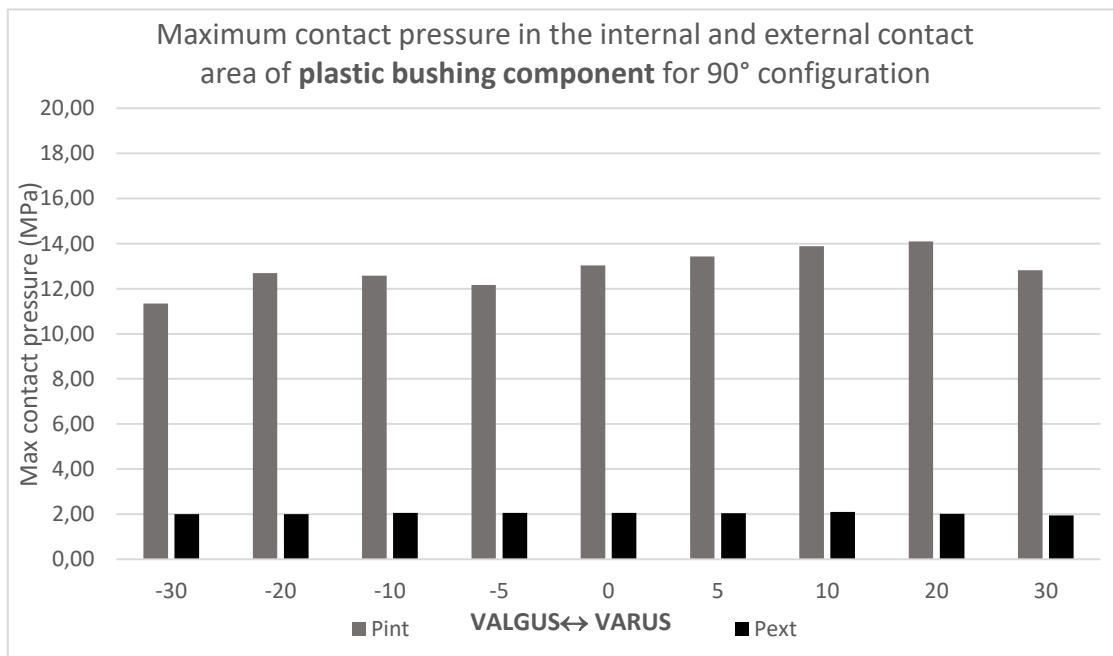


Figure 72, Maximum contact pressure in the internal and external contact area of plastic bushing component for 90° configuration with cementless stem of 160 mm

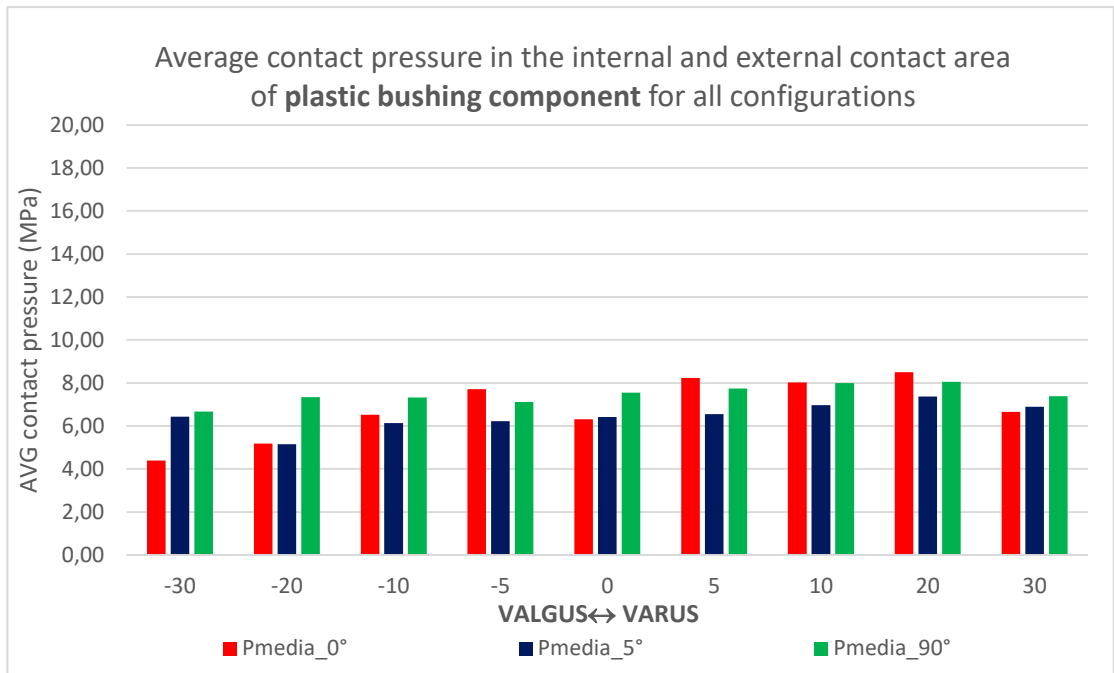


Figure 73, average contact pressure in the internal and external contact area of plastic bushing component for all configurations with cementless stem of 160 mm

## 4.2 Part II

Fig.74 report a graphical overview of the average Von Mises stress on polyethylene insert with cemented stem of 50 mm of length. As before, each row represents Valgus and Varus alignment, while the columns indicate positioning of the knee in three different configurations (0°-5°-90°). While, fig. 75 reports the contact pressure and area.

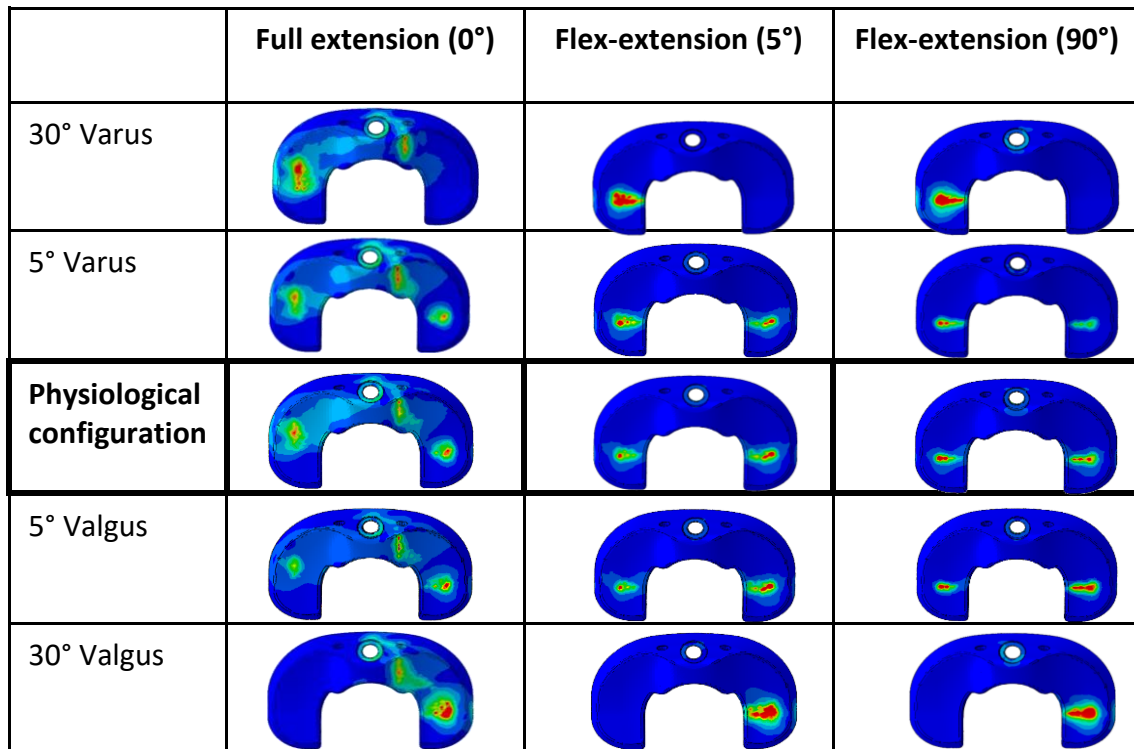


Figure 74, average von Mises stress on polyethylene component. Each row represents a Varus/Valgus configuration, while the columns indicate each flex-extension configuration.

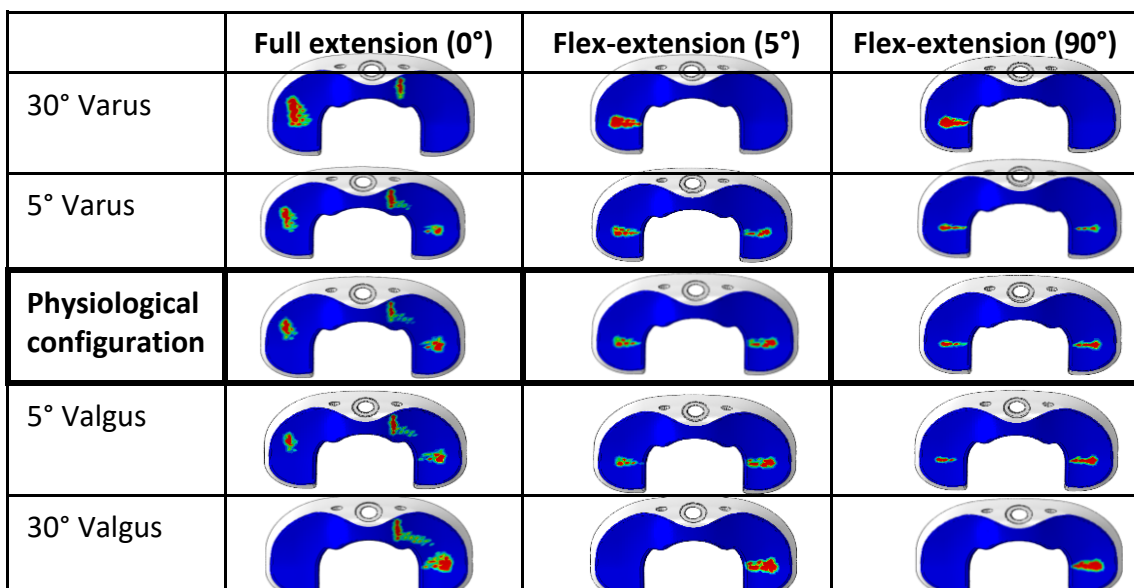


Figure 75, graphical overview of the contact pressure for each configuration

Qualitative results are reported also for plastic bushing component. Fig. 76 and 77 report results in term von Mises stress and contact pressure for plastic bushing component.

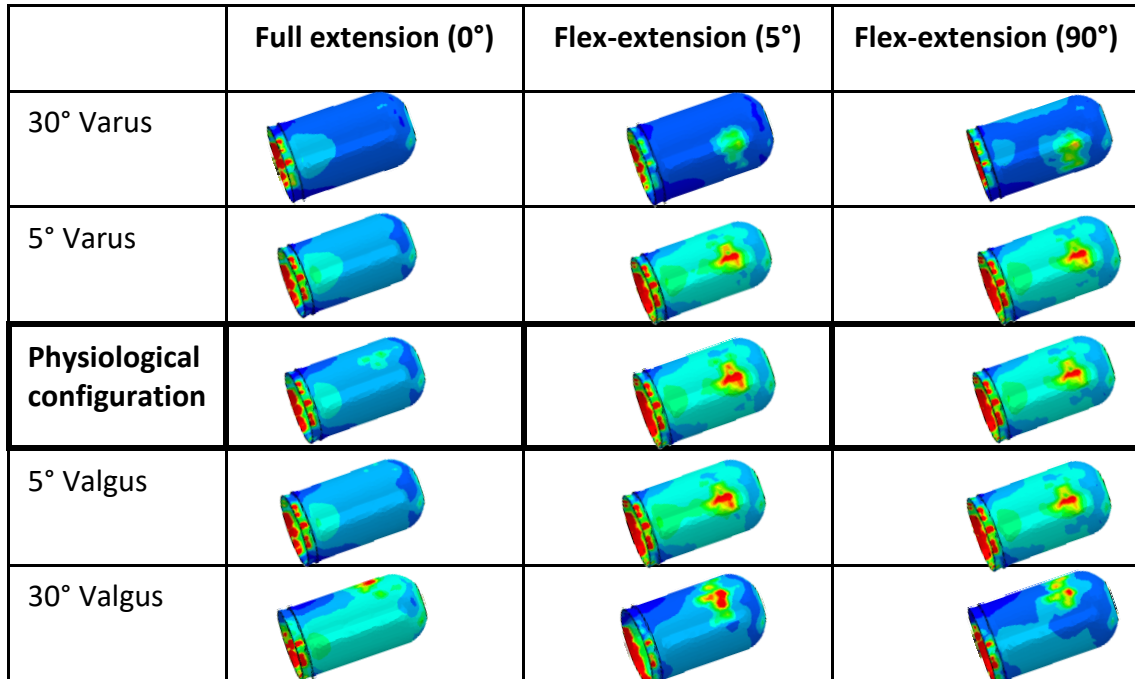


Figure 76, average von Mises stress on plastic bushing. Each row represents a Varus/Valgus configuration, while the columns indicate each flex-extension configuration.

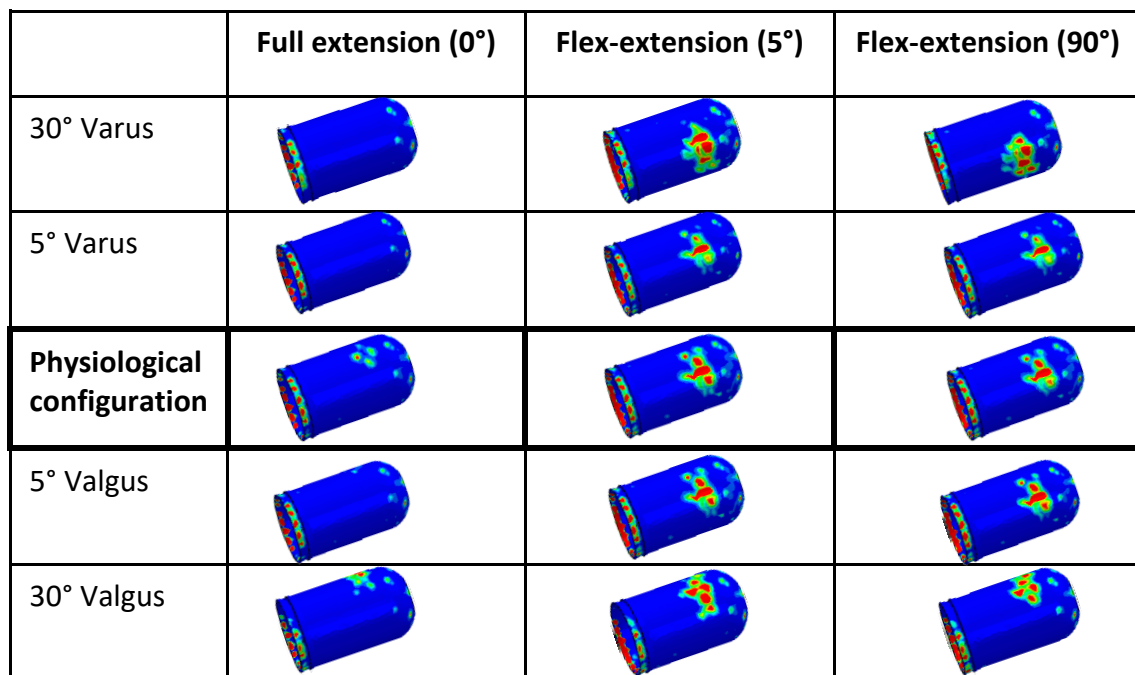


Figure 77, graphical overview of the contact pressure for each configuration.

The results of von Mises stress and contact pressure on tibiofemoral compartment with cemented femoral of 120 mm of length are illustrate in fig. 78 and fig. 79. While fig. 80 and 81 show the von Mises stress on polyethylene component and contact pressure on plastic bushing component.

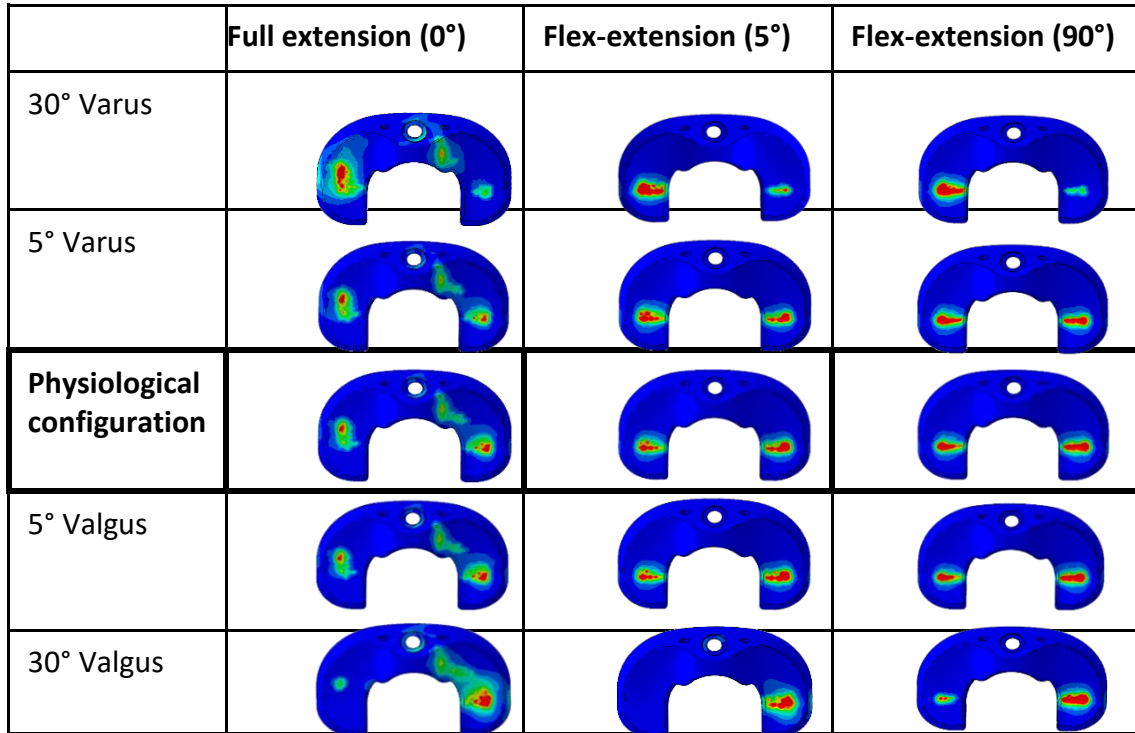


Figure 79, average von Mises stress on polyethylene component. Each row represents a Varus/Valgus configuration, while the columns indicate each flex-extension configuration.

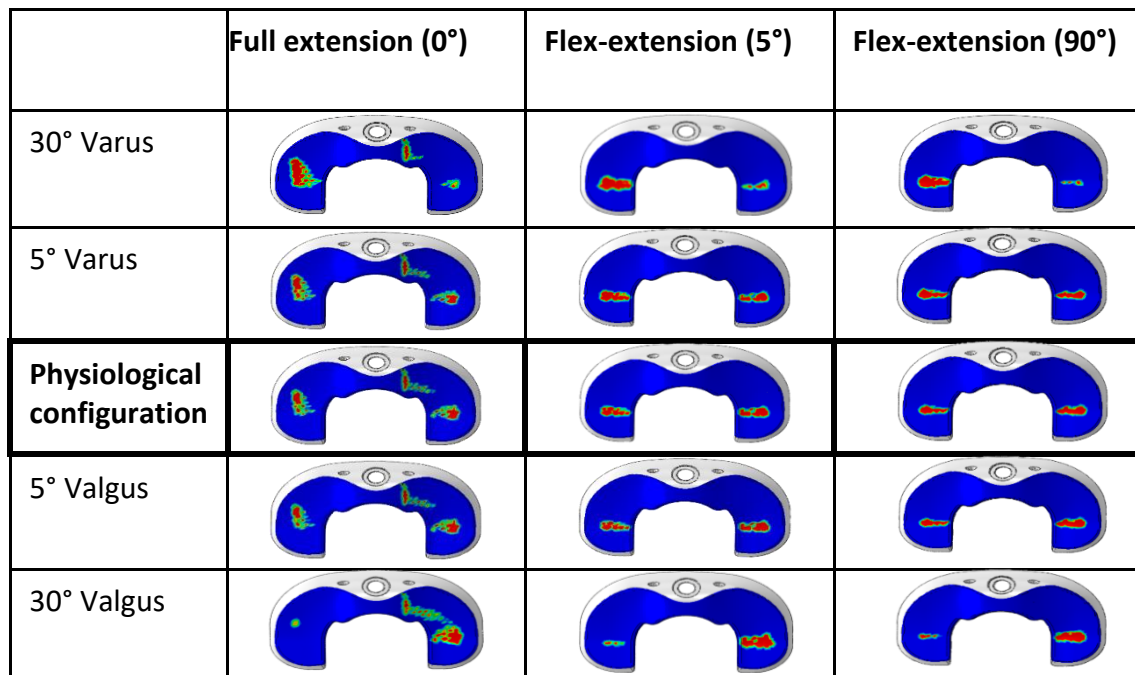


Figure 78, average von Mises stress on plastic bushing. Each row represents a Varus/Valgus configuration, while the columns indicate each flex-extension configuration.

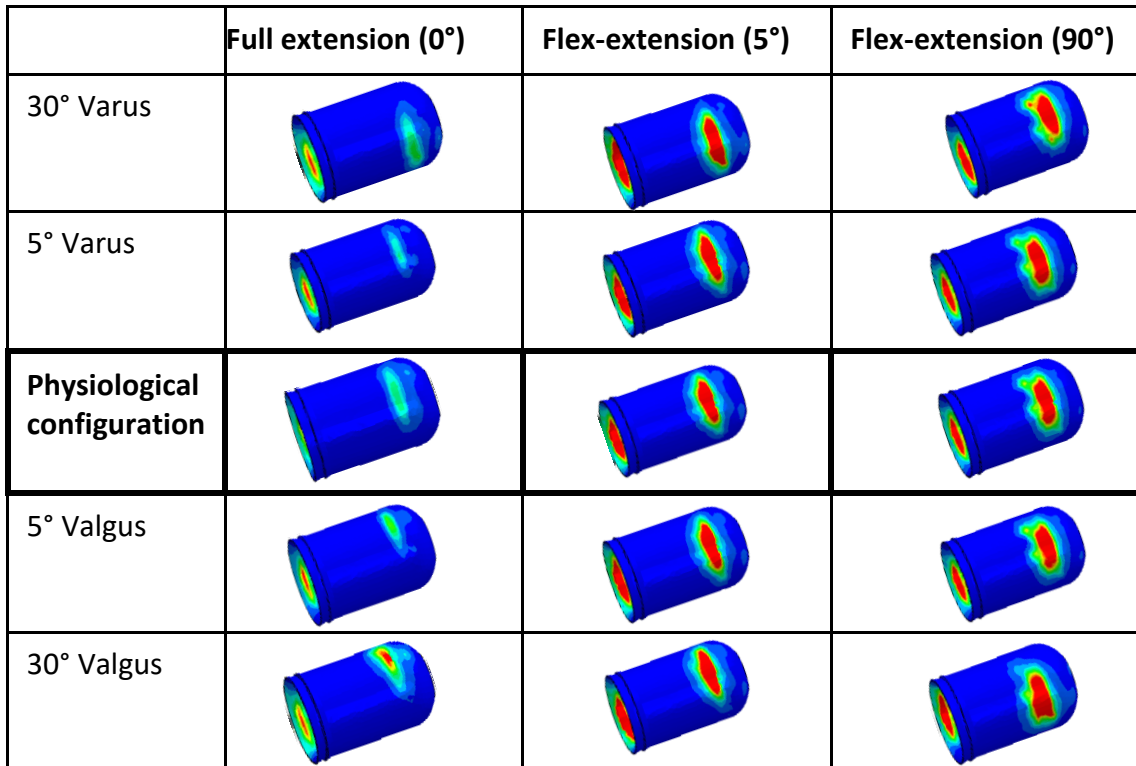


Figure 80, graphical overview of the contact pressure for each configuration

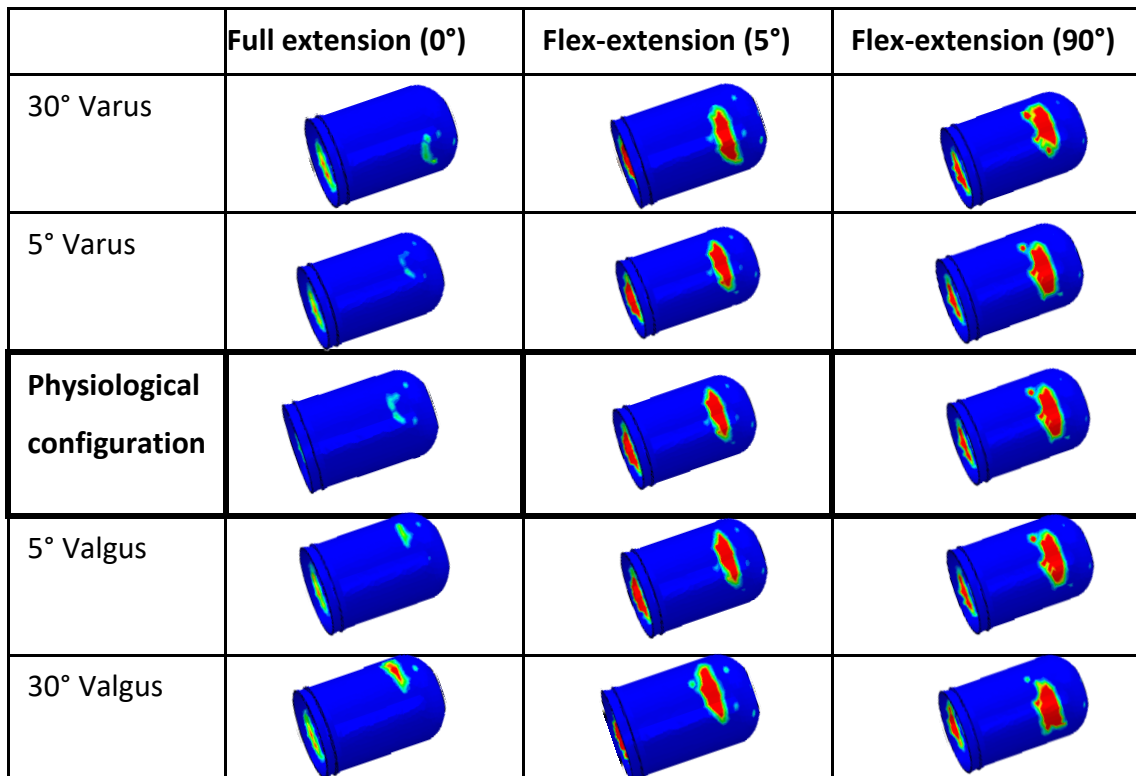


Figure 81, graphical overview of the contact pressure for each configuration.

The results of von Mises stress and contact pressure on tibiofemoral compartment with cemented femoral of 160 mm of length are illustrate in fig. 82 and fig. 83. While, the trend of contact force is reported in fig. 75.

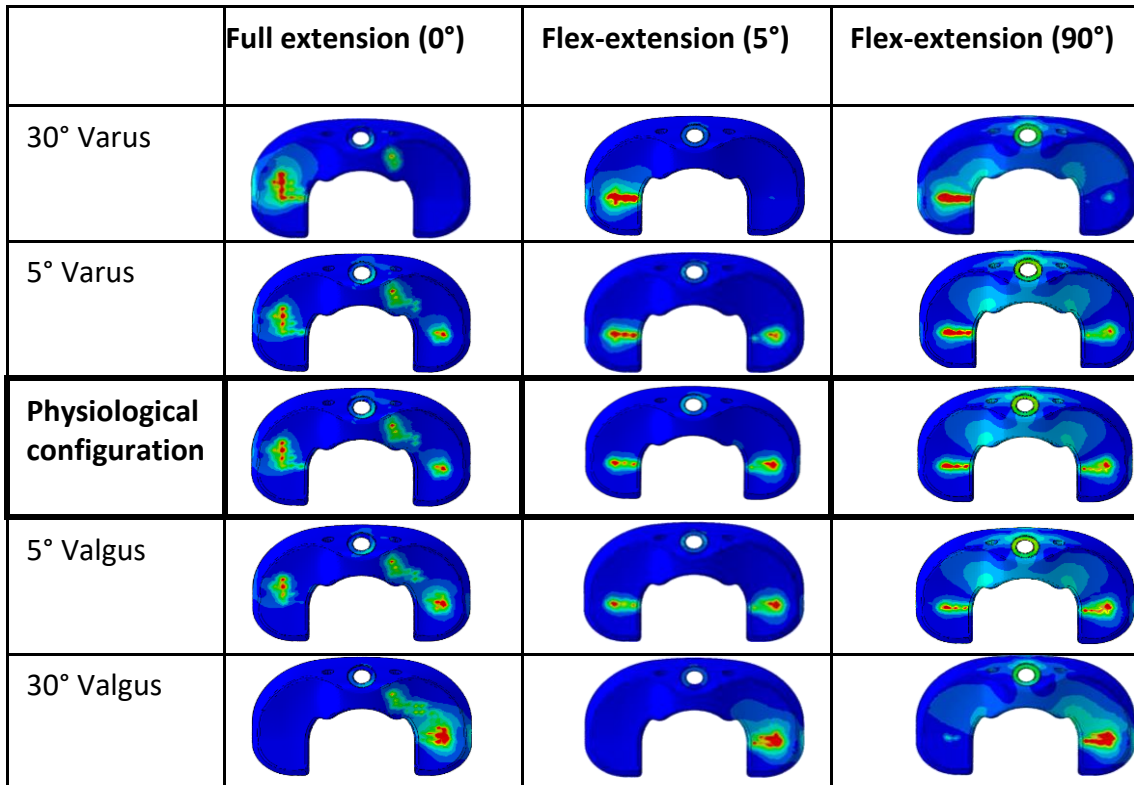


Figure 82, average von Mises stress on polyethylene component. Each row represents a Varus/Valgus configuration, while the columns indicate each flex-extension configuration.

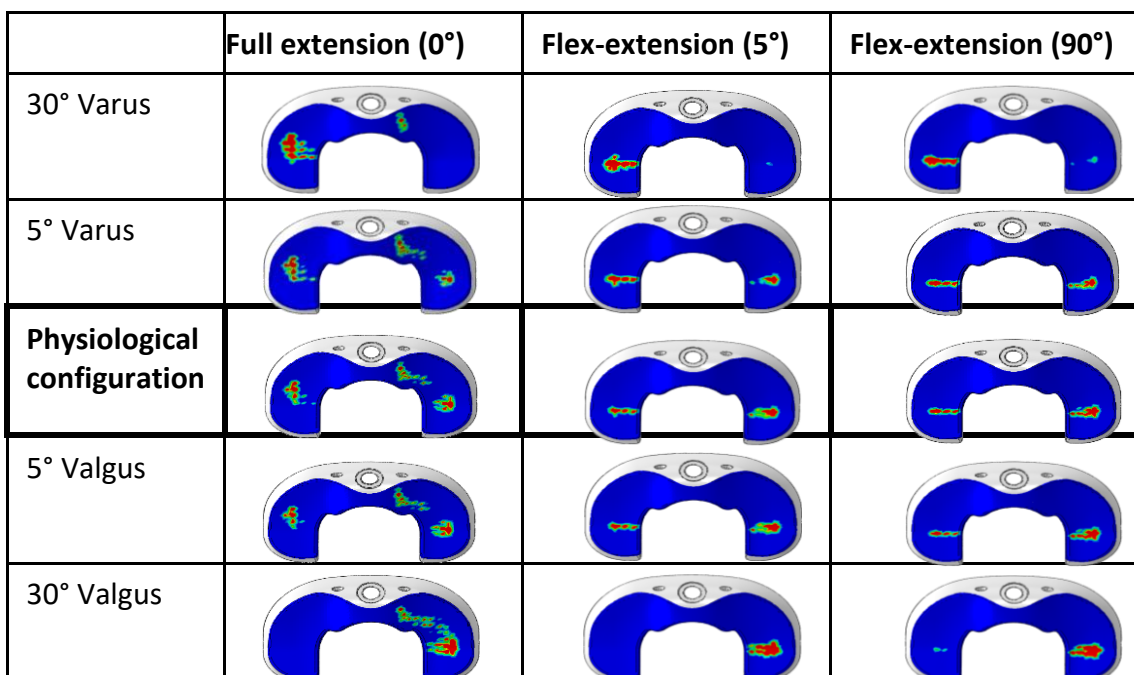


Figure 83, graphical overview of the contact pressure for each configuration

Moreover, von Mises stress and contact pressure on plastic bushing are shown in fig. 83 and fig. 84, considering the same configuration.

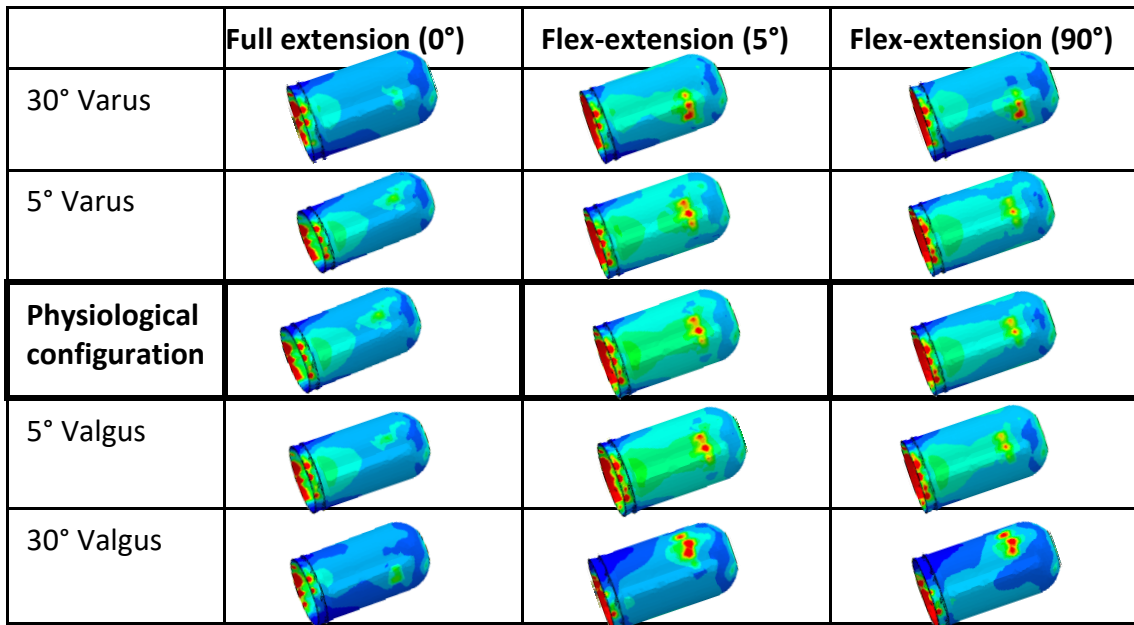


Figure 84, average von Mises stress on plastic bushing. Each row represents a Varus/Valgus configuration, while the columns indicate each flex-extension configuration.

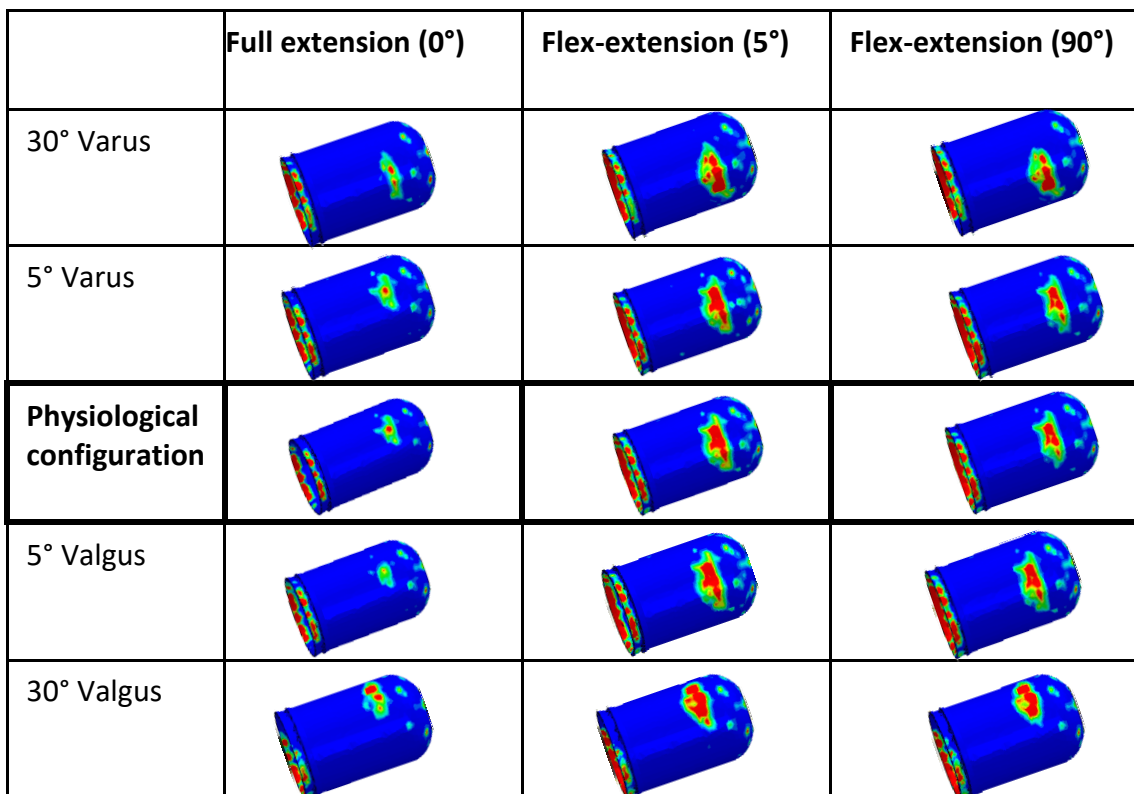


Figure 85, graphical overview of the contact pressure for each configuration.

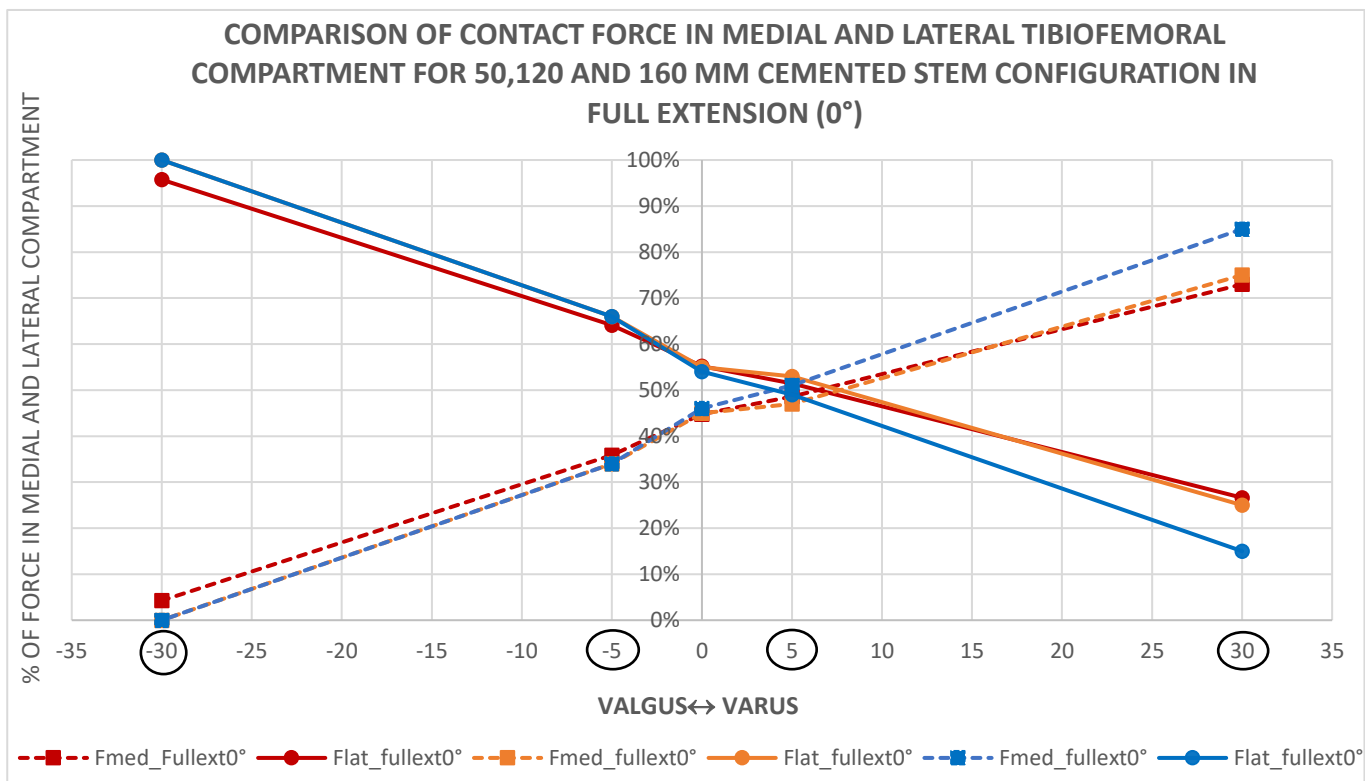


Figure 86, Trend of force in medial and lateral tibiofemoral compartment for Valgus and Varus deformity at 0° of flexion

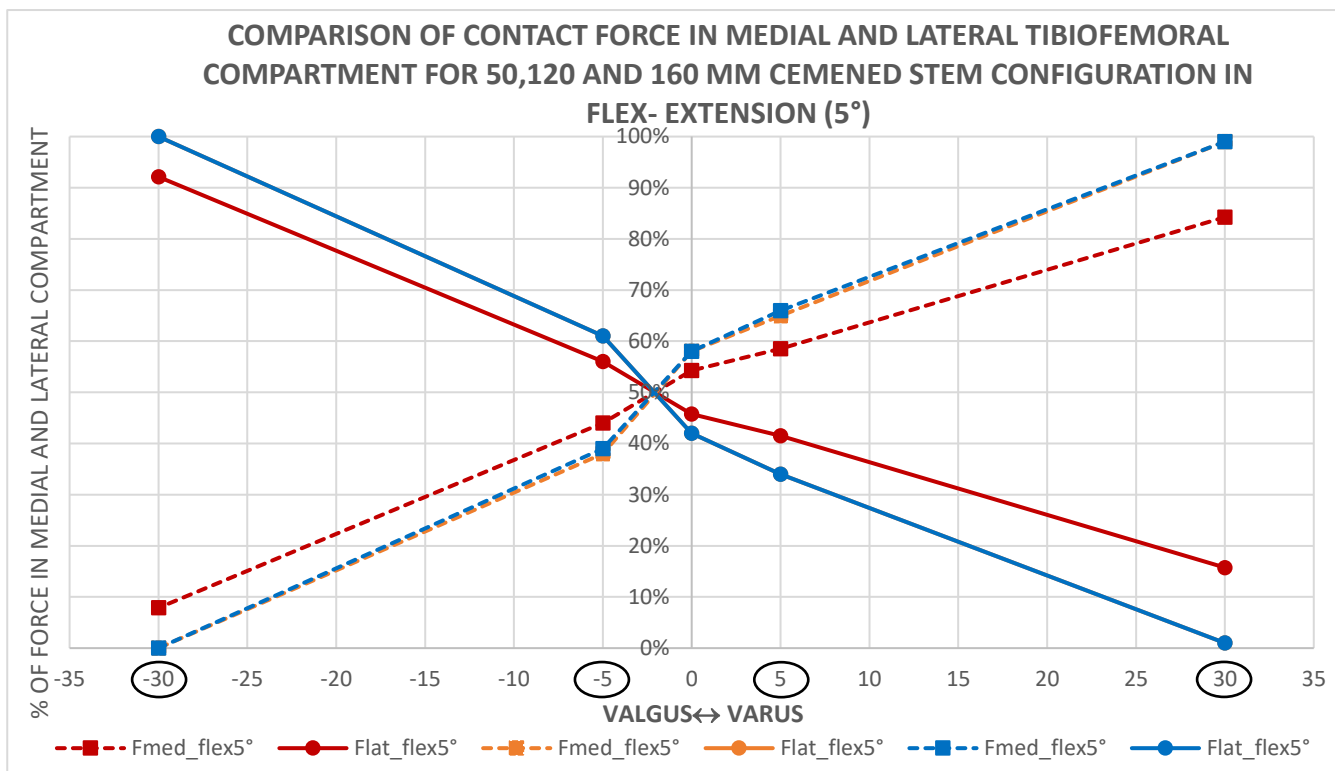


Figure 87, Trend of force in medial and lateral tibiofemoral compartment for Valgus and Varus deformity at 90° of flexion

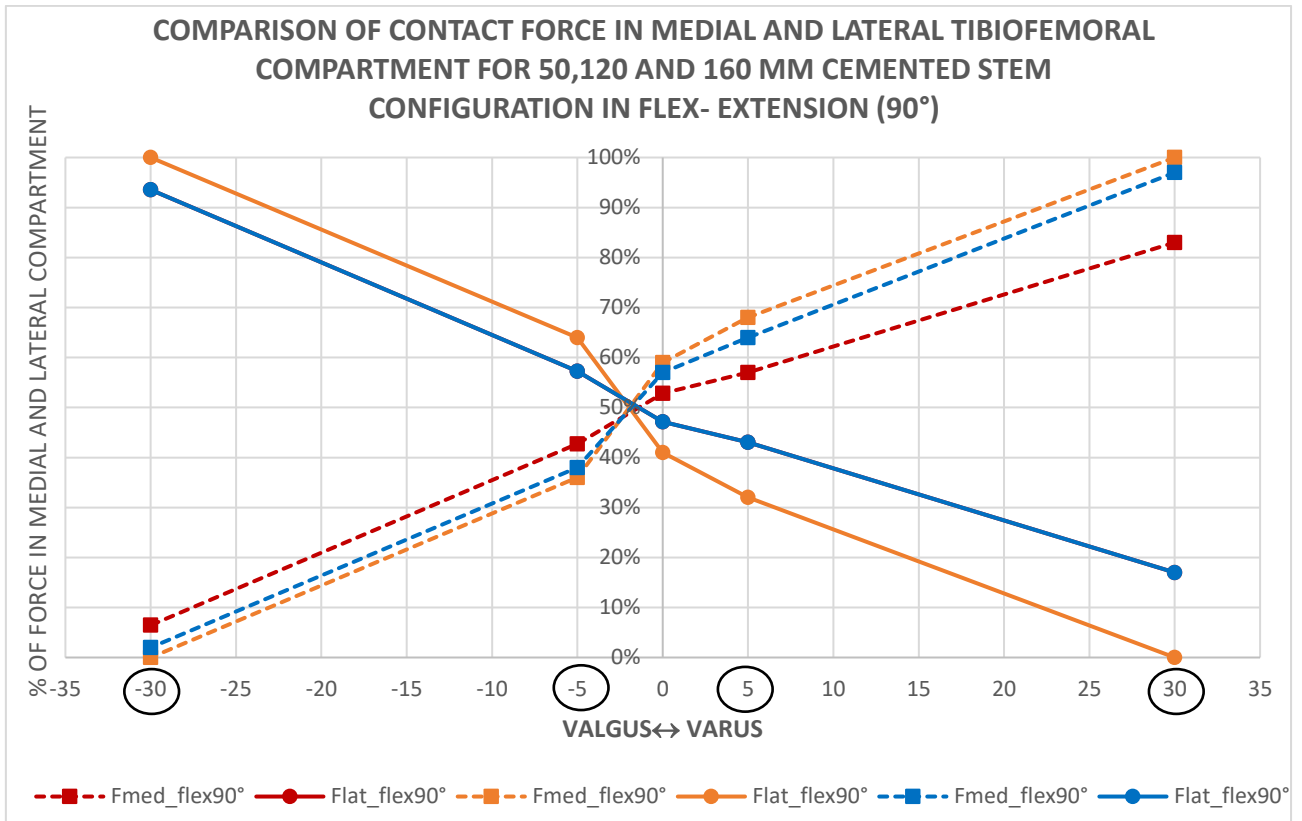
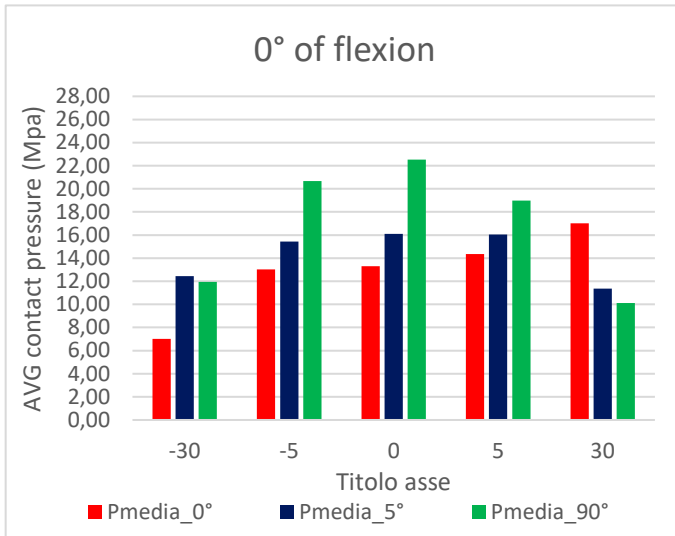


Figure 88, Trend of force in medial and lateral tibiofemoral compartment for Valgus and Varus deformity at 5° of flexion

To better understand the difference between 50, 120 and 160 mm cemented stems, Fig. 86, 87 and 88 report a comparison of contact force in medial and lateral tibiofemoral compartment at 0°, 5° and 90° for 50, 120 and 160 mm cemented stems. Red lines indicate the trend of force for 120 mm cemented stem, orange lines represent the percentage of force for cemented stem of 50 mm of length and blue lines indicates the trend of contact force with the model using 160 mm cemented stem.

From results obtained with cementless models, the graphs report only results for -5° and 5°, and for -30° and 30° Varus and Valgus configurations. The trend of force in medial and later compartment of polyethylene insert is similar for 50 and 160 mm cemented models. While 120 mm cemented shows a better distribution of force for severe Valgus and Varus degree.

**AVERAGE CONTACT PRESSURE ON POLYETHYLENE COMPONENT FOR ALL CONFIGURATIONS**



**AVERAGE CONTACT PRESSURE IN THE INTERNAL AND EXTERNAL CONTACT AREA OF PLASTIC BUSHING COMPONENT FOR ALL CONFIGURATIONS**

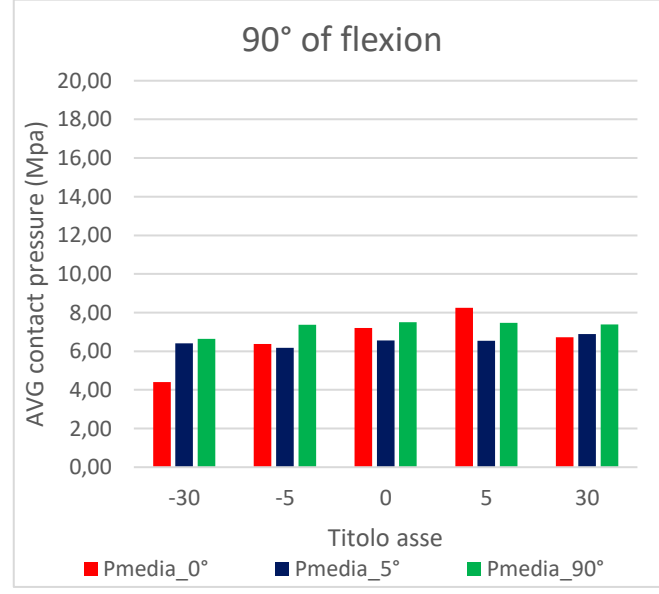
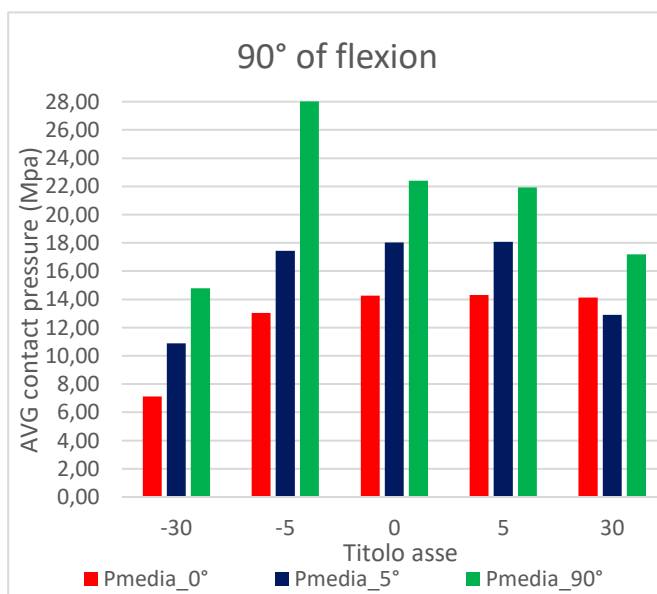
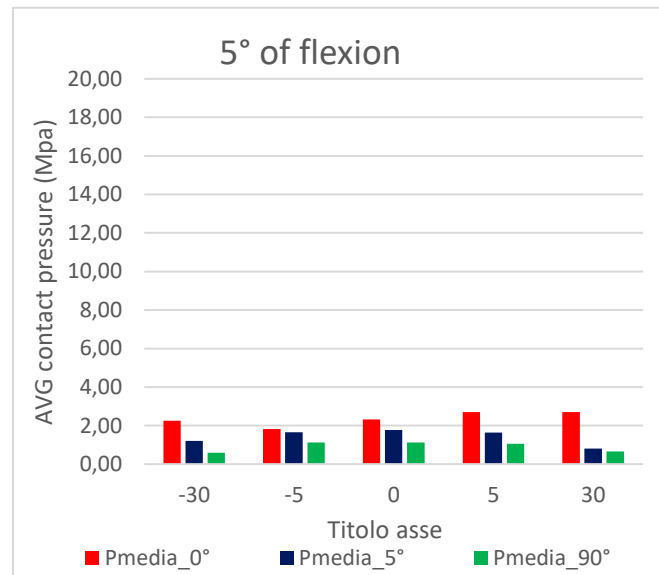
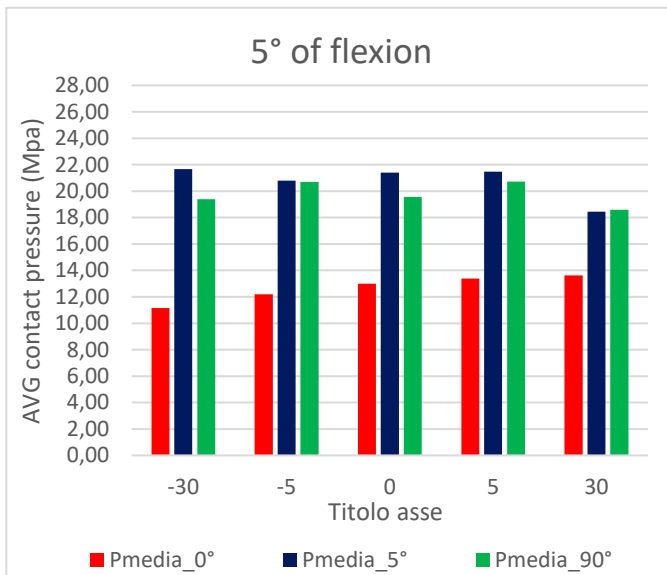
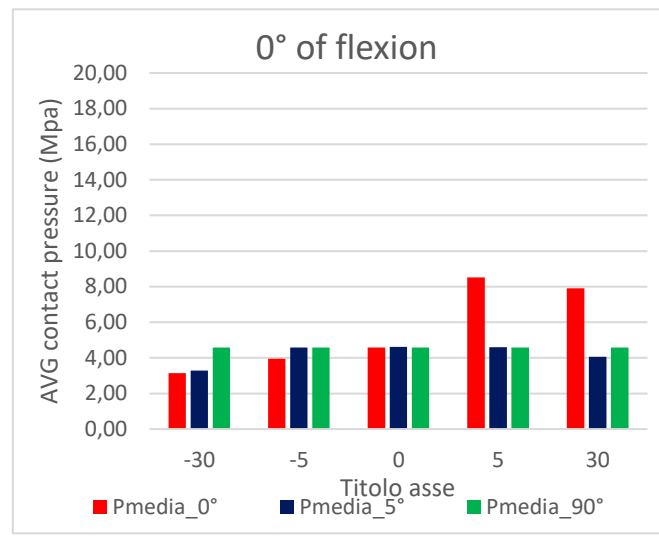


Figure 89, graphical overview of average contact pressure on polyethylene component (left) and average contact pressure in the internal and external contact area of plastic bushing component (right) for all configurations (0°, 5° and 90°).

### 4.3 Part III

Fig. 90 and 91 report a graphical overview of von Mises stress and contact pressure and area on polyethylene insert. While, fig. 92 and 93 show the von Mises stress and contact pressure on plastic bushing component, both for 50 mm cementless stem with osteoporotic bone.

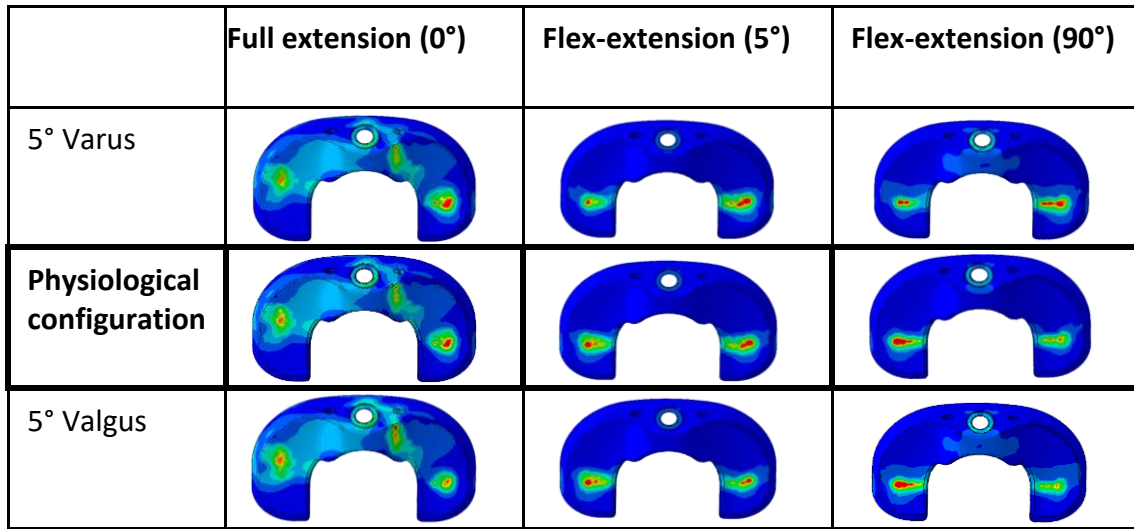


Figure 90, average von Mises stress on polyethylene component. Each row represents a Varus/Valgus configuration, while the columns indicate each flex-extension configuration.

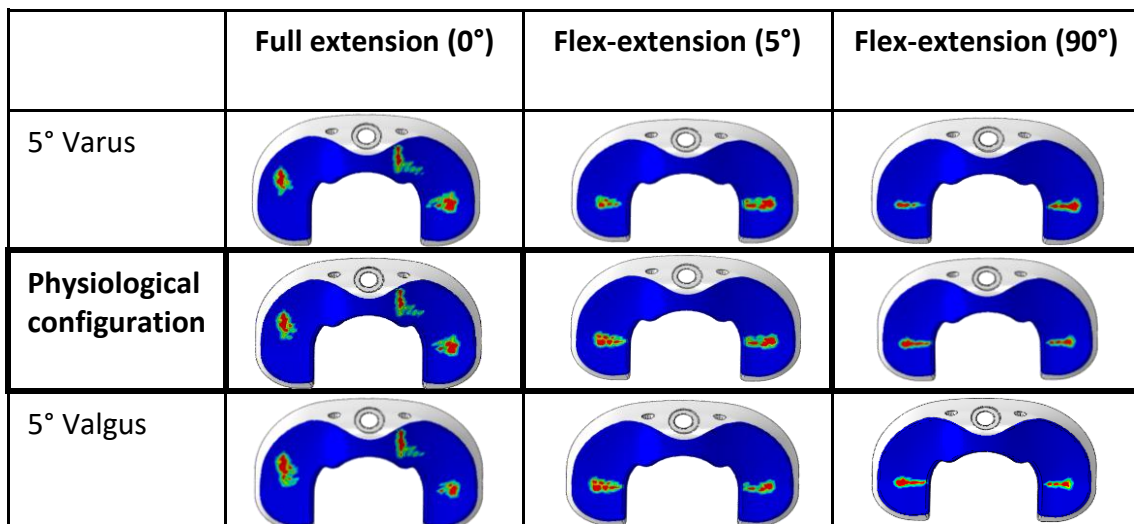


Figure 91, graphical overview of the contact pressure for each configuration.

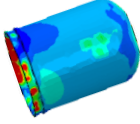
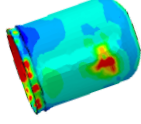
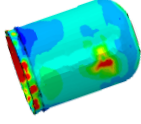
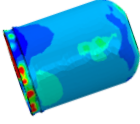
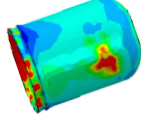
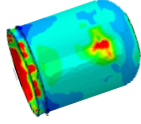
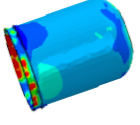
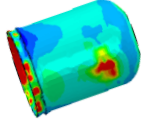
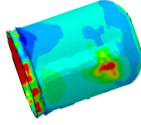
	Full extension (0°)	Flex-extension (5°)	Flex-extension (90°)
5° Varus			
Physiological configuration			
5° Valgus			

Figure 92, average von Mises stress on plastic bushing. Each row represents a varus/valgus configuration, while the columns indicate each flexo-extension configuration.

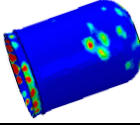
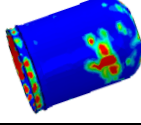
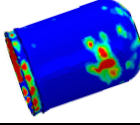
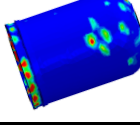
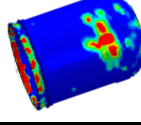
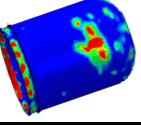
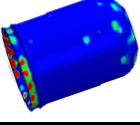
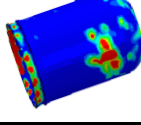
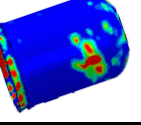
	Full extension (0°)	Flex-extension (5°)	Flex-extension (90°)
5° Varus			
Physiological configuration			
5° Valgus			

Figure 93, graphical overview of the contact pressure for each configuration

The results of von Mises stress and contact pressure on tibiofemoral component for cementless femoral stem with a length of 120 mm and osteoporotic bone are illustrate in fig. 94 and fig. 95.

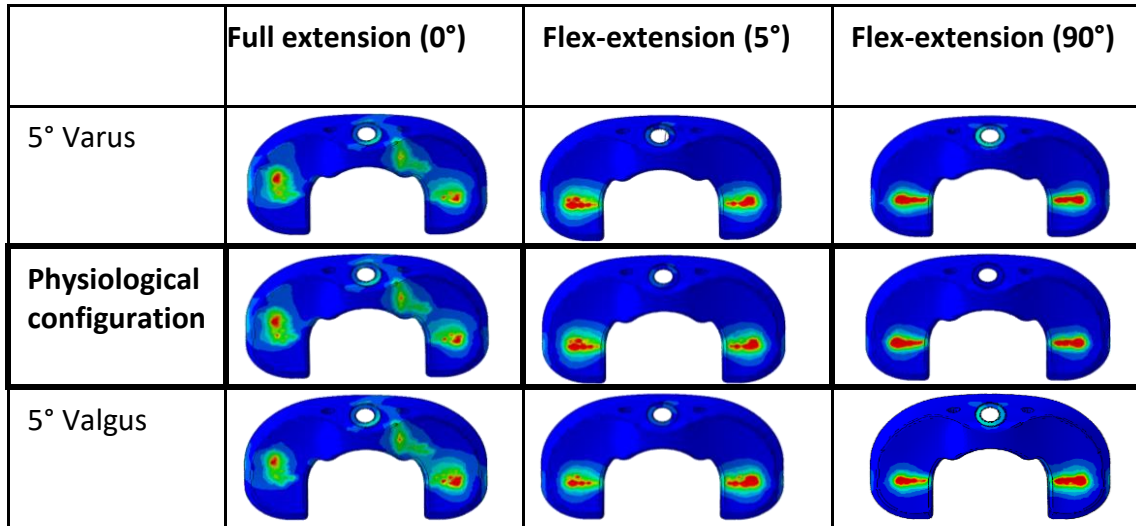


Figure 94, average von Mises stress on polyethylene component. Each row represents a Varus/Valgus configuration, while the columns indicate each flex-extension configuration.

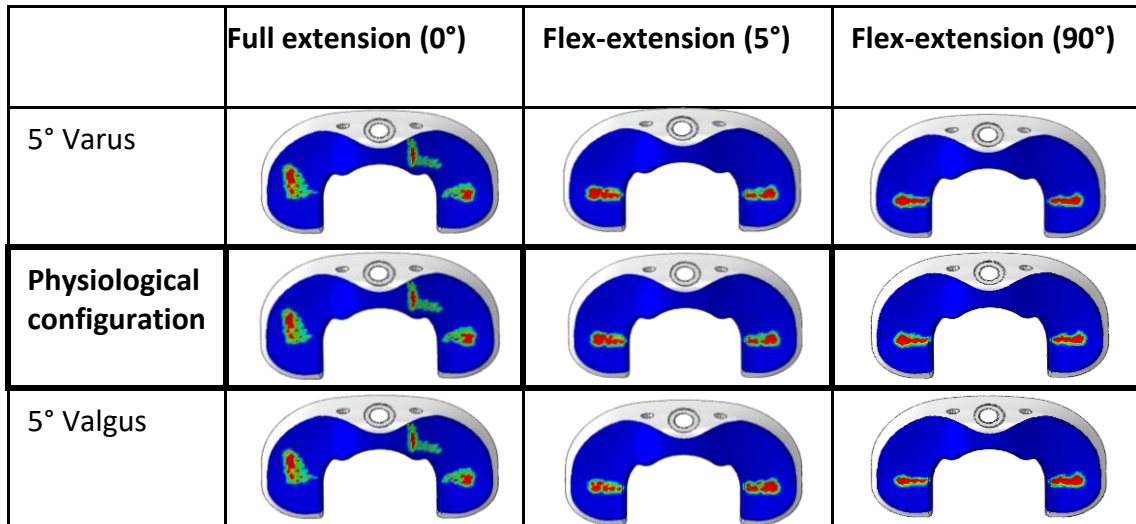


Figure 95, graphical overview of the contact pressure for each configuration.

The results in terms of von Mises stress and contact pressure for plastic bushing component are shown below (fig. 96 and 97).

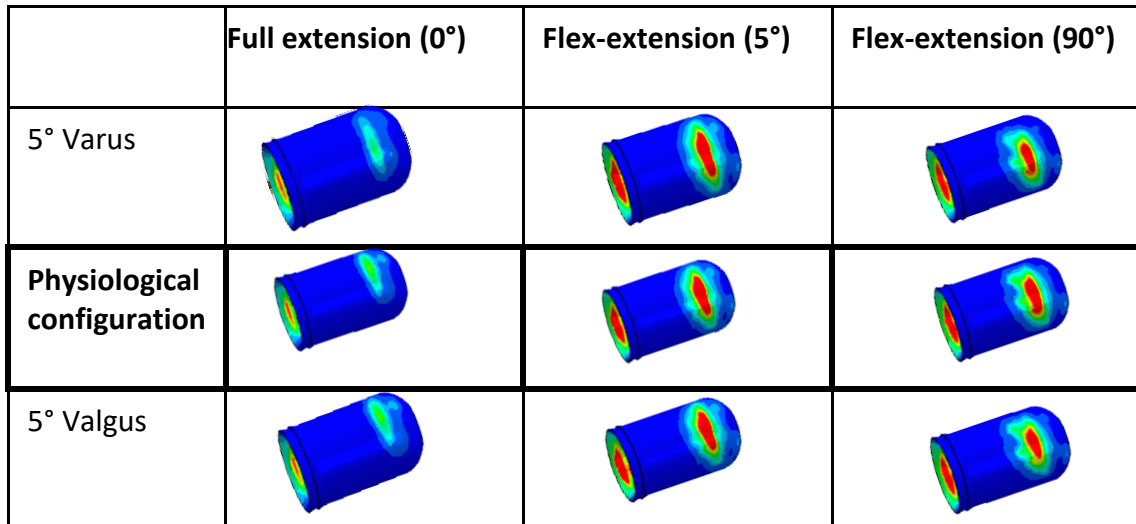


Figure 96, average von Mises stress on plastic bushing. Each row represents a varus/valgus configuration, while the columns indicate each flexo-extension configuration.

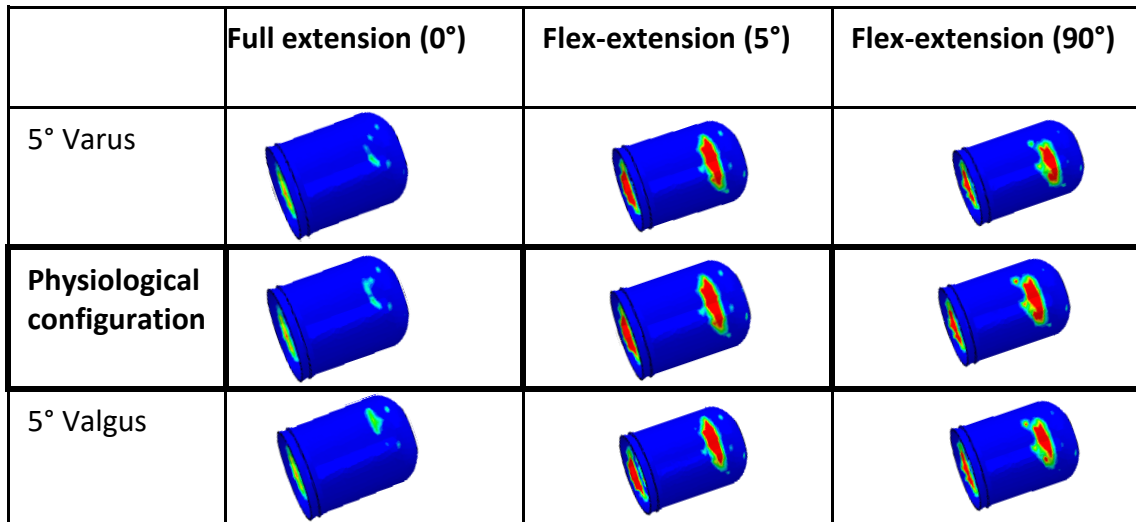


Figure 97, graphical overview of the contact pressure for each configuration

Finally, fig. 98, 99 100 and 101 show the results of von Mises stress and contact pressure both for polyethylene insert and plastic bushing component with cementless stem of 160 mm of length.

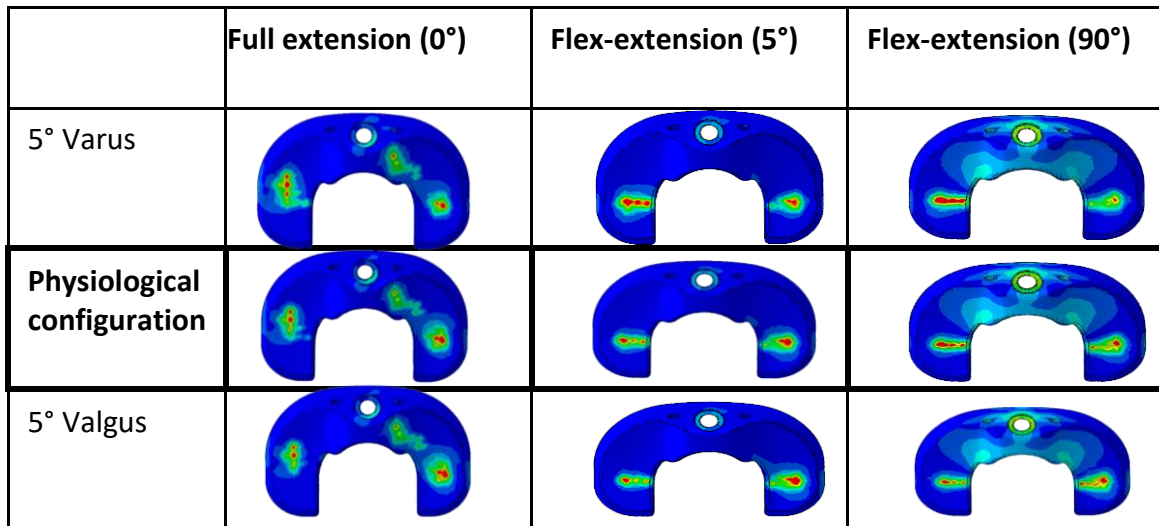


Figure 98, average von Mises stress on polyethylene component. Each row represents a varus/valgus configuration, while the columns indicate each flex-extension configuration.

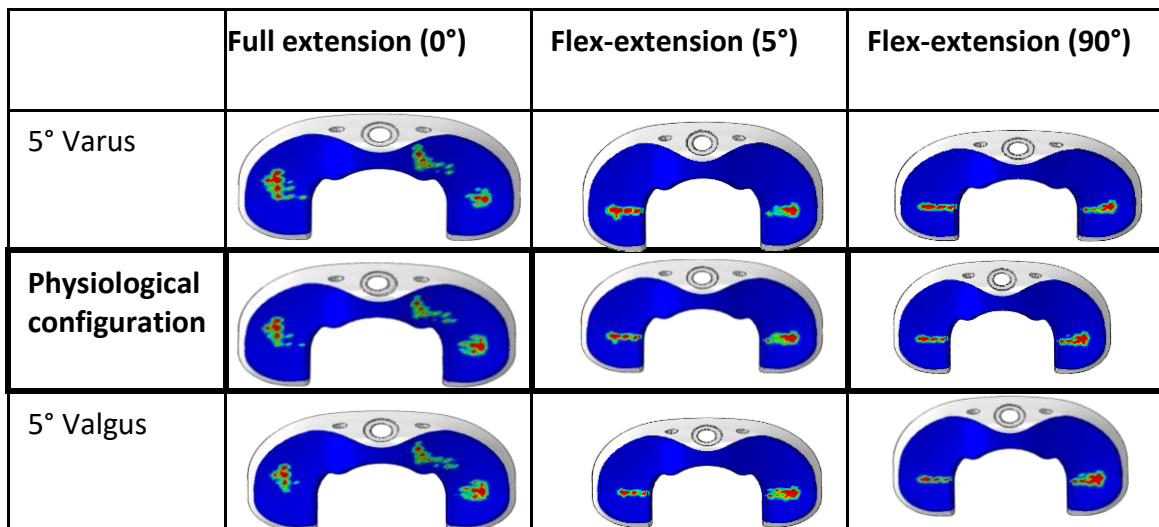


Figure 99, graphical overview of the contact pressure for each configuration.

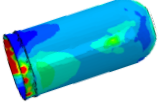
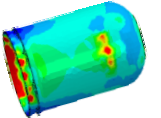
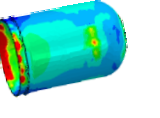
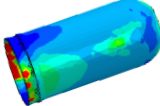
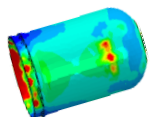
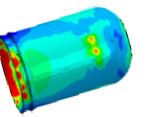
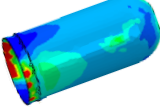
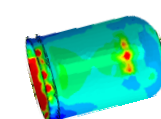
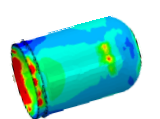
	Full extension (0°)	Flex-extension (5°)	Flex-extension (90°)
5° Varus			
Physiological configuration			
5° Valgus			

Figure 100, average von Mises stress on plastic bushing. Each row represents a varus/valgus configuration, while the columns indicate each flex-extension configuration.

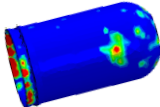
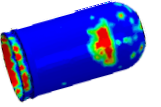
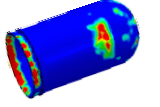
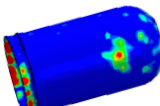
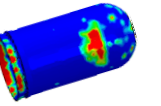
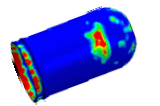
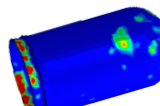
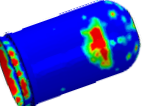
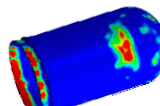
	Full extension (0°)	Flex-extension (5°)	Flex-extension (90°)
5° Varus			
Physiological configuration			
5° Valgus			

Figure 101, graphical overview of the contact pressure for each configuration

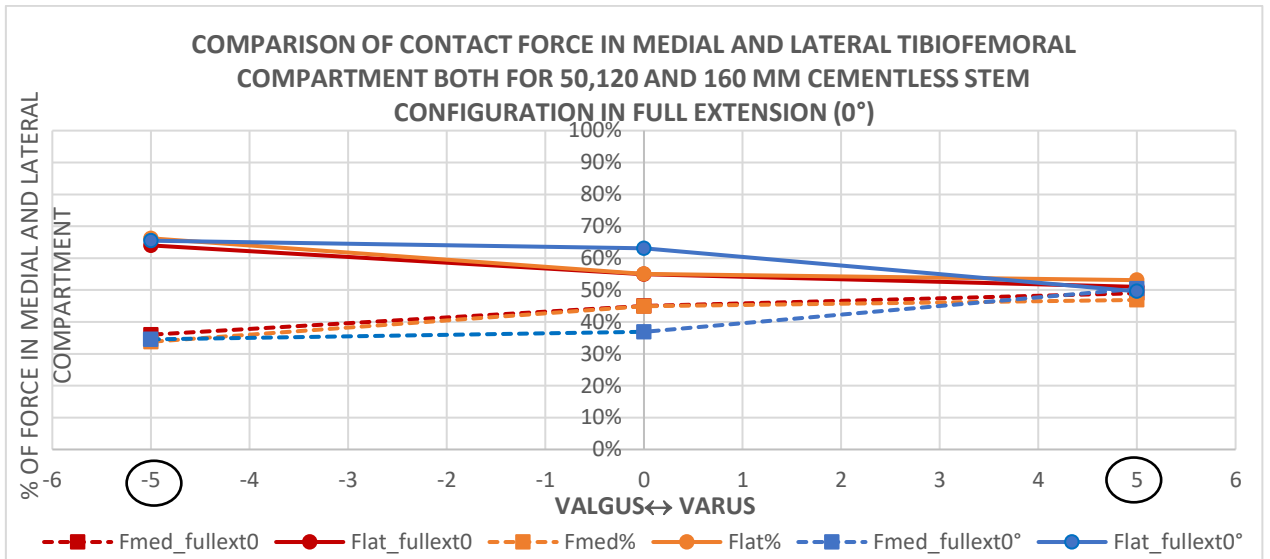


Figure 102, Trend of force in medial and lateral tibiofemoral compartment for Valgus and Varus deformity at 0° of flexion with osteoporotic bone

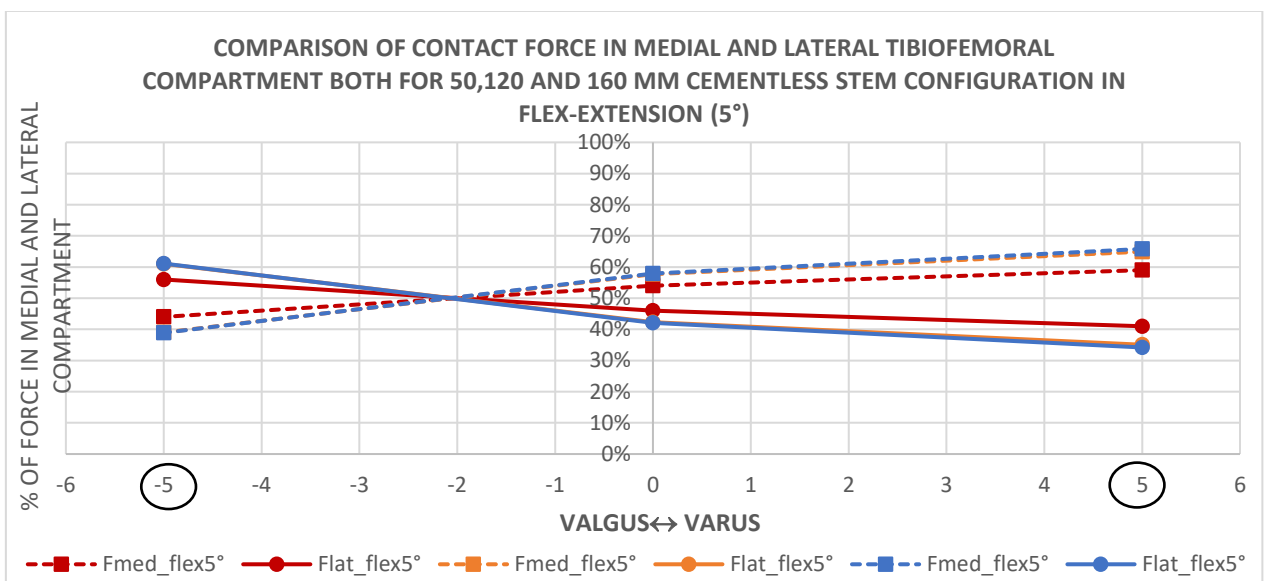


Figure 103, Trend of force in medial and lateral tibiofemoral compartment for Valgus and Varus deformity at 5° of flexion with osteoporotic bone

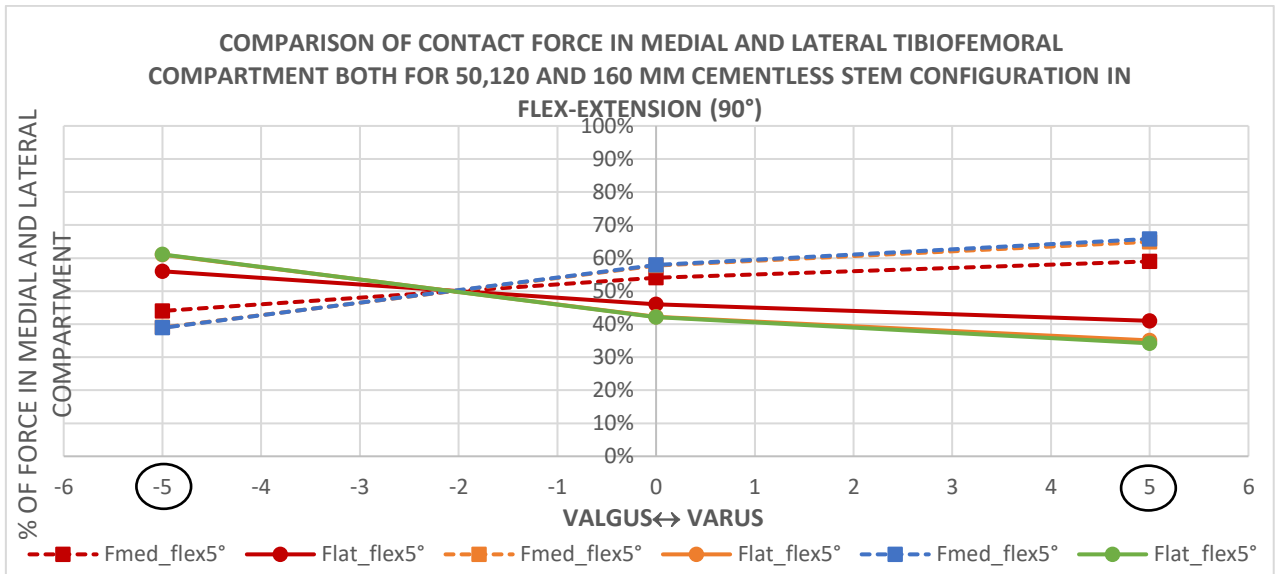


Figure 104, Trend of force in medial and lateral tibiofemoral compartment for Valgus and Varus deformity at 0° of flexion with osteoporotic bone

## 5. Discussion

The aim of this study was to evaluate the distribution of stress and contact area on polyethylene and bushing components in patients with Varus and Valgus deformity. One key finding is that Varus and Valgus malalignment cause an increase of stress on polyethylene component compared to alignment configuration. From results, it is possible to note that shifting from physiological configuration to Varus alignment, the stress increases in the medial region of polyethylene. Accordingly, the stress decreases in the medial region and increases in the lateral side in Valgus configuration compared to the aligned model.

According to results found in literature studies, there is an asymmetric distribution of contact force on the polyethylene insert. In fact, the percentage of force, in full extended knee, in the medial and lateral region is 45% and 55% respectively, both for 50 and 120 mm cementless stems. While, the load split is 37% and 63% with 160 mm cementless stem. Different results are observed for the knee at 5° and 90° of flexion, in fact the contact zone moves from anterior to posterior part of polyethylene component. This causes an overload of the medial compartment. In particular, the percentage of distribution of force in the medial side is 58% and 42% in the lateral side with 50 mm cementless stem. A similar behaviour is found for 160 mm cementless stem. While, the distribution of contact force is 54% and 46% in the medial and lateral region respectively with 120 mm cementless stem.

Another important key finding is that an inclination of 5° of the femoral component could be optimal for all cementless stems. A hyperextension of implant components could lead to overload the anterior part of the prosthesis, resulting in instability of the implant. Based on literature studies, an alignment of approximately 5° is optimal to ensure stability of the implant. In fact, the distribution of medial-lateral force is approximately equal on polyethylene insert. Moreover, it is well noted that the models with cementless stems of 50 and 160 mm lengths have a similar behaviour. As a result, from aligned configuration up to 10° of Varus and Valgus alignment, there are no significant problems. After that, the percentage of force increases sharply after 10° of Varus and

Valgus alignment, with values of 100% of total force in medial and lateral region. On the other hand, the model with cementless stem of 120 mm of length presents an approximately linear trend of force, both for Valgus and Varus alignment. The percentage of force increases slightly from physiological configuration to 30° of Varus in medial region. While, a similar behaviour can be noted for valgus alignment, where the contact force rises in lateral region and drop in medial side. Nevertheless, an asymmetric distribution of force in medial and lateral side, for both configurations, is observed for all models. This fact confirm data found in literature.

Therefore, the model with 120 mm cementless stem seems to have a better distribution of force than other two stems. The graphs of contact force show a roughly linear trend between -10° and 10° of Valgus and Varus configurations. Moreover, the values obtained from this model demonstrate a better distribution of force on each side for moderate and severe Varus and Valgus alignment at 5° and 90° of flexion. In particular, at 10° of Valgus there is a variation of 40% of total contact force on medial-lateral side of polyethylene component with 50 mm cementless stem, while a variation of 20% is found with 120 mm cementless stem.

The results thus demonstrate that changes of force in medial and later condyle are relevant for 120 mm cementless stems. This model results a perfect compromise between 50 and 160 cementless stems, mainly, for severe Valgus configuration. The stem of femoral component with a length of 120 mm thus become essential in severe Valgus and Varus alignment.

To emphasize the quantitative results of contact force, bar histograms shows the values of contact pressure on polyethylene component and bushing component in MPa. Contact pressure increases with flexion achieving values in a range between 0 and 24 MPa with 120 mm cementless stem. Bar graphs show the same behaviour of contact force, as the contact pressure increase on medial region of polyethylene insert and decrees in lateral side for Varus configurations. An opposite behaviour occurs for Valgus configurations. There are no noticeable problems of plasticization because the

maximum values of pressure are mainly in a range of 20-25 MPa. Moreover, the values of average contact pressure on polyethylene and bushing component, resulting with 120 cementless model, are lower than other two models. Moreover, it is needed to say that the polyethylene was considered isotropic linearly elastic, which could lead to incorrect estimation of values of contact pressure. Therefore, the cementless stem of 120 mm of length remain a good compromise between 50 and 160 mm cementless stems.

Similar results were found for cemented and osteoporotic models.

Finally, in case of Valgus and Varus deformity, both cementless and cemented stems of 120 mm of length ensure good stability due to better stress distribution on polyethylene insert. This state is true mainly for several case of Valgus deformity.

## 6. Conclusions

The aim of this study was to obtain relevant results in order to provide support surgeon's treatment decision. A biomechanical study was conducted to predict the behaviour of implant with different models and under clinical problems, such as Varus and Valgus deformity and osteoporotic bone. To date, the use of Endo-Model rotating-hinge is mainly based on surgeon experience because does not exist a protocol which indicate the proper length and method of fixation of stems. Therefore, the results obtained can be considered a good support for decision-making process during complex knee replacement surgeries. Moreover, the aim of this study was not to give accurate values of contact pressure or stress on polyethylene and plastic bushing components, but only give an overview of distribution of contact force and stress on implant components. Additionally, the goal of the research was to analyse how deviation from neutral mechanical alignment led to an increase of stress in such area of implant and study which configurations could ensure better stability of the implant.

In conclusion, future developments could be considered. For instance, studying the performance of the hinged knee arthroplasty during a squat movement, therefore performing a dynamic study. Moreover, considering other movements, such as walking. Other studies could investigate the micromotions between the implant and the bone or take in consideration other lengths of the stem.

## 7. Figures

Figure 1, articulations of the knee joint. Distal view of the femur and proximal view of the tibia	5
Figure 2, Proximal view of tibia bone	5
Figure 3, Distal view of femur bone	5
Figure 4, bones of the knee	6
Figure 5, (A) Anterior view of the distal femur and the proximal tibia. (B) Posterior view of the distal femur and the proximal tibia. (C) Top view of the proximal tibia	8
Figure 6, Anterior view of quadriceps	9
Figure 7, Posterior view of hamstrings muscles	10
Figure 8, forces and moments of the knee with six degrees of freedom	12
Figure 9, mechanical and anatomical axis of the lower limb.	14
Figure 10, physiological knee (a), Valgus knee (b), Varus knee (c)	15
Figure 11, healthy knee joint (left), osteoarthritic knee (right)	16
Figure 12, Procedure of TKA	18
Figure 13, femur, tibia and patella after bone resection. The damaged joint is completely removed. The TKA is performed with the removed parts replace by TKA components.	19
Figure 14, components of TKA	20
Figure 15, Movements of Hinged Knee Prosthesis (a), Rotational (b) and flexion movement(c).	23
Figure 16, Cemented Stems	24
Figure 17, Cementless Stems	
Figure 18, the UHMWPE plateau is pressed down into the metal tray and firmly fixed by the self-locking screw	25
Figure 19, Screw fixation	25
Figure 20 , Insertion of modular stems	25
Figure 21, internal components of Endo-Model Hinge Knee Prosthesis	26
Figure 22, the instrumented baseplate to compute forces and moments. $M_y$ =moment. $F_x$ =mediolateral force, $F_z$ =axial force, $l$ =distance between condyles, $l_z$ =lever arm z, $F_{lat}$ =force on the lateral compartment and $F_{med}$ =force on the medial compartment.	30
Figure 23, coupling of lateral (a) and medial (b) forces.	31
Figure 24, lateral view of femur bone at 0° (a), 5° (b) and 90°(c) of flexion.	32
Figure 25, cementless stem of 50 mm of length	32
Figure 26, cementless stem of 120 mm of length	33
Figure 27, cementless stem of 160 mm of length	33
Figure 28, cemented stem of 50 mm of length	33
Figure 29, cemented stem of 120 mm of length	34
Figure 30, cemented stem of 160 mm of length	34

Figure 31, overview of meshed prosthesis-----	35
Figure 32, average von Mises stress on polyethylene component. Each row represents a Varus/valgus configuration, while the columns indicate each flexo-extension configuration.-----	36
Figure 33, graphical overview of the contact pressure for each configuration.-----	37
Figure 34, Trend of force in medial and lateral tibiofemoral compartment for Valgus and Varus deformity-----	38
Figure 35, average von Mises stress on plastic bushing. Each row represents a Varus/valgus configuration, while the columns indicate each flexo-extension configuration.-----	40
Figure 36, graphical overview of the contact pressure for each configuration.-----	41
Figure 37, average von Mises stress on polyethylene component. Each row represents a Varus/valgus configuration, while the columns indicate each flexo-extension configuration-----	42
Figure 38, graphical overview of the contact pressure for each configuration -----	43
Figure 39, Trend of force in medial and lateral tibiofemoral compartment for Valgus and Varus deformity-----	44
Figure 40, average von Mises stress on plastic bushing. Each row represents a Varus/valgus configuration, while the columns indicate each flexo-extension configuration.-----	45
Figure 41, graphical overview of the contact pressure for each configuration.-----	46
Figure 42, average von Mises stress on polyethylene component. Each row represents a Varus/valgus configuration, while the columns indicate each flexo-extension configuration-----	47
Figure 43, graphical overview of the contact pressure for each configuration -----	48
Figure 44, Trend of force in medial and lateral tibiofemoral compartment for Valgus and Varus deformity-----	49
Figure 45, average von Mises stress on plastic bushing. Each row represents a Varus/valgus configuration, while the columns indicate each flexo-extension configuration.-----	50
Figure 46, graphical overview of the contact pressure for each configuration.-----	51
Figure 47, Trend of force in medial and lateral tibiofemoral compartment for Valgus and Varus deformity at 0° of flexion -----	52
Figure 48, Trend of force in medial and lateral tibiofemoral compartment for Valgus and Varus deformity at 5° of flexion -----	52
Figure 49, Trend of force in medial and lateral tibiofemoral compartment for Valgus and Varus deformity at 90° of flexion -----	53
Figure 50, Maximum contact pressure for medial and lateral contact area on polyethylene component for 0° configuration with the cementless stem of 50 mm.-----	54
Figure 51, Maximum contact pressure for medial and lateral contact area on polyethylene component for 5° configuration with the cementless stem of 50 mm-----	54
Figure 52, Maximum contact pressure for medial and lateral contact area on polyethylene component for 90° configuration with the cementless stem of 50 mm -----	55

Figure 53, Average contact pressure on polyethylene component for all configurations with the cementless stem of 50 mm for 0°, 5° and 90° of flexion. ....	55
Figure 54, Maximum contact pressure in the internal and external contact area of plastic bushing component for 0° configuration with cementless stem of 50 mm .....	56
Figure 55, Maximum contact pressure in the internal and external contact area of plastic bushing component for 5° configuration with cementless stem of 50 mm .....	57
Figure 56, Maximum contact pressure in the internal and external contact area of plastic bushing component for 90° configuration with cementless stem of 50 mm.....	57
Figure 57, average contact pressure in the internal and external contact area of plastic bushing component for all configurations with cementless stem of 50 mm at 0°, 5° and 90° of flexion. --	58
Figure 58, Maximum contact pressure for medial and lateral contact area on polyethylene component for 0° configuration with cementless stem of 120 mm. ....	58
Figure 59, Maximum contact pressure for medial and lateral contact area on polyethylene component for 5° configuration with cementless stem of 120 mm. ....	59
Figure 60, maximum contact pressure for medial and lateral contact area on polyethylene component for 90° configuration with cementless stem of 120 mm.....	59
Figure 61, average contact pressure on polyethylene component for all configurations with cementless stem of 120 mm .....	60
Figure 62, Maximum contact pressure in the internal and external contact area of plastic bushing component for 0° configuration with cementless stem of 120 mm .....	60
Figure 63, Maximum contact pressure in the internal and external contact area of plastic bushing component for 5° configuration with cementless stem of 120 mm .....	61
Figure 64, maximum contact pressure in the internal and external contact area of plastic bushing component for 90° configuration with cementless stem of 120 mm .....	61
Figure 65, average contact pressure in the internal and external contact area of plastic bushing component for all configurations with cementless stem of 120 mm .....	62
Figure 66, Maximum contact pressure for medial and lateral contact area on polyethylene component for 0° configuration with cementless stem of 160 mm .....	62
Figure 67, Maximum contact pressure for medial and lateral contact area on polyethylene component for 5° configuration with cementless stem of 160 mm .....	63
Figure 68, Maximum contact pressure for medial and lateral contact area on polyethylene component for 90° configuration with cementless stem of 160 mm.....	63
Figure 69, average contact pressure on polyethylene component for all configurations with cementless stem of 120 mm .....	64
Figure 70, Maximum contact pressure in the internal and external contact area of plastic bushing component for 0° configuration with cementless stem of 160 mm.....	64

Figure 71, Maximum contact pressure in the internal and external contact area of plastic bushing component for 5° configuration with cementless stem of 160 mm	65
Figure 72, Maximum contact pressure in the internal and external contact area of plastic bushing component for 90° configuration with cementless stem of 160 mm	65
Figure 73, average contact pressure in the internal and external contact area of plastic bushing component for all configurations with cementless stem of 160 mm	66
Figure 74, average von Mises stress on polyethylene component. Each row represents a Varus/Valgus configuration, while the columns indicate each flex-extension configuration.	67
Figure 75, graphical overview of the contact pressure for each configuration	67
Figure 76, average von Mises stress on plastic bushing. Each row represents a Varus/Valgus configuration, while the columns indicate each flex-extension configuration.	68
Figure 77, graphical overview of the contact pressure for each configuration.	68
Figure 78, average von Mises stress on polyethylene component. Each row represents a Varus/Valgus configuration, while the columns indicate each flex-extension configuration.	69
Figure 79, graphical overview of the contact pressure for each configuration	70
Figure 80, average von Mises stress on plastic bushing. Each row represents a Varus/Valgus configuration, while the columns indicate each flex-extension configuration.	69
Figure 81, graphical overview of the contact pressure for each configuration.	70
Figure 82, average von Mises stress on polyethylene component. Each row represents a Varus/Valgus configuration, while the columns indicate each flex-extension configuration.	71
Figure 83, graphical overview of the contact pressure for each configuration	71
Figure 84, average von Mises stress on plastic bushing. Each row represents a Varus/Valgus configuration, while the columns indicate each flex-extension configuration.	72
Figure 85, graphical overview of the contact pressure for each configuration.	72
Figure 86, Trend of force in medial and lateral tibiofemoral compartment for Valgus and Varus deformity at 0° of flexion	73
Figure 87, Trend of force in medial and lateral tibiofemoral compartment for Valgus and Varus deformity at 5° of flexion	74
Figure 88, Trend of force in medial and lateral tibiofemoral compartment for Valgus and Varus deformity at 90° of flexion	73
Figure 89, graphical overview of average contact pressure on polyethylene component (left) and average contact pressure in the internal and external contact area of plastic bushing component (right) for all configurations (0°, 5° and 90°).	75
Figure 90, average von Mises stress on polyethylene component. Each row represents a Varus/Valgus configuration, while the columns indicate each flex-extension configuration.	76
Figure 91, graphical overview of the contact pressure for each configuration.	76

Figure 92, average von Mises stress on plastic bushing. Each row represents a varus/valgus configuration, while the columns indicate each flexo-extension configuration.-----	77
Figure 93, graphical overview of the contact pressure for each configuration -----	77
Figure 94, average von Mises stress on polyethylene component. Each row represents a Varus/Valgus configuration, while the columns indicate each flex-extension configuration.-----	78
Figure 95, graphical overview of the contact pressure for each configuration.-----	78
Figure 96, average von Mises stress on plastic bushing. Each row represents a varus/valgus configuration, while the columns indicate each flexo-extension configuration.-----	79
Figure 97, graphical overview of the contact pressure for each configuration -----	79
Figure 98, average von Mises stress on polyethylene component. Each row represents a varus/valgus configuration, while the columns indicate each flex-extension configuration.-----	80
Figure 99, graphical overview of the contact pressure for each configuration.-----	80
Figure 100, average von Mises stress on plastic bushing. Each row represents a varus/valgus configuration, while the columns indicate each flex-extension configuration.-----	81
Figure 101, graphical overview of the contact pressure for each configuration-----	81
Figure 102, Trend of force in medial and lateral tibiofemoral compartment for Valgus and Varus deformity at 0° of flexion with osteoporotic bone -----	82
Figure 103, Trend of force in medial and lateral tibiofemoral compartment for Valgus and Varus deformity at 5° of flexion with osteoporotic bone -----	82
Figure 104, Trend of force in medial and lateral tibiofemoral compartment for Valgus and Varus deformity at 0° of flexion with osteoporotic bone -----	83

## 8. Tables

Table 1, materials properties used for all models .....	29
Table 2, Percentage of force applied in all models .....	31

## REFERENCES

- [1] Roland Becker et al., "Alignment in total knee arthroplasty", *Knee Surgery, Sports Traumatology, Arthroscopy*, August 2016.
- [2] Innocenti B. et al., "Deviations From Optimal Alignment in TKA: Is There a Biomechanical Difference Between Femoral or Tibial Component Alignment?" *J Arthroplasty*. 2016 Jan; 31(1):295-301.
- [3] Flandry F1, Hommel G. "Anatomy and Biomechanics of the knee" *Sports Med Arthrosc Rev*. 2011 Jun; 19(2):82-92.
- [4] Blackburn TA, Craig E., "Knee anatomy: a brief review" *Phys Ther*. 1980 Dec;60(12):1556-60.
- [5] Petersen W1, Zantop T, "Anatomy of the anterior cruciate ligament with regard to its two bundles" *Clin Orthop Relat Res*. 2007 Jan;454:35-47.
- [6] Woo SL et al., "Biomechanics of knee ligaments" *Am J Sports Med*. 1999 Jul-Aug;27(4):533-43.
- [7] Darryl D. D'Lima et al., "Knee joint forces: prediction, measurement, and significance" *Proc Inst Mech Eng H*. 2012 Feb; 226(2): 95–102.
- [8] R.Shenoy et al., "Biomechanics of the knee and TKR" *Orthopaedics and Trauma* 27:6
- [9] Kuster MS et al., "Joint load considerations in total knee replacement" *J Bone Joint Surg Br*. 1997 Jan;79(1):109-13.
- [10] Gupton M et al., "Anatomy, Bony Pelvis and Lower Limb, Fibula" *StatPearls [Internet]*. Treasure Island (FL): StatPearls Publishing; 2019-.2018 Dec 6.
- [11] Stephen Kishner, MD, MHA et al., "Knee Joint Anatomy" *Medscape*
- [12] "Knee Anatomy, Function and Common Problems", Web, <https://www.healthpages.org/anatomy-function/knee-joint-structure-function-problems/>

- [13] Raviprasad K. "Component Alignment in Total knee Replacement". Ortho & Rheum Open Access J 2018;11(3): 555815.
- [14] "Osteoarthritis: Care and Management in Adults". Web, <https://www.ncbi.nlm.nih.gov/pubmed/25340227>
- [15] Haq I1, Murphy E, Dacre J. "Osteoarthritis", Postgrad Med J. 2003 Jul;79(933):377-83.
- [16] Gregory M Martin, MD et al., "Patient education: Total knee replacement (arthroplasty)", Web, <https://www.uptodate.com/contents/total-knee-replacement-arthroplasty-beyond-the-basics>
- [17] Matthew Varacallo et al., "Total Knee Arthroplasty (TKA) Techniques", StatPearls [Internet]. Treasure Island (FL): StatPearls Publishing; 2019-.2019 Jan 19. [PubMed]
- [18] "Knee Replacement Implants", Web, <https://orthoinfo.aaos.org/en/treatment/knee-replacement-implants/>
- [19] Yousef Abu-Amer et al., "Aseptic loosening of total joint replacements: mechanisms underlying osteolysis and potential therapies", Arthritis Research & Therapy 2007, 9(Suppl 1):S6 (doi:10.1186/ar2170)
- [20] Niraj V Kalore et al., "Diagnosis and Management of Infected Total Knee Arthroplasty", Niraj V Kalore
- [21] "Total Knee Replacement", Web, <http://kneehipreplacement.com/>
- [22] B. Guenoun et al., Complications following rotating hinge Endo-Modell (LINK) knee arthroplasty,
- [23] Endo-Model® Standard/ – M Knee System with Segmental Bone Replacement Components and MIRETO™ Instrument Set, Implant and Instrument.
- [24] Halder A et al., "Influence of limb alignment on mediolateral loading in total knee replacement: in vivo measurements in five patients", J Bone Joint Surg Am. 2012 Jun;94(11):1023

## ***Ringraziamenti***

Dopo un lungo percorso pieno di ostacoli e difficoltà finalmente posso dire di avercela fatta. Dunque, è un mio dovere e un piacere ringraziare tutte le persone che hanno fatto parte di questo capitolo importante della mia vita.

In primis vorrei ringraziare la Professoressa Cristina Bignardi, il Professore Alberto Audenino e il Professore Bernardo Innocenti per la disponibilità e la cortesia dimostratami durante questo percorso di tesi, per i preziosi insegnamenti che mi hanno aiutata a crescere sia a livello professionale che umano.

A *mia Madre e mio Padre*, per tutti i sacrifici, per avermi supportata in ogni mia scelta, per avermi sempre sostenuta ed aver creduto sempre in me anche quando pensavo di non potercela fare. Per aver macinato chilometri per venirmi a trovare, fino in capo al mondo. Per avermi sempre spronata ad andare avanti e non mollare. Per aver gioito con me nei momenti belli ed essermi stati accanto nei momenti difficili. Un grazie immenso va a loro, a cui devo tutto.

A *mia zia Simona*, che con il suo ottimismo e positività mi ha sempre risollevato il morale. Per avermi insegnato a vedere sempre il lato positivo delle cose ed affrontare i fallimenti non come rinunce ma punti di partenza per migliorare sempre. Un grazie anche a mio zio Raffaele per i consigli e le indicazioni che mi ha fornito da quando ho intrapreso questo percorso.

Grazie alle mie sorelle, *Alessia e Irma*, per avermi sopportato e supportato soprattutto in questo ultimo periodo. Per avermi fatto svagare ed essere venute a trovarmi fino in Belgio.

Un ringraziamento particolare va a *Marika*, oltre che compagna di università è diventata parte fondamentale della mia vita. Abbiamo iniziato insieme questo percorso di Laurea Magistrale, è stata come un'ancora di salvezza in mezzo al mare. Ci siamo supportate a vicenda, abbiamo condiviso momenti difficili ma soprattutto belli di questi anni. Anche se le nostre strade inevitabilmente si divideranno, noi non ci divideremo mai.

Un grazie agli *amici* che ho conosciuto a Torino in particolare *Daria, Laura, Giada e Giovanni* per aver contribuito a rendere questi anni più leggeri ed indimenticabili. Per essere venuti fino in Norvegia, per avere condiviso ore di lezioni ma anche sbronze. Grazie perché senza di voi questi anni non sarebbero stati gli stessi.

Un grazie agli *amici di sempre*, perché nonostante abbiamo intrapreso strade diverse quando ci ritroviamo è come se non fosse cambiato nulla. A chi voleva essere presente oggi ma non ha potuto.

Grazie a *Roberta e Stefano*, per avermi fatto sempre sentire a casa, per il rapporto sincero che si è instaurato. Per aver condiviso ansie e gioie. Siete stati come una famiglia.

Grazie a *Maila*, per aver condiviso il periodo più impegnativo e stressante di questo percorso. L'unica persona che poteva capire a pieno il mio stato d'animo. Grazie per le chiacchierate, le parole di conforto, le risate e i nostri aperitivi. Sei entrata da poco a far parte della mia vita, ma sei già entrata nel mio cuore.

Grazie ai *miei zii e i miei cugini* per aver fatto km e km pur di esserci oggi e condividere con me questo traguardo importante. Per avermi raggiunto fino in capo al mondo ed aver avuto sempre un pensiero per me.

Grazie anche a *Gina, Antonio e Alberto* per avermi accolto come una figlia e una sorella, per avermi sostenuta con il vostro affetto e per essere qui presenti oggi a festeggiare con me.

Ultimo ma il più importante grazie va a te, *Nicola*, il mio punto fermo, il mio porto sicuro per una nave in tempesta come la mia. Grazie per aver compreso ogni mia paura e ogni mio sbalzo d'umore ed essermi stato accanto spronandomi a dare sempre il meglio di me. Grazie perché mi hai insegnato, con il tuo immenso Amore, che la distanza è solo un numero e nonostante nazioni e chilometri che ci dividevano siamo ancora qua, più forti di prima. Grazie perché con la tua determinazione e testardaggine mi hai insegnato che se vuoi puoi arrivare dove vuoi. Grazie per rendermi ogni giorno felice. Soprattutto grazie perché ci sei sempre stato e sei presente ogni giorno della mia vita.

*Più di ieri, meno di domani.*

Un grazie speciale a tutti,

*Lilia*

*22/07/2019*